（千葉大学審査学位論文）

Land Subsidence Mapping and Risk Assessment in Kathmandu Valley, Nepal, using DInSAR and GIS Techniques

July 2017

Chiba University

Graduate School of Science

Division of Geosystem and Biological Sciences

Department of Earth Sciences

Richa Bhattarai

ABSTRACT

Land subsidence is identified as a global problem and intensive studies are being conducted worldwide to detect and monitor this problem. However, in Nepal no research has been done regarding subsidence even though the existing conditions indicate the probability of subsidence occurrence. Therefore, this study will be the first to detect land subsidence and assess its risk in Kathmandu valley, Nepal.

Differential Synthetic Aperture Radar Interferometry (DInSAR) is a remote sensing technique that is capable of detecting land surface deformation with centimeter accuracy with a large spatial coverage. In this research, this technique was applied to two pairs of Advanced Land Observing Satellite (ALOS) Phased Array L-band SAR (PALSAR) data to detect land subsidence in Kathmandu valley from 2007 to 2010. DInSAR was also applied to three pairs of ALOS 2 PALSAR 2 data (from 2014 to 2015) to detect land subsidence in Kathmandu valley after the 2015 Gorkha earthquake event and see if the earthquake event had any effect on the subsidence.

Risk assessment is simply an evaluation of the probability and frequency of occurrence of a hazardous event, exposure of people and property to the hazard and consequence of that exposure. Disaster Risk Index method, Analytic Hierarchy Process (AHP) along with Geographic Information System (GIS) tools were used to assess risk of land subsidence in Kathmandu Valley, Nepal.

The DInSAR result for ALOS PALSAR data revealed several subsidence areas towards the center of the valley ranging from a maximum of 9.9 km^2 to a minimum of 1 km^2 coverage. Majority of the subsidence was observed in old settlement areas with mixed use development namely, Central Kathmandu, Chauni, Lalitpur, Imadol, Thimi, Madhyapur Thimi, New Baneshwor, Koteshwor and Gothatar. The subsidence depth was found to be gradually increasing from the periphery towards a center in almost all detected subsidence area. The subsidence depth was found to be in a range of 1 cm to 17 cm and the maximum subsidence velocity was found to be 4.8 cm/yr. The subsidence volume for each subsidence affected area was also calculated using a simple mathematical formula.

It was found that the concentration of deep water extraction wells was higher in areas with higher subsidence rates. It was also found that the detected subsidence area was situated over geological formations mainly consisting of silica, sand, silt, clay and silty sandy gravel.

DInSAR results for ALOS 2 PALSAR 2 revealed that no difference was found in the location of subsidence occurrence to that from 2007 to 2010 data. However, a little change in velocity and area covered were observed. The subsidence depth was found to be in a range of 1cm to 25 cm. The maximum subsidence velocity was found to be 15 cm/yr.

The location where maximum subsidence was observed (i.e. Maximum depth of 17 cm and 14 cm in Central Kathmandu and Lalitpur) was found to at high risk of experiencing land subsidence induced damage. Other location where subsidence was observed was found to be at medium risk and the rest of the Kathmandu valley was found to be at low risk with current data situation.

Due to lack of previous land subsidence measurement data and difficulty to acquire GPS measurement data, the outcomes of this study have not been validated. But, owing to that fact that DInSAR is a well-developed methodology that has been capable of accurately detecting land subsidence is similar location to that of Kathmandu valley, the accuracy can be assumed to be acceptable.

This study can be considered as the first step towards other comprehensive study relating to land subsidence. The outcome of this research provides a basic understanding of the current situation that can further assist in developing prevention and risk management techniques.

ACKNOWLEDGEMENT

I would like to express my sincere gratitude to **Graduate School of Science** for providing the opportunity to conduct my PhD at Chiba University. I would also like to extend my deepest gratitude to **Prof. Dr. Ryutaro Tateishi** for his guidance and supervision during the initial stages of this research and **Prof. Dr. Akihiko Kondoh** for his guidance and supervision during the final stages of the research. This research would not have been possible without the constant valuable advices from both the supervisors. I am blessed to have such encouraging and supporting supervisors.

I would also like to take this opportunity to thank my reviewers **Dr. Sci. Atsushi Higuchi** (CEReS), **Prof. Dr. Kazuhito Ichii** (CEReS) and **Prof. Dr. Nozomu Takeuchi** for their precious comments and advices which helped me improve this dissertation.

I would specially like to thank the **Super Global University- Ministry of Education, Culture, Sports, Science and Technology (SGU-MEXT) scholarship** for financially supporting the educational expenses during the period of this research. I would also like to thank **Jspacesystems** for providing the necessary ALOS PALSAR data. The ALOS 2 PALSAR 2 data was obtained from **Japan Aerospace Exploration Agency (JAXA)** under the Research Agreement for the Advanced Land Observing Satellite-2 with the help of **Aikebaier Maitiniyazi**. I would like to thank both for providing the necessary data. I acknowledge **Kathmandu Valley Water Supply Management Board (KVWSMB)**, **Ministry of Water Supply and Sanitation, Kathmandu Valley Development Authority (KVDA)** and **National Accounts Section, Central Bureau of Statistics**, Government of Nepal for providing necessary data to conduct this study.

I express my acknowledgement to **Toshiyuki Kobayashi** and **Tomohiro Shirahata** for tutoring me and helping me with the Japanese translations and basic daily life matter of Japan. I am also grateful to **Haireti Alifu**, **Aikebaier Maitiniyazi** and **Ayihumaier Halipu** for their immense help during my research. I would also like to acknowledge the help of all the members of **Tateishi lab** and **Kondoh lab.**

I would also like to thank my brother **Suyesh Bhattarai** for his suggestions, encouragement and helping me obtain all the necessary data from Nepal. A special thanks to my husband **Nikhil Raj Poudyal** for his constant encouragement, guidance, suggestions and support; Thank you for making my life so much easier. I would also like to thank my **parents, parents-in-law,** and all my **family members** and **friends** for their encouragement and moral support during my PhD study.

A very special gratitude goes out to my 19 months old daughter **Vedanshi Poudyal**; achieving my goal would have been impossible without her love and patience… I owe this degree to her.

Finally, I would like to thank **GOD** for everything.

Thank you all for your support and encouragement!

Richa Bhattarai

TABLE OF CONTENTS

LIST OF FIGURES

Chapter 1

Chapter 2

Chapter 3

Chapter 4

LIST OF TABLES

Chapter 2

Chapter 3

Chapter 4

1. INTRODUCTION

1.1 Background

In general terms, subsidence refers to the sudden sinking or gradual downward settling of the ground surface with very less or no horizontal motion at all (Jackson, 1997). Land subsidence can also be defined as an environmental geological phenomenon that causes the slow lowering of ground surface elevation (Hu, B., et al., 2009). It is often a result of the natural compaction of sediments and extraction of ground water, geothermal fluids, oil, gas, coal and other solids through mining (Corapcioglu, 1989; Strozzi et al., 2001). Land subsidence tends to change the topographic gradients and thus causes infrastructure damage, ruptures in the land surface, aggravates flooding, causes inundation of land and reduces the capacity of aquifers to store water, ultimately posing a risk for the society and economy (Holzer and Galloway, 2005). The occurrence of land subsidence has been studied in many places around the world, including Tokyo, Japan (Yamaguchi, 1969), Mexico (Adrian et al., 1999), Saudi Arabia (Bankher and Al-Harthi, 1999), Texas, USA (Gabrysch, 2000), Jakarta, Indonesia (Abidin et al., 2001), Ravenna, Italy (Teatini et al., 2005), Bangkok, Thailand (Bergado et al., 1987; Phien-wej et al., 2006), Pingtung Plain, Taiwan (Hu et al., 2006) and China (Xu et al., 2008).

Scientific studies reveal that unrestricted groundwater exploitation has the potential to cause a slow but significant land subsidence (Pratt et al., 1926; Poland et al., 1969; Bell et al., 1986; Shi et al., 2007). A close relationship between the amount of groundwater withdrawal for industrial activities and advancement of land subsidence was recognized early in Japan during 1954 to 1960 observations (Inaba et. al., 1969). Additionally, geology also plays a vital role in acceleration of land subsidence. Large amounts of groundwater extraction from certain types of underlying sediments, such as fine-grained sediments result in compaction of these sediments because the groundwater is partly responsible for the subsurface support. This ultimately triggers land subsidence (Perlman, 2016).

Land subsidence is just a geological phenomenon either triggered by natural or anthropogenic activities and the risk to human and their immediate artificial environment are almost negligible in remote and uninhabited areas (Tomás et al., 2014b). But, when this phenomenon has the probability of resulting harmful consequences or the expected loss (of lives, property, livelihoods, economic activities or environment) mostly in developed areas then it is considered to pose a risk (Kappel et al., 1999; Autin, 2002; Hu et al., 2009). Risk factors are compounded by rapid increase in urban population and economic development (Wang et al., 2012). The physical damage caused by land subsidence (i.e. the hazard due to land subsidence can be mainly categorized into two forms: damage on artificial (manmade) infrastructures and damage on natural systems. Significant damage is seen in areas corresponding to land subsidence occurrence.

The main damage on manmade infrastructure reported worldwide are mostly related to water transport structures (Sato et al., 2003; Faunt et al., 2015). Since land subsidence affects the elevation of the ground, and owing to the fact that water transportation infrastructures are very sensitive to minor gradient changes, subsidence can hugely affect such structures. Other reported problems include damage to buildings and transportation facility (i.e. roads, bridges, railways).

Although, damage to manmade infrastructures are more emphasized and easily noticeable unlike the damage to natural systems which is invisible are generally more threatening. The main reason being that artificial infrastructures damages can generally be repaired opposed to natural system damage which is generally permanent. Some of the examples of natural structure damage are permanent compaction of aquifer system, change in topography which ultimately affects the river patterns and low lying areas.

The other main factor affected by land subsidence is damage to the social environment which includes the human society and the economic development level. The physical damage caused by land subsidence will eventually affect the social environment directly or indirectly but the intensity is determined by the recoverable capability of life, property and various economic activities in the disaster affected areas. Remarkable economic losses have been caused by land subsidence throughout the world (Zhang et al., 2003; Holzer et al., 2005; Liu et al., 2015).

Kathmandu valley, the capital and the urban core of a developing country Nepal is lagging in terms of data documentation and research work regarding land subsidence and its risk assessment. The

factors that make a location prone to land subsidence risk (i.e. geology and groundwater extraction characteristics) are in favor of the valley, yet research is not being conducted. Also, the valley is experiencing rapid increase in population and economic development in the past few decades that will ultimately contribute to increase in risk of damage induced by land subsidence if no counter measures are considered.

Therefore, it is necessary to assess land subsidence risk for decision and policy makers to prevent a huge potential disaster. Risk assessment is simply an application of a methodology for evaluating risk, where risk is defined as the probability and frequency of occurrence of a hazardous event, exposure of people and property to the hazard and consequences of that exposure (Hu et al., 2009).

Kathmandu is a bowl-shaped valley with two principle landforms: alluvial and flood plains, which makes it even more prone to subsidence. Groundwater has always been a significant source of water supply in Kathmandu valley since early 1970s (Pandey et al., 2012). Constantly increasing population, industrialization and urbanization have triggered the increase in groundwater consumption. Extraction of groundwater has increased from 2.3 million-liters-a-day (MLD) in 1979 to 80 MLD in 2011 (Shrestha, 2016). Groundwater fulfills nearly 50% of the total water demand during wet season and 60-70% during the dry season (ICIMOD, 2007). Consequently, annual extraction is exceeding recharge leading to tremendous depletion in groundwater levels. Considering the relation of groundwater exploitation and land subsidence from the case studies of various countries, it can be assumed that the same may occur in Kathmandu valley as well. Nonetheless, no published research has been done to the authors' knowledge to determine if land subsidence is taking place in actual due to ground water extraction; therefore, no evidence of land subsidence in Kathmandu valley is available (Pandey et al., 2012).

Researches have been done focusing on the land deformation caused by the crustal movements in the region. On April 25, 2015, a devastating earthquake of Mw 7.8 (US Geological Survey, 2015) struck central Nepal. It was followed by a strong aftershock of Mw 7.3 on 12 May 2015 and many other aftershocks greater than Mw 6 thereafter. It was only after this event that a few literatures mentioned subsidence; the sole cause being the earthquake (Kobayashi et al., 2015). A developing country, struck by a natural disaster recently is moving forward to rebuilding and if subject like land subsidence that has been troubling the globe is not addressed immediately then the

consequences can be unaffordable. Therefore, mapping, continuous monitoring and risk assessment of land subsidence is critical in a place like Kathmandu Valley.

Differential Synthetic Aperture Radar interferometry (DInSAR) is an advanced remote sensing tool that has the ability to map displacements over vast areas at a very high spatial resolution with a lower cost as compared to other conventional techniques such as GPS, topographic measure and extensometers (Tomás et al., 2014). Previously, several researchers have applied this method to map and monitor groundwater extraction induced subsidence all around the world with successful results. For example; in Antelope Valley, California (Galloway et. al., 1998); Coachella Valley, California (Sneed et. al, 2001); Kolkata, India (Chatterjee, 2006); Iran (Motagh, 2008); Jakarta (Bayuaji, 2010); Alto Guadalentin Basin, Spain (Boni et. al., 2015).

Most frequently deployed approach for land subsidence risk assessment are by the means of Geographic Information System (GIS) techniques and Disaster Risk Index Method and Analytic Hierarchy Process (AHP) (Hu et al., 2009; Westen et al., 2011; Zhu et al., 2013; Liu et al., 2015). GIS provides robust tools for inclusive spatial modeling and analysis. Disaster Risk Index method is an approach where the hazard, the vulnerability and the capability of disaster prevention and reduction are considered for the quantitative evaluation a risk. AHP is a multi-criteria mathematical evaluation method used for decision making where hierarchical structures are used to quantify relative priorities for a given set of elements on a ratio scale set by the user (Hu et al., 2009).

1.2 Objectives of the Research

The main objective of this research is

1. To detect the current situation of land subsidence in Kathmandu valley by the application of Differential Synthetic Aperture Radar Interferometry (D-InSAR) technique to Advanced Land Observing Satellite (ALOS) Phased Array L-band Synthetic Aperture Radar (PALSAR) data.
2. To assess land subsidence risk by using GIS techniques, Disaster Risk Index Method and Analytic Hierarchy Process (AHP).

1.3 Scope of the Research

Although very little is known about land subsidence in Nepal, no studies are being done to actually detect the occurrence of land subsidence. Therefore, the outcome of this research will help in understanding the current situation, that would further help to develop prevention techniques and risk management. After comparing with land measurement data and conveying a field survey, it is expected to be useful for the government and interested stakeholders for better understanding of the situation for sustainable development and policy-making for disaster prevention.

The results from this study can serve as a significant benchmark for Kathmandu Valley, Nepal as it is developing towards sustainable urbanization but lacks proper data and research.

1.4 Study Area

Kathmandu Valley, the largest urban agglomerate of Nepal is located between 27°34'33" and 27°49'4" N latitudes and 85°11'19" and 85°34'57" E longitudes covering an area of 654.7km^2 (RSLUP report, 2015). The valley consists of three major cities namely Kathmandu: the capital city, Bhaktapur and Lalitpur: ancient cultural gem cities. The Landsat image of Kathmandu valley is shown in **Figure 1.1.**

Kathmandu valley is the capital city of Nepal and hence has been a center of ever growing economic activities from a very long time. Kathmandu valley is an urban agglomerate with a core urban center surrounded by extended urban economic zones. The lack of decentralization of developmental activities has propagated Kathmandu valley to be one of the most desired city to live in the country consequently, increasing the internal migration rates. The population density of Kathmandu valley is 2793 people per square kilometer as the 2011 census (CBS, 2012). The increasing population and failure in implementing strict regulation has resulted in haphazard development of the valley both in terms of infrastructure and economy.

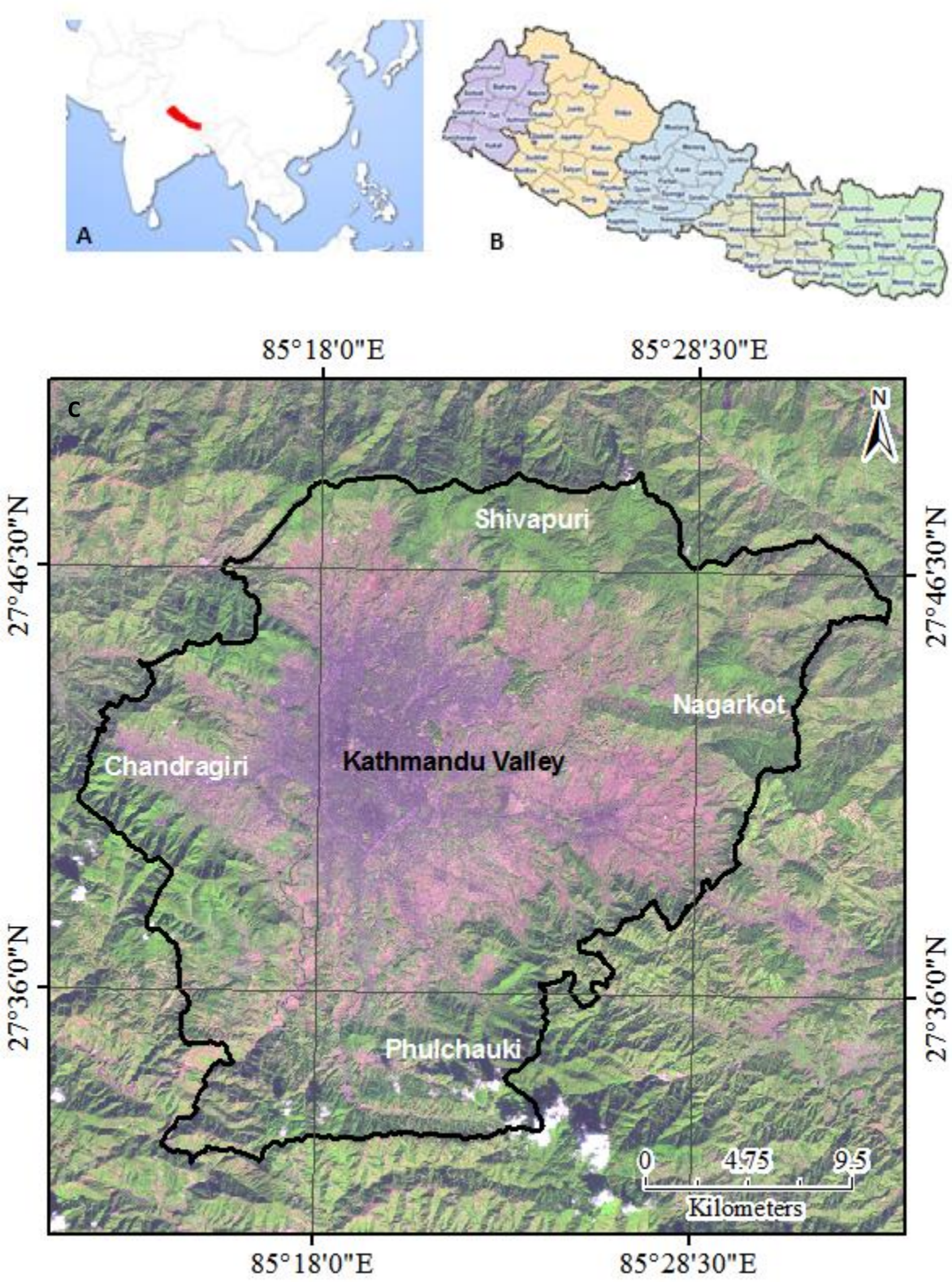

Figure 1.1 Study Area: (A) Location of Nepal in the world. (B) Map of Nepal showing Kathmandu Valley. (C) Landsat Image (R: G: B = Band 2:3:4) observed on 10th November 2016 along with the administrative boundary of Kathmandu Valley and surrounding mountain ranges.

This bowl-shaped valley is filled by more than 650 m thick quaternary lacustrine and fluvial deposits at the central part of the valley (Baneshwor) and gradually reduces towards the marginal boundaries (Moribayashi et al., 1980) which makes it prone to land subsidence (Pandey, 2016). Land subsidence potential can be determined by a primary factor and an immediate factor. In case of Kathmandu valley, the primary factor is the geology and the immediate factor is the haphazard groundwater extraction activity.

Geology of Kathmandu Valley:

Kathmandu valley is surrounded by Shivapuri mountain range (2732 m) in the North, Phulchauki mountain range (2762 m) in the south, Nagarkot mountain range (1895 m) in the east and Chandragiri mountain range (2356 m) in the west (Piya, 2004). The average elevation of the valley is approximately 1,400 meters above sea level. The main composition of geology of Kathmandu valley is the quaternary lacustrine sediments over basement rocks (Nautiyal et al., 1961). The basement rock is formed by Precambrian to Devonian rocks which mainly consist of Limestone, Dolomite, Slate, Metasandstone, Phyllite, Marble, Schist, Quartzite and Garnet-schist (Moribayashi et al., 1980). The quaternary sediments consist of thick (more than 650m deep) semi-consolidated fluvio-lacustrine sediments of Pliocene to Pleistocene age. It is composed of fine to coarse-grained sand, gravel, clay, silt, peat, lignite and diatomite (Stocklin and Bhattarai, 1977). Through various geological, boring and gravity survey it has been known that Kathmandu valley has a three-layer of this quaternary underground deposits. The bottom layer consists of the river sediment, the center layer consists of the sediments of mud lake formation and the top most layer consists of sediments of upper lake formation delta and rivers. The central lake sediment deposit layer reaches a thickness of about 200m in the central part of the Kathmandu basin and is laterally thinned and sharpened at the edge of the basin and sediments of deltas and rivers. The main composition of this layer is the black organic silt, sand and clay (locally named as Kalimati). This central layer is unique as it consists of fossils of plants from the former paleo lake along with clay layer formed as a result of weathering of granitic rocks (Sakai, 2015).

The geological map of Kathmandu valley and a geological cross-section of Kathmandu Basin showing north-south sediment distribution through the center of Kathmandu valley is shown in **Figure 1.2** and **Figure 1.3** respectively.

A boring survey conducted by (Sakai et al., 2001) during 2000 to 2003 under the Clock Tower (Ghantaghar) located inside the Tribhuvan University, Tri-Chandra Campus, discovered that the uppermost unconsolidated layer was 10-15 m deep and composed of coarse granite granules with high moisture content. This layer was followed by a weak high in moisture Kalimati layer spread to nearly 40-45 m deep whose main composition was methane gas. The constituents were in a more solidified state at depth more than 100m. The existence of the fragile Kalimati layer throughout Kathmandu is one of the main factor that intensifies the earthquake waves and other movements further causing structures to collapse (Sakai, 2015).

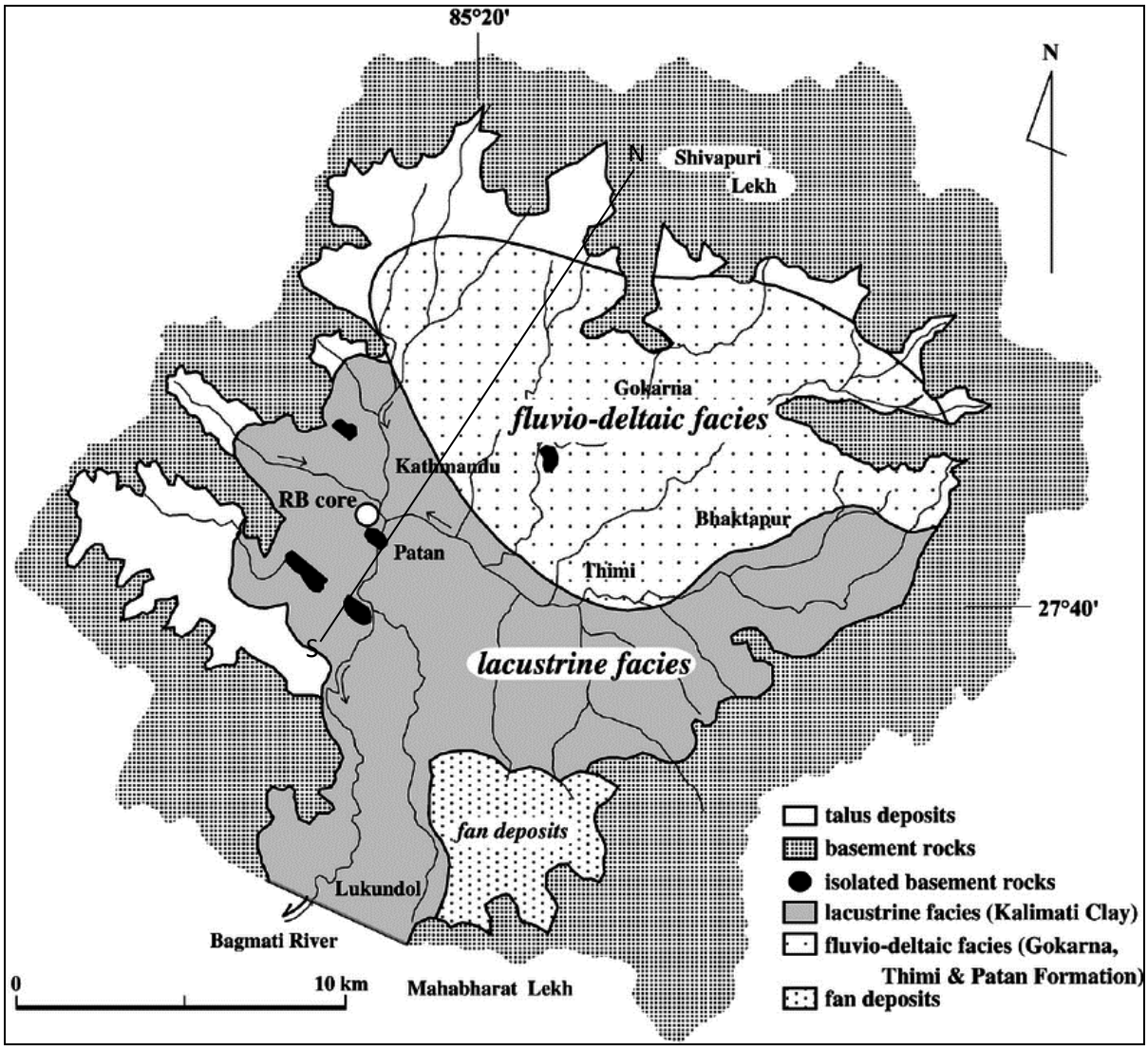

Figure 1.2. Geological map of Kathmandu Valley (Source: Kuwahara et al., 2010)

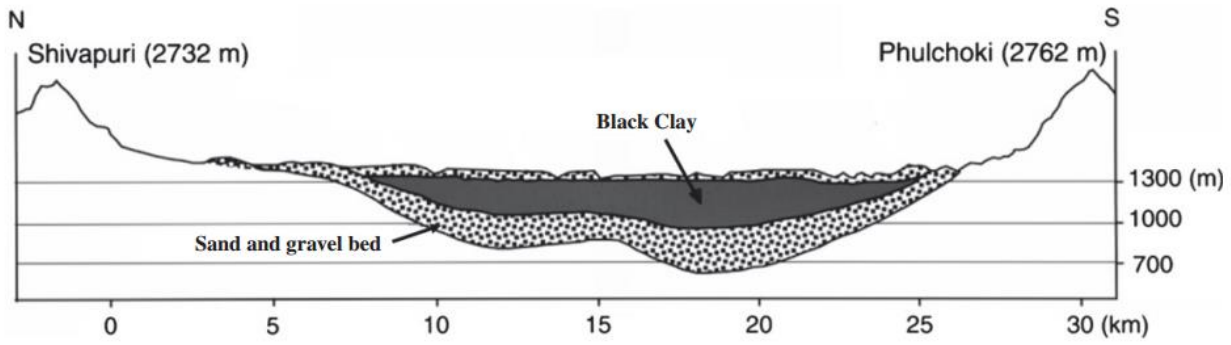

Figure 1.3. A geological cross-section of Kathmandu Basin, showing north-south sediment distribution through the center of Kathmandu Valley. (Source: Katel et al., 1996; Sakai et al., 2002)

The thickness and variation of the lacustrine sediments plays a vital role in land subsidence occurrence. The contour map of the basement topography of Kathmandu basin generated by Paudyal et al., (2013) is shown in **Figure 1.4.** The thickness and variations of the sediments is discussed based on the result obtained from this contour map. The intermix of unconsolidated sediment and basement layer is deep in the center of the Kathmandu Valley Basin and is shallow towards the outskirts of the valley. Some points (A with sediment thickness 48m and B with sediment thickness 30 m) in Figure 3.4 show swift change in the sediment thickness which indicates that the basement rock is present near the surface in those areas.

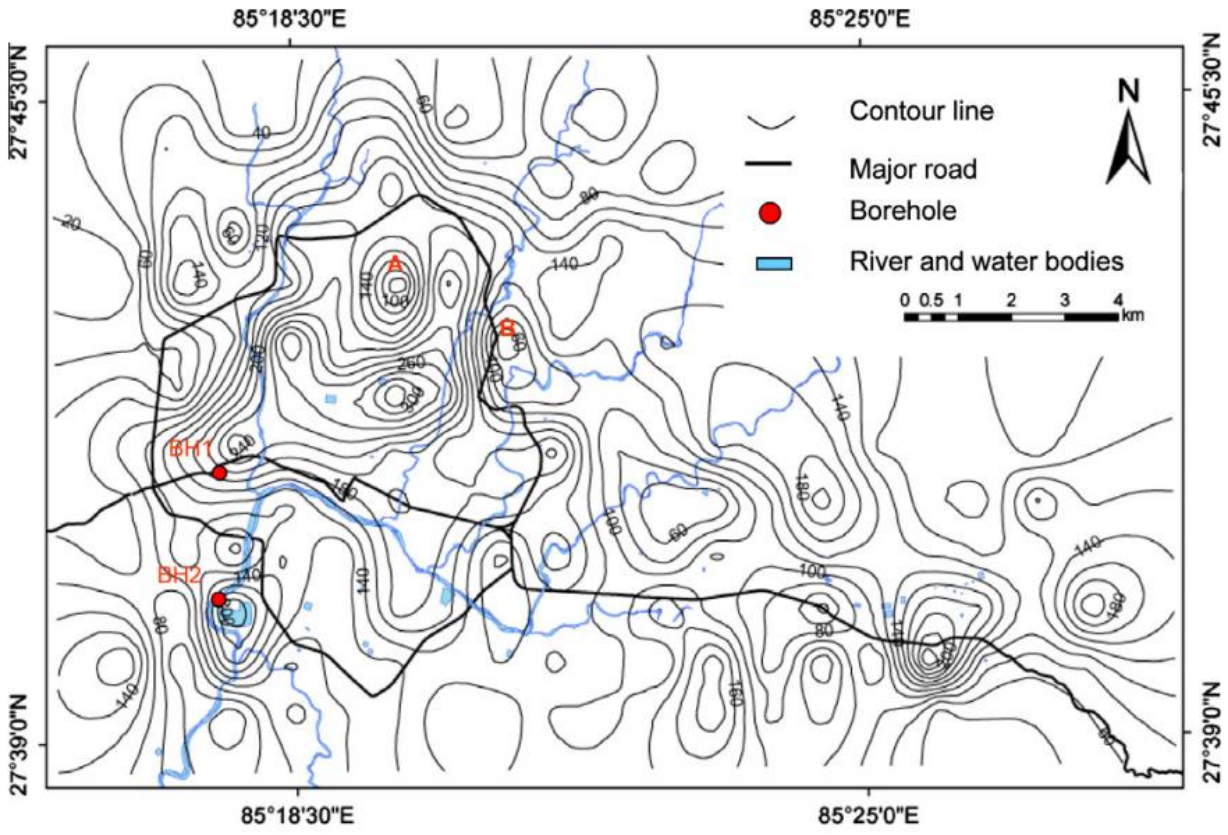

Figure 1.4. Contour map of the basement topography of Kathmandu basin with major roads network indicated by dark black lines and river network indicated by blue lines. (Source: Paudyal et al., 2013)

Hydrogeology of Kathmandu Valley:

Kathmandu valley is situated near to the source of Bagmati River Basin (BRB) which has a superficial outlet towards the southwest. The valley generally consists of three hydrogeological layers namely, shallow aquifer, aquitard and deep aquifer. According to Pandey and Kazama, (2011), the shallow aquifer is thicker towards the north of the valleys groundwater basin with estimated thickness within the range 0 to 85m whereas the deep aquifer is thicker towards the central and south part with an estimated thickness of 25m to 285m. The aquitard layer with clay as the main constituent separates the two aquifers and its thickness is estimated to be in the range of 5m to 200m. The main natural recharge area is towards the northern part and a small area contributing to recharge is located towards the southern part (Pandey et al., 2012). The main source

of aquifer recharge is through direct infiltration of monsoonal rainwater and surface water infiltration (Shrestha et al., 1996; Gautam et al., 2014).

Kathmandu valley has a closed and isolated groundwater system and consists of some interconnected aquifers. The presence of sand and gravel beds has created a deep confined aquifer that serves as a significant source of water supply to the central urban area of Kathmandu valley.

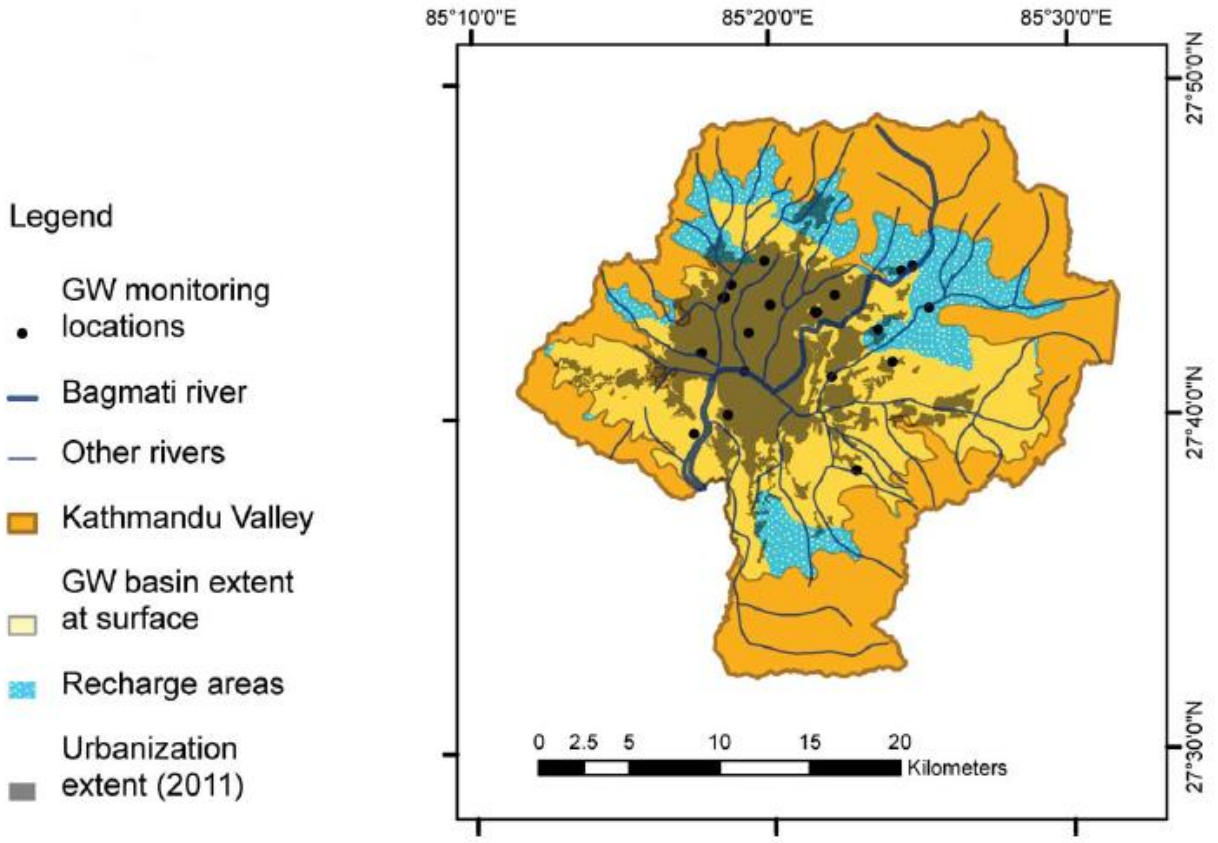

Figure 1.5. Kathmandu valley map showing river networks, groundwater basin extent, recharge areas and urbanization extent. (Source: Shrestha et al., 2017)

1.5 Structure of the thesis

The basic organization of this dissertation is as follows:

Chapter 1 INTRODUCTION includes the background, objectives and the scope of this research. It also includes the detail description of the study area.

Chapter 2 LITERATURE REVIEW comprises of the history and mechanism of land subsidence. An overview of land subsidence in Kathmandu valley along with a brief description of the 2015 Gorkha Earthquake is also included in this chapter. Also, microwave remote sensing, radar interferometry and ALOS PALSAR and ALOS 2 PALSAR 2 along with the concept of risk assessment are introduced here.

Chapter 3 METHODOLOGY explains in detail the methods used for land subsidence mapping, volume estimation and risk assessment. The data used in this research are also included in this chapter.

Chapter 4 RESULT AND DISCUSSION presents the results obtained from this research along with discussion.

Chapter 5 CONCLUSION AND RECOMMENDATION provides the overall conclusion and summary of this study. The recommendations for future study is also provided in this chapter.

2. LITRETURE REVIEW

2.1 Land Subsidence

Land subsidence is a visible evidence of superficial or deep underground deformation triggered by various subsurface processes (Tomás et al., 2014(b)). The first ever case of land subsidence was discovered in the lowlands of Tokyo as a result of repeated precise levelling carried out in 1924, to study the post-seismic crustal disturbance due to the Kwanto Earthquake of 1923 (Inaba et al., 1969). Since then this problem has been documented throughout the globe. About 150 major cities throughout the globe is suffering from a significant amount of land subsidence (Heath and Spriull, 2003). In the United States alone, more than 17000 square miles have been affected by land subsidence out of which approximately 80% of the identified subsidence occurred due to groundwater exploitation (Perlman, 2016). Highly urbanized and industrialized areas of Europe have also been suffering from groundwater abstraction related subsidence for centuries (USGS, 2017).

Along with the discovery of land subsidence occurrence, the method to detect it has also been developing. During the 1920's precise leveling methods were used (Inaba, 1969). All through 1960's to 1980's extensometers and spirit leveling were used and developed (USGS, 2017). The implication of ground based measurement using GPS and InSAR technologies were introduced from 1990's (Galloway, 1998). Since, then this method has been used and developed to detect land subsidence around the world.

The relationship between subsidence and exploitation of groundwater was recognized in 1928 by Meinzer, a pioneer researcher at United States Geological Survey after he discovered that aquifers were compressible (Meinzer, 1928).

2.1.1 Mechanism of land subsidence

In general terms of physics, land subsidence can be defined as the loss in surface elevation that is caused by the removal of subsurface support (USGS, 2017). Land subsidence is a very complex phenomenon with diverse cause and effects. Its occurrence is mainly a combination of a primary factor and an immediate factor; Primary factor being the existence of unconsolidated sediments deposits that consists the aquifer system and immediate factor being the diminishing groundwater level (Holzer, 1984; Budhu, 2010; Galloway, 2011).

An area is potentially prone to land subsidence if a thick sediment deposit prone to consolidation exists in the subsoil, along with water which is susceptible to be pumped. Lowering of water table due to groundwater harvesting is the triggering factor of subsidence (Martinez, 2015). Nonetheless, even if the water table is reduced land subsidence will not occur if the aquifer system lacks the presence of unconsolidated sediments.

The mechanism of land subsidence phenomenon due to aquifer compaction is shown in **Figure 2.1.** The major factor in occurrence of land subsidence due to ground water extraction is the presence of unconsolidated fine-grained sediments mainly clay and silt in an aquifer system. These fine-grained sediments are naturally deposited in a haphazard manner creating lots of space for water storage. When groundwater level reduces, these haphazardly deposited sediments get rearranged into a compacted stack like formation decreasing the water storage space; hence resulting in land subsidence occurrence.

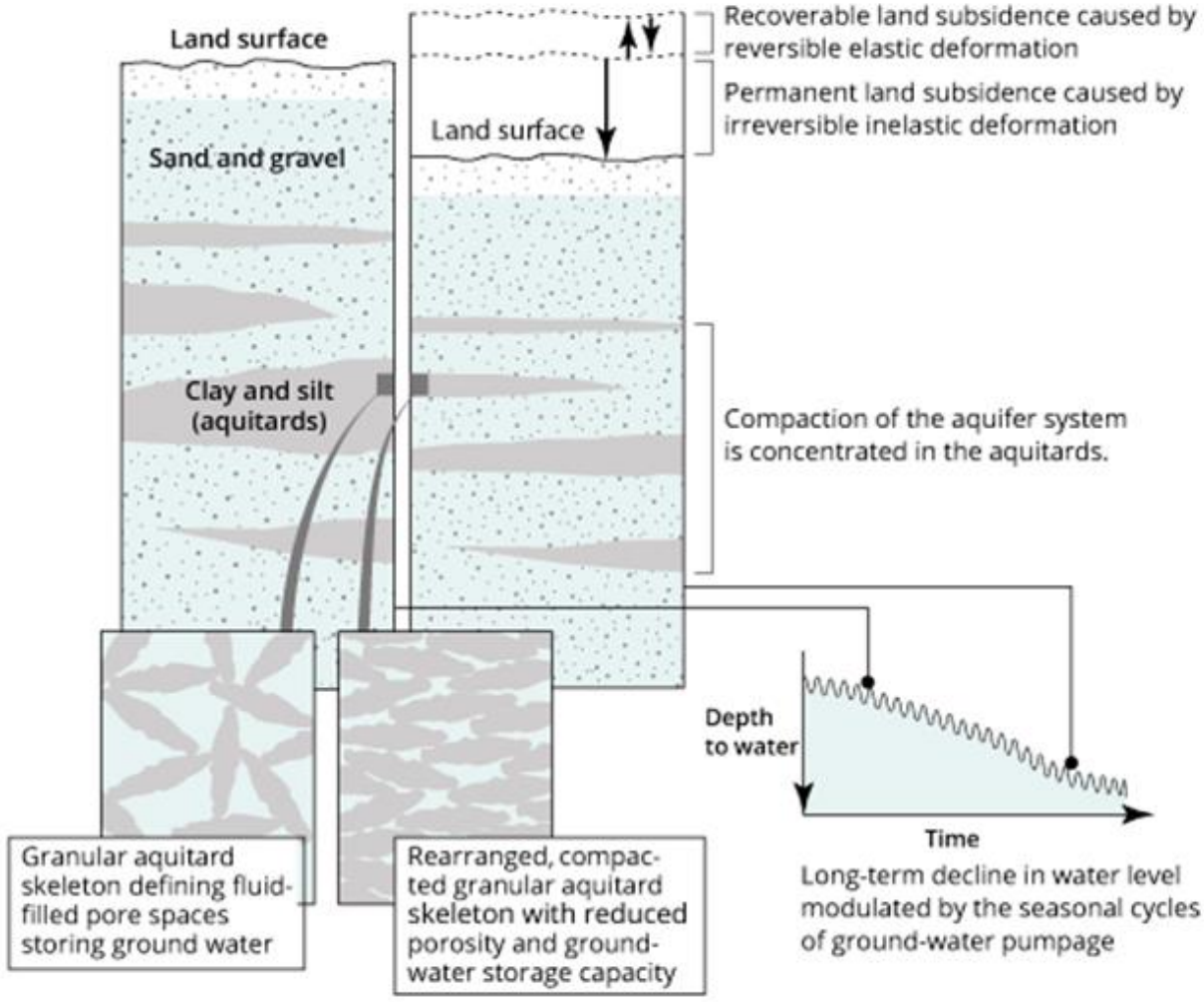

Figure 2.1 Mechanism of land subsidence due to aquifer compaction. (Source: USGS, 2017)

2.1.2 Land Subsidence in Kathmandu valley, Nepal

Historically, Kathmandu valley was a former paleo lake just like Mexico City. The lake was formed due to tectonic activities that uplifted edges of the valley. The lake receded as the water dissolved soft limestone rocks at Chobar and started flowing out. As flat fertile land started emerging along with the main Bagmati River and its tributaries, settlements started to grow. Currently, Kathmandu valley is the most densely populated region of the country. The history of origin of Kathmandu valley clearly states that the landform is unsettled lacustrine deposits which make it prone to land subsidence.

As mentioned earlier, the triggering factor for land subsidence is lowering of the water table. The history of groundwater development as described by Pandey et al., 2012 is discussed here. Groundwater extractions in the valley started in the early seventies, when the availability was high and supply was low (Pandey et al., 2012). As the water demand started exceeding the supply, private and governmental institutions started to pump groundwater through private wells. Visible impacts on water levels were observed during the mid-eighties, when the Nepal Water Supply Corporation (NWSC) started including groundwater into its supply system (Metcalf, 2000). During the nineties, the number of private wells increased so rapidly that the extraction exceeded the water recharge levels. With ever increasing population, development activities and lack of groundwater resources policy, the water demand is bound to increase exerting more pressure to the groundwater table. This in turn will result in aquifer compaction in areas consisting highly compressible clay and silt layers raising the risk of land subsidence (Pradhanang et al., 2012)

Land subsidence had been reported in the past in Hyumat tole area (27°41'57" N and 85°18'12" E), Shantibasti area (27°40'42" N and 85°18'03" E), and Imadol area (27°39'36" N and 85°21'00" E) without detailed scientific study and evidence (Rana et al., 2007). Although, many scientists and researchers have suggested to initiate study and monitoring of land subsidence (Rana et al., 2007; Pandey et al., 2012; Pradhanang et al., 2012; Gautam et al., 2014; KV-RSLUP report, 2015; Shrestha et. al., 2017) no published research has been done to the authors' knowledge to determine if land subsidence is taking place in actual due to ground water extraction; therefore, no evidence of land subsidence in Kathmandu valley is available (Pandey et al., 2012).

Also, a drilling project conducted in 2000, revealed that the underground geology of Kathmandu valley is so weak that while constructing tall buildings the foundations must be secured up to a deep level (Sakai, 2015).

Recently, Shrestha et al., 2017 published a scientific paper entitled "Model-based estimation of land subsidence in Kathmandu valley, Nepal". A calibrated groundwater flow model was developed based on the coupled surface subsurface modelling system. This model was used for land subsidence simulations. The invalidated result shows subsidence vulnerability towards the northern part of the groundwater basin. The author predicts that land subsidence will occur as a result of deep aquifer compaction caused by large amounts of groundwater extraction.

2.1.3 Effect of 2015 Gorkha Earthquake in Kathmandu Valley

On April 25, 2015, a devastating earthquake of Mw 7.8 (US Geological Survey, 2015) struck the Gorkha region in central Nepal. It was followed by a strong aftershock of Mw 7.3 on 12 May 2015 and many other aftershocks greater than Mw 6 thereafter. This earthquake was a result of stress released from the under thrust movement of the Indian tectonic plate beneath the Eurasian tectonic plate (Kobayashi et al., 2015). The earthquake ruptured the Main Himalayan Thrust fault (MHT) **(Figure 2.2)** which stopped halfway at 11km under Kathmandu valley. Therefore, there are chances of future fault rupture up to the surface (Elliott et al., 2016).

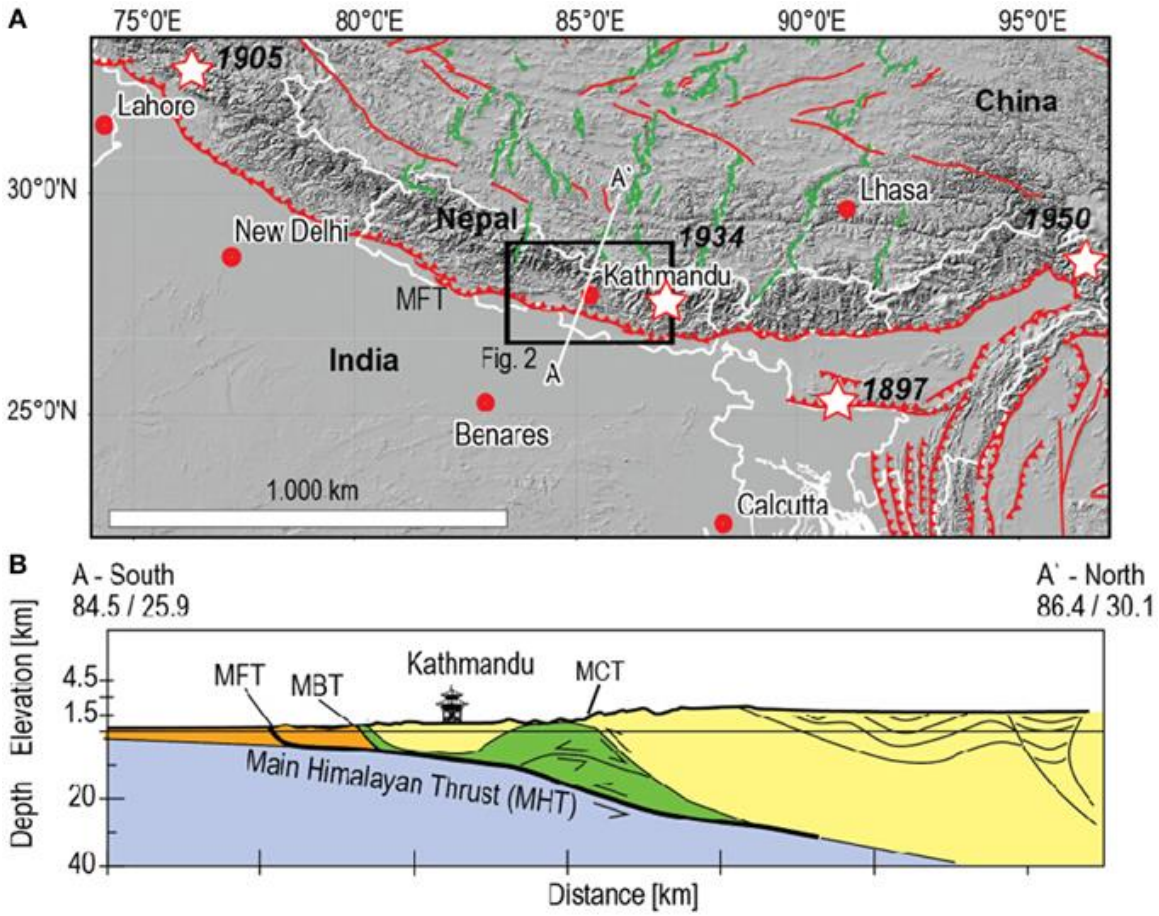

Figure 2.2 (A) Geodyanmic map of Nepal showing SRTM topography, fault lines, earthquake events since 1895 (represented by stars) and Main Frontal Thrust (MFT). (B) Cross section of the main tectonic faults. (Source: Diao et al., 2015).

An uplift of about 1.4 m and 1 m was observed approximately 20 km northeast and 30 cm westward from Kathmandu respectively along with local subsidence around the city (Kobayashi et al., 2015; Diao et al., 2015). **Figure 2.3** shows the area of land uplift and sink due to the 2015 earthquake obtained from Sentinel- 1A data analyzed by DLR German Aerospace Center. Blue color indicates the uplift of up to 0.8m near the Indian and Eurasian tectonic plates boundary whereas the yellow color indicates subsidence. A horizontal 2 m shift in the north–south direction was also detected (DLR, 2015).

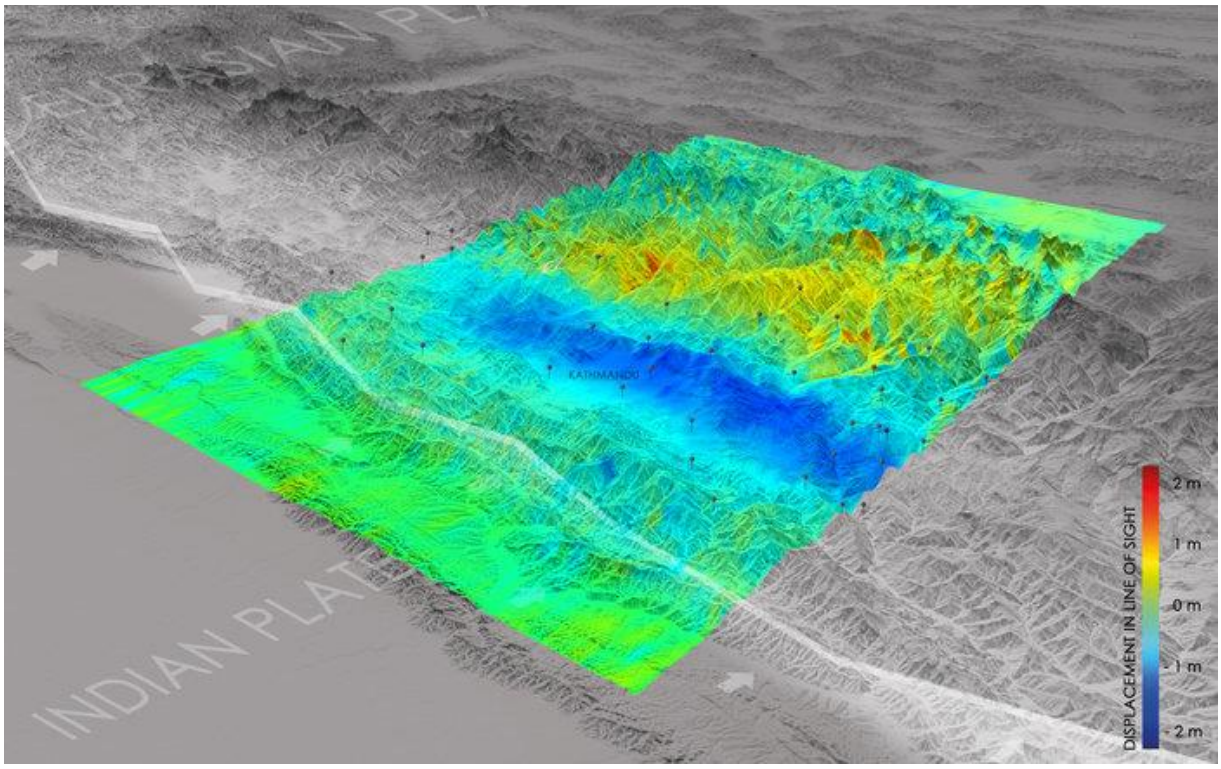

Figure 2.3 Displacement caused by Gorkha 2015 earthquake obtained from Sentinel 1A satellite data. (Source: DLR, German Aerospace Center).

2.2 Introduction to Microwave Remote Sensing

In general, remote sensing refers to the acquisition of information about an object or a phenomenon by using satellite or aircraft based sensor technologies without making any physical contact with the object.

Microwaves are electromagnetic waves that include wavelengths approximately ranging from one meter to one millimetre. The electromagnetic spectrum is shown in **Figure 2.4.** There are basically two types of microwave sensors: active and passive. An active sensor system supplies its own radiation source, which is directed at the object to measure the returned emission. On the other hand, a passive sensor system depends on other sources of energy like sunlight or thermal infrared.

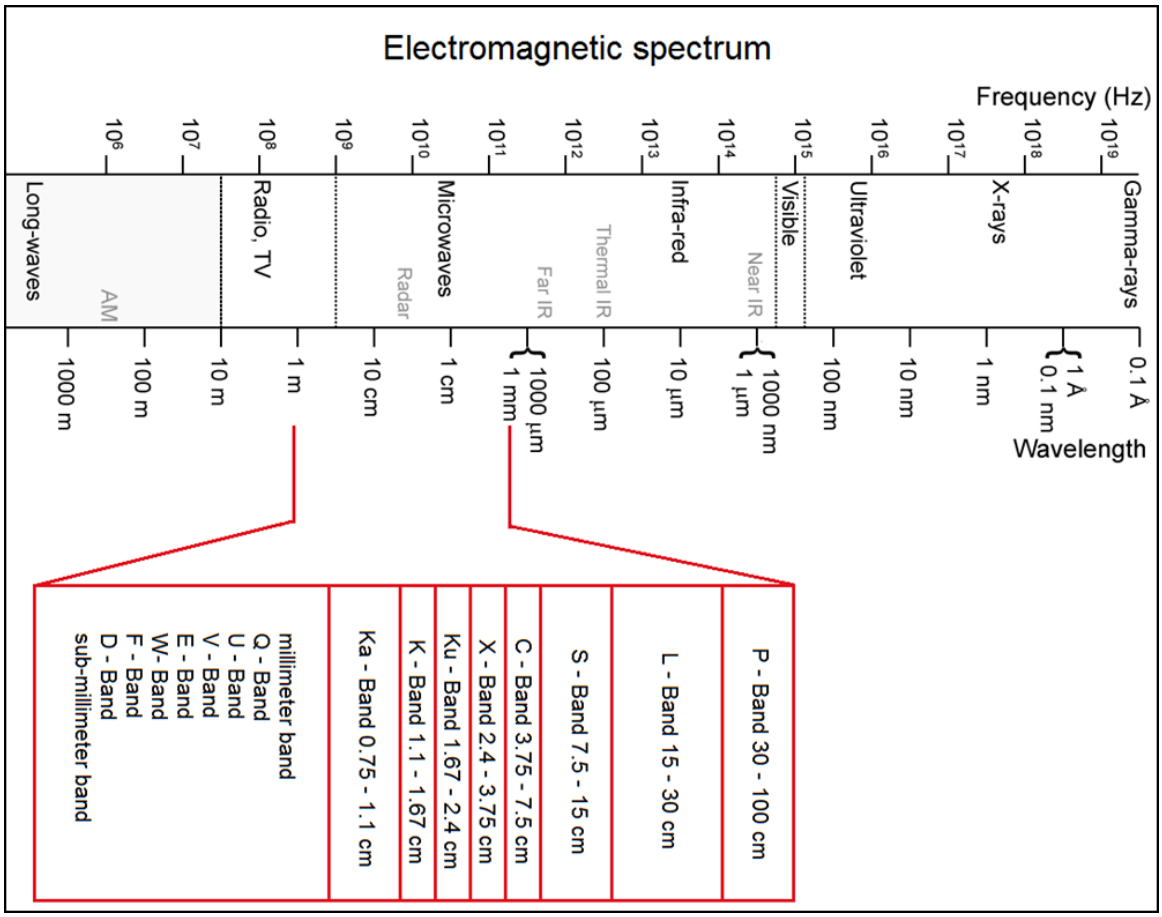

Figure 2.4 Electromagnetic Spectrum

The most prevalent form of imaging active microwave sensor is RADAR (Radio Detection and Ranging). The radar sensor transmits a microwave signal towards the object of interest and then detects the backscattered signal.

The strength of the backscattered signal depends on the roughness of the object and the degree of slope in relation to the radar. This strength is measured to distinguish between different objects and the time delay between the transmission and reflection of signals determines the distance from the sensor to the object. Radar sensor systems have many advantages. It is capable of penetrating clouds, light rain, smoke, haze and snow. It can operate in both day and night. It is also able to penetrate more deeply into vegetation than optical waves.

Radar sensor systems are divided into two categories: Real Aperture Radar (RAR) and Synthetic Aperture Radar (SAR). RAR transmits and receives microwave signals with a long antenna and are therefore incapable of producing fine resolutions. SAR transmits and receives signals with shorter antenna and is exclusive to moving platforms. Through appropriate signal processing it is possible to simulate antenna length up to hundred meters or more. When the signals transmitted from the synthetic aperture radar source reflects from the ground to the advancing platform, the object of interest appears to be in motion. Changing frequencies that gives rise to phase and amplitude variations in the returned pulses are results of this motion. All these data are recorded for later processing where the moderated signals are analysed and recombined to synthesize signals.

SAR data consists of high-resolution reflection of emission from the surface that has been illuminated by an administered beam of pulse generated by the sensor. The physical characteristics like surface roughness, orientation and geometric structure of the surface; the electrical characteristics like dielectric constant, conductivity and moisture content and the radar frequency of the sensor determines the radar reflection from the surface. European Space Agency's (ESA) European Remote Sensing Satellite (ERS-1 and 2), Japanese Earth Resources satellite (JERS-1), RADARSAT 1 and 2, Advanced Land Observing Satellite (ALOS and ALOS 2), TerraSAR-X, Sentinel-1 are some of the satellite system that provide SAR data.

2.2.1 Introduction to Radar Interferometry

Radar interferometry was first used by Graham in 1974 for topographic mapping (Graham, 1974). Zebker and Goldstein used the side looking airborne radar in 1986 and obtained the first ever practical results (Zebker and Goldstein, 1986). Research and studies expanded with the launch of European Space Agency's (ESA) ERS-1 and ERS-2 satellite in 1991 and innumerable papers have been published since then. Gens et al., (1996); Rocca et al., (2000) and Burgmann et al., (2000) have described the detailed theory and application of radar interferometry.

Radar interferometry technology utilizes the phase difference between two or more SAR data that are acquired from different orbit position at different times. Geodetic information like topographic information, surface deformation (such as volcano, subsidence, landslide, earthquake, etc), glacier flow etc. can be derived from this technique. Interferometric SAR (InSAR) is the process when the phase difference between two images are utilized to derive local topography whereas Differential InSAR (DInSAR) is the process that utilizes the phase difference to detect and quantify ground displacement that has occurred during the time between two acquired images. This process is complementary to ground-based methods such as levelling and global positioning system measurements. Through this process land deformation information can be obtained for a wide coverage area even when the area is inaccessible (Raucoules et al., 2007).

The concept of DInSAR was first explained by Gabriel et al., (1989). It has also been thoroughly reviewed in many scientific papers (Massonnet et al., 1998; Ferretti et al., 2001; Crosetto et al., 2005; Kampes 2006; Prati et al., 2010; Tomas et al 2014b). The DInSAR technique can be categorized into two groups Persistent scatterers method and small baseline method. Persistent scatterers methods are mainly focused on localized targets whereas small baseline method is used for spatially distributed targets. These DInSAR technology methods has been applied in various fields.

Tectonic and Volcanic events: DInSAR has been applied to measure tectonic deformation and ground movements caused by earthquakes (Massonnet et al., 1993; CNES/ ESA/ ESRIN study, 2000; Colesanti et al., 2003; Yen et al., 2008; Tsuji et al., 2009; Pezzo et al., 2014). Eruption

induced deformation and volcano-tectonic deformation has also been measured by application of DInSAR (Massonnet et al., 1995; Rosen et al., 1996; Lagios et al., 2005).

Landslides and glacier movements: Landslides have been measured and monitored by application of DInSAR (Guzzetti et al., 2009; Herrera et al., 2010; Jebur et al., 2013; Tomas et al., 2014a; Schlőgel et al., 2015) It has also been used for monitoring glacier movements and ice flow measurements (Goldstein et al., 1993; Berthier et al., 2007; Hu et al., 2014).

Infrastructure and building monitoring: The stability of buildings and other man-made structures like highway and railway can also be monitored using DInSAR. (Tomás et al., 2012; Yu et al., 2013;).

DEM generation: Digital elevation maps (DEMs) are also produced using this technique. In 1995, DEM was produced using the two ERS satellites with one-day separation time interval. In 2000, DInSAR technique was utilized by NASA's SRTM mission aboard the space shuttle.

Subsidence events: Land subsidence occurrences as a result of various natural and human induced processes has been successfully measured using DInSAR (Galloway et al., 1998; Nakagawa et al., 1999; Strozzi et al., 1999; Sneed et al., 2001; Raucoules et al., 2007; Tomás et al., 2014b, Wempen et al., 2017). The pros of DInSAR technique (i.e. higher data acquisition frequency and spatial coverage; lower annual cost per point measurement and per area) as compared to the conventional techniques (i.e. GPS measurements, extensometers, etc.) has made this technique an indispensable tool for land subsidence studies (Tomás et al., 2014b).

The accuracy of results obtained from DInSAR processing is generally derived by comparing it with the actual land measurement data. A general accuracy of ± 1 mm/year for average displacement rates and ± 5 mm/year for line of sight displacement have been suggested by authors (Colesanti et al., 2006; Lanari et al., 2007; Raucoules et al., 2007; Prati et al., 2010; Hooper et al., 2012). Since, land measurement data for the study area could not be obtained; this general accuracy is assumed for the generated DInSAR results in this study.

The dominant advantages of DInSAR are as follows:

- Low cost as compared to conventional methods
- High frequency monitoring of a location due to the short revisiting time for orbital sensors.

- Large spatial coverage
- Very sensitive to vertical displacements caused by subsidence due to the low incidence angle (i.e. angle between the satellite LOS and a line perpendicular to the surface)

The distortions, errors and decorrelation are explained further in this chapter. However, some of the limitations of DInSAR are as follows:

- Availability of image is governed by the satellite repeat orbit cycle.
- Less sensitive to horizontal displacements.

This research utilized the small baseline DInSAR technique to detect and quantify land subsidence therefore the methodology of this technique will be explained in detail in Chapter 3.

2.2.1.1 Radar System Geometry and Distortion

The imaging geometry of a radar system is shown in **Figure 2.5**. A radar system operates in a side looking mode imaging a swath on one of the sides of the aircraft. The swath width depends on the altitude of the aircraft and is limited by the range beam width. Larger swath width can be obtained by increasing the altitude. Since, radar system is a side-looking system, the radar images generated display abnormal features and distortions (Woodhouse, 2005). These distortions are explained as follows:

Foreshortening

This is the most dominant effect in SAR images for hilly and mountainous area. Generally, an object closer to the antenna in the ground range direction returns the signal earlier than the object that is far away from the antenna. But in case of objects with high altitude, it may be assumed to be closer to the antenna than its actual geographical location. This is called the foreshortening effect. This effect is mainly observed when the slope steepness is less than the radar incidence angle. The severity increases as the slope angle approaches the incidence angle. This effect can be indemnified by incorporating a Digital Elevation Model (DEM) of the region while geocoding.

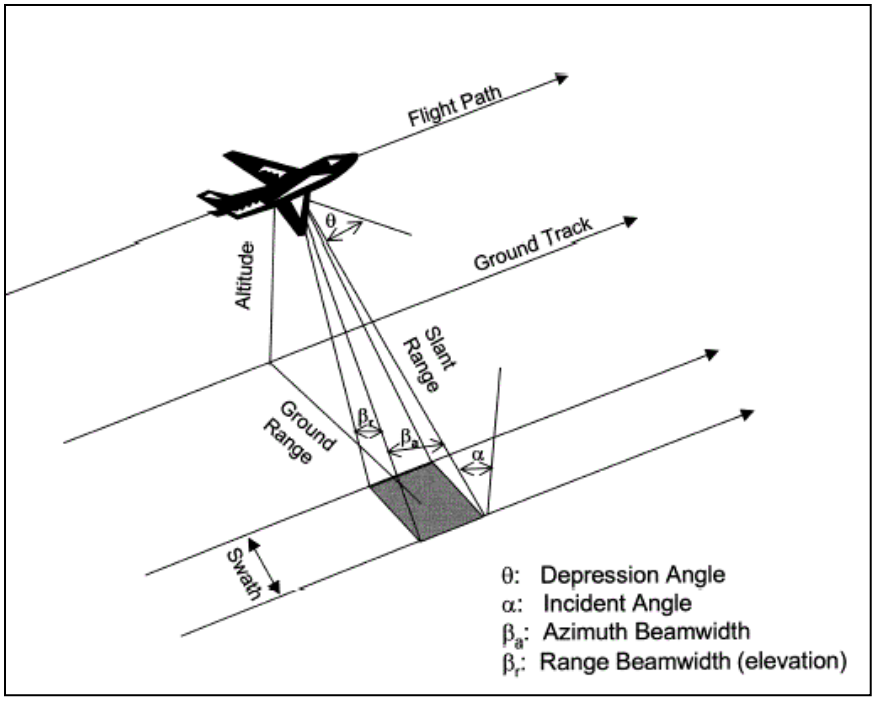

Figure 2.5. Radar System Geometry. (Source: Shuchman et al., 2005)

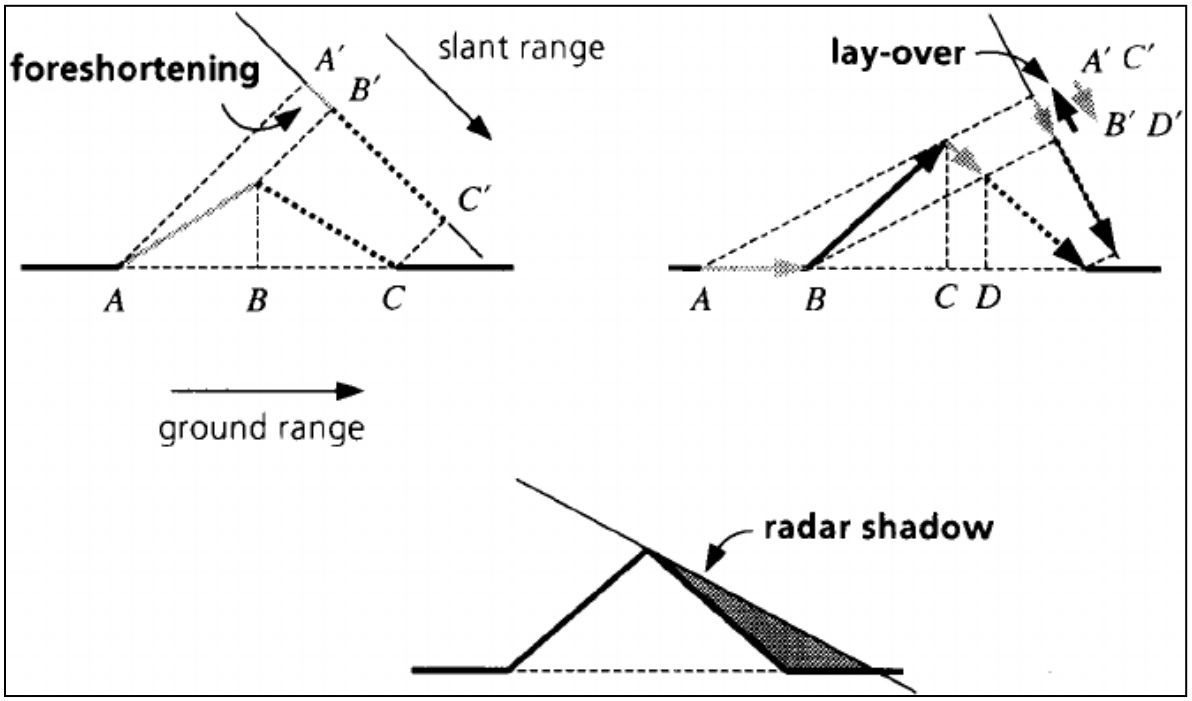

Figure 2.6. Geometric distortions of radar system. (Source: Bamler, 2000)

Layover

Layover is a severe case of foreshortening which occurs when the slope facing the antenna is steeper than the radar incidence angle. This effect leads to the inversion/ reversal of the image geometry. In simple words, the top of the slope is imaged before the base **(Figure 2.6).**

Shadow

Since, radar beam is at an angle, it will not be able to reach the regions behind a vertical structure resulting in failure to reflect. This in turn results in a black spot on the image and is known as shadow. The length of the shadow and the height of the vertical structure are proportional.

2.2.1.2 Errors and Decorrelation in Radar Interferometry

As discussed earlier, radar interferometry uses the phase information between two SAR acquisitions to derive the terrain and height information. This resultant phase information may also consist of phase information from other sources like topography, land surface/ cover type, atmospheric noise, noise from the radar instrument etc. The dominance of these components depends on the modes and characteristics of the interferometric data pair used. For instance, the atmospheric noise and phase difference due to land displacement is insignificant in single-pass radar interferometry whereas it can be significant in repeat-pass radar interferometry.

In DInSAR processing, atmospheric effect, orbit effect and topographic residuals also act as sources of errors. Such phase noises and errors degrade the accuracy of radar interferometry and therefore, the quality of the interferometry is dependent on proper or improper elimination of phase noise and other undesired phase generating components. The decorrelation and errors are explained as follows:

Decorrelation

Correlation is the measure used to detect the similarity among the dielectric properties of the imaged pixel of two SAR data. The better the correlation the lesser the phase noise present which means decorrelation gives rise to low coherence that leads to more phase noise. Decorrelation occurrence depends on the characteristics of the site selected for study like the complexity of the terrain, land cover/land use, climatic condition etc. Decorrelation is the most acute in sites with

complex terrain, high vegetation cover and continuously changing climatic condition. Decorrelation can be categorized into three categories which are described as follows:

Spatial Decorrelation: This type of decorrelation is caused by the physical separation (baseline) between the location of two SAR antennas. To reduce this error, image pair within baseline band 100 m to 500 m can be considered (Hanssen, 2002).

Temporal Decorrelation: This decorrelation is caused by the dissimilarity of the dielectric properties of objects present on ground over time between two repeat-pass data acquired. The ground objects that contribute to this error are moving leaves and branches, water surface, vegetation cover change and growth etc. To minimize this type of decorrelation, a minimal temporal baseline should be considered.

Volume Decorrelation: This type of decorrelation is caused by the unstable phase of image pixel over time over vegetated regions. The dielectric properties and orientation of tree leaves and branches in a canopy cover, weather conditions (i.e. rain and wind) results in the variation of the backscattered radar signal. To reduce this type of decorrelation, finer SAR imaging resolution can be utilized.

Atmospheric effect

The speed with which the electromagnetic radiation travels is different in mediums with different values of refractive index. The refractive index of the atmosphere varies with variation in electron density in the ionosphere and water vapour in the troposphere Therefore, the microwave radar signal may travel at different speed at different acquisition time through the atmosphere resulting in phase variation in interferogram results even for no deformation cases. This error can be minimized by using long radar wavelength possible and using multiple observations and then averaging the derived products for surface deformation (Zebker et al., 1997).

Orbit error

Incorrect orbital information can cause an erroneous interferogram and hence can generate wrong displacement map. This type of error usually occurs during co-registration of two SAR data (Hanssen, 2002) where false orbital fringes parallel to the azimuth direction is observed. This error can be removed by using ground control points appointed on the DEM of the site in interest.

2.2.2 Introduction to ALOS PALSAR and ALOS 2 PALSAR 2

Advanced Land Observation Satellite (ALOS), one of the largest Earth observing satellite was launched by JAXA in January 2006. The main objective was Cartography, Regional Observation, Disaster Monitoring, Resources Surveying and Technology Development. Three remote-sensing instruments were onboard ALOS. Panchromatic Remote-sensing Instrument for Stereo Mapping (PRISM) for digital elevation mapping, Advanced Visible and Near Infrared Radiometer type 2 (AVNIR-2) for precise land coverage observation, and the Phased Array L-band Synthetic Aperture Radar (PALSAR) for day-and-night and all-weather land observation.

PALSAR is an active microwave sensor that uses L-band frequency to attain cloud-free and day-and-night land observation. It was developed to provides higher performance than the JERS-1's SAR. The specification of PALSAR characteristics are shown in **Table 2.1**.

Table 2.1 Characteristics of ALOS PALSAR (Source: EORC, JAXA)

Mode	**Fine**		**ScanSAR**	**Polarimetric**
Center Frequency	1270 MHz(L-band)			
Bandwidth	28MHz	14MHz	14MHz,28MHz	14MHz
Polarization	HH or VV	HH+HV or VV+VH	HH or VV	HH+HV+VH+VV
Incident angle	8 to 60deg.	8 to 60deg.	18 to 43deg.	8 to 30deg.
Range Resolution	7 to 44m	14 to 88m	100m (multi look)	24 to 89m
Swath	40 to 70km	40 to 70km	250 to 350km	20 to 65km
Bit Length	5 bits	5 bits	5 bits	3 or 5bits
Data rate	240Mbps	240Mbps	120Mbps, 240Mbps	240Mbps

ALOS 2 was launched on May 2014 as the successor of ALOS. The factors such as resolution, observation area and time lag for data provision has been improved in ALOS 2 PALSAR 2 thus ALOS 2 is wider, more precise and has high responsiveness. The specification of PALSAR 2 characteristics is shown in **Table 2.2** and **Table 2.3.**

Table 2.2 Characteristics of ALOS 2 PALSAR 2 (Source: PASCO)

Observation Mode	**Spotlight**	**ScanSAR**		
		[28MHz]	[14MHz]	[490km]
Obs. Mode ID	SBS	WWS/WWD	WBS/WBD	VBS/VBD
Length of Range Direction	25km	350.5km	350.5km	489.5km
Length of Azimuth Direction	25km	355km	355km	355km
Range Resolution	3.0m	47.5m (5look)	95.1m (5look)	44.2m (2look)
Azimuth Resolution	1.0m	77.7m (3look)	77.7m (3look)	56.7m (1.5look)
Polarization	Single（HH, HV, VH, or VV）	Single（HH, HV, VH, or VV） Dual（HH+HV or VH+VV）		

Table 2.3 Characteristics of ALOS 2 PALSAR 2 (continued) (Source: PASCO)

Observation Mode	**Stripmap**			**Full (Quad.) Polarimetry**	
	[3m]	[6m]	[10m]	[6m]	[10m]
Obs. Mode ID（code）	UBS/UBD	HBS/HSD	FBS/FBD	HBQ	FBQ
Length of Range Direction	55km（max）	55km（max）	70km（max）	40-50km	30km
Length of Azimuth Direction	70km	70km	70km	70km	70km
Range Resolution	3.0m	6.0m	9.1m	5.1m	8.7m
Azimuth Resolution	3.0m	4.3m	5.3m	4.3m	5.3m
Polarization	Single（HH, HV, VH, or VV） Dual（HH+HV or VH+VV）			Full (Quad.) Polarimetry （HH+HV+VH+VV）	

2.3 Risk Assessment of Land Subsidence

One of the application of results obtained from DInSAR is incorporating it with the geophysical, geographical and social data to develop risk maps (Palà et al., 2006; Hu et al., 2009; Tomás et al., 2014(b); Chen et al., 2014; Liu et al., 2015). Risk maps can be further utilized for risk analysis and mitigation planning.

Risk assessment in relation to disaster is defined as a process that helps to determine the nature and extent of a risk. This is done by analysing hazards and prevailing vulnerability conditions which are considered to have the potential to harm exposed people, property, economic activities, livelihoods and their environment (Monitoring and Evaluation studies, "Disaster Risk Assessment Process"). The significance of risk assessment is its contribution as an intrinsic part of the decision-making process in disaster risk management. Assessing risk empowers all the directly and indirectly affected parties to understand the current risk scenario and further aids to produce an appropriate mitigation and prevention measure/s (European Commission, 2010).

Defining the terminologies in risk assessment is very important as the definition significantly varies among different fields of study and a different conceptual understanding could change the whole meaning of the study. The terms used for risk assessment of land subsidence in this study has been defined as follows:

Hazard

Hazard, in general can be defined as a natural or an artificial phenomenon that has the potential to disrupt and damage people, property and their immediate environment. This term can be used to describe the intensity of an actual hazard event as well as the underlying condition that may increase the probability of occurrence of a hazardous event in future (UNISDR, 2009). In this study, hazard is used to describe the intensity of the actual hazard event (i.e. land subsidence). Some examples of hazards are floods, droughts, earthquake, epidemics, accidental release of toxic chemicals etc.

Vulnerability

Vulnerability, in general can be defined as a concept that describes the factors (including economic, social and physical) aiding to reduce the ability to cope with the potential hazards impacts. In other words, vulnerability can be defined as the characteristic feature and conditions of a community or a system that makes it susceptible to the damages caused by a hazard (UNISDR, 2009). Some of the characteristics and conditions that make a community vulnerable to damages caused by a hazard are concentration and crowdedness of buildings, population and resource base; proximity to the possible hazard; interdependency of lifelines in urban areas etc. (ADPC).

Capability of disaster prevention and reduction

Capability of disaster prevention and reduction can be defined as the resources, technology and potency possessed by a community or a country which empowers them to cope; prevent or reduce or recover quickly and efficiently from the effects of a hazard (ADPC). The factors that significantly affect the capability of disaster prevention and reduction are awareness, strict implementation of suitable laws and regulations, prevention and mitigation activities, preparedness etc.

Risk

Risk can be defined as the probability of occurrence of a negative consequence when a hazard interacts with a vulnerable component (ADPC). The synergy between hazard, exposure and vulnerability is risk. Hazard is the main factor that creates risks by exposing pre-existing vulnerabilities. If any of the factors among hazard, exposure and vulnerability can be reduced or eliminated then the risk can also be reduced or eliminated.

Concept of Risk Assessment

Scientific literature regarding risk assessment of various hazards are well established (Brabb, 1984; Bolotin, 1993; Westen et al., 2002; Remondo et al., 2008;). Nonetheless, very few literature relating to risk assessment of land subsidence are available (Hu et al., 2008, Hu et al., 2009; Yu et al., 2008; Chen et al., 2013, 2014; Liu et al., 2015). The basic methodology followed by all these literature is similar. First the indicators on which the risk of land subsidence depends are identified. The indicators are then normalized and weighted to determine its significance to risk by using

methods like AHP. The weighted indicators are then used for hazard and vulnerability evaluation. Finally, risk is calculated by utilizing the hazard and vulnerability evaluation.

According to the ISO 31010, (which is a standard guide for selection and application of systematic techniques for risk management and assessment) risk is the combination of negative consequence of a hazard and the likelihood of occurrence of the hazard along with the capability to prevent and reduce it. The term likelihood of occurrence is also termed as probability of occurrence when it can be quantified (European Commission, 2010). Since, the three terms are interdependent; risk is expressed as the functional relationship of these three terms.

$$\text{Risk} = f(\text{hazard} * \text{vulnerability} * \text{Capability of disaster reduction and prevention})$$

The detail methodology of risk assessment along with the equation is explained in Chapter 3.

The three factors are interrelated in such a way that application of effective prevention and preparedness measures reduces the vulnerability which in turn reduces the impact of the hazard finally leading to reduction of the risk. The number and complexity of the factors used to measure/ quantify risk can vary depending on the impacts involved.

Risk Assessment in Nepal

It has always been difficult for a developing country like Nepal, to afford costly preventive measures and implement strict land-use or other policies. However, regular risk assessment of various commonly occurring hazards like landslides, floods, glacier lake outburst floods (GLOF) is done (Kayastha et al., 2013; Shrestha et al., 2010). The subject of land subsidence is very new to Nepal, hence, no risk assessment study for land subsidence exist.

3. METHODOLOGY

3.1 Data

Three **ALOS PALSAR** fine-mode, single-polarization data acquired at different acquisition times within 2007 to 2010 with same observation parameters like path/row 510/54, off nadir angle 34.3° were selected for land subsidence mapping of Kathmandu Valley. The details of the two pairs generated from this data are shown in **Table 3.1**.

Table 3.1. ALOS PALSAR (fine mode/HH) 10m data, ascending (Source: Jspacesystems)

InSAR Pair	Process Level	Off Nadir Angle		Observation Date	Interval (days)	Perpendicular Baseline (m)	Path/Row
Pair 1	1.0	34.3	Master	2007/11/02	138	417	510/54
			Slave 1	2008/03/19			
Pair 2			Master	2007/11/02	828	257	
			Slave 2	2010/02/07			

Table 3.2. ALOS 2 PALSAR 2 (fine mode Stripmap/HH) 10m data, descending (Source: AUIG JAXA)

InSAR Pair	Process Level	Off Nadir Angle		Observation Date	Interval (days)	Perpendicular Baseline (m)	Path/ Center Frame
Pair 3	1.1	29.1	Master	2014/11/07	182	300.4	49/3060
			Slave	2015/05/08			
Pair 4			Master	2015/05/08	56	148.8	
			Slave	2015/07/03			
Pair 5			Master	2015/07/03	112	68.2	
			Slave	2015/10/23			

Similarly, four **ALOS 2 PALSAR 2** Stripmap fine-mode, single polarization data with same observation parameters like path/center frame 49/3060, off nadir angle 29.1° were selected to study the effect of 2015 Gorkha Earthquake in the study area. The details of the three pairs generated from this data are shown in **Table 3.2**.

Since, the perpendicular baseline value between 150 m to 450 m gives the best interferogram result (Ardiansyah, 2013) this factor was also considered while selecting the pair images. The ALOS PALSAR data used in this research was purchased from Japan Space Systems whereas the ALOS 2 PALSAR 2 data was obtained from ALOS User Interface Gateway (AUIG), provided by Japan Aerospace Exploration Agency (JAXA) under the Research Agreement for Advanced Land Observing Satellite-2.

Digital Elevation Model (DEM) extracted from Shuttle Radar Topography Mission (SRTM) 1 Arc second (resolution of 30m) global elevation data was also used in the DInSAR processing. This data was downloaded from Earth explorer data portal.

Groundwater exploitation intensity data used for hazard mapping of land subsidence was provided by the Kathmandu Valley Water Supply Management Board (KVWSMB), Ministry of Water Supply and Sanitation, Government of Nepal.

Population density, Gross Domestic Product (GDP) and Construction Land Proportion data was used for Vulnerability mapping. Population density data was obtained from the Kathmandu Valley Development Authority (KVDA), Government of Nepal. GDP data for the study area was obtained from National Accounts Section, Central Bureau of Statistics, Government of Nepal. Construction land proportion data was obtained from the Ministry of Land Reform and Management, Nepal.

3.2 Methodology for Land Subsidence Mapping

Synthetic Aperture Radar (SAR) is a system able to obtain high resolution complex images from wide areas of terrain, usually onboard an orbital or airborne platform, but also in ground based deployments (Yerro et al., 2014). D-InSAR is a remote sensing technique useful for detecting land displacement or deformation accurately in a wide coverage area by utilizing the phase difference between two or more SAR data taken on different acquisition times. The phase difference between an interferometry data pair can be expressed as follows:

$$Int = \phi disp + \phi atm + \phi noise + \phi topo + \phi flat \quad (1)$$

Where, $\phi disp$ refers to the phase difference from ground displacement along the slant range; ϕatm refers to the atmospheric effect; $\phi noise$ refers to the noise from the radar instrument and temporal deceleration; $\phi topo$ refers to the topographic height information and $\phi flat$ refers to the assumption of an ideally flat earth terrain (Bayuaji et. al., 2010). In the DInSAR technique, the ground displacement is estimated in a slant range direction; therefore, the following Equation 2 can be used to obtain ground displacement in a vertical direction (Curlander and McDonough, 1991).

$$\Delta z = \Delta sl \cos\theta \quad (2)$$

where, Δz is ground displacement in vertical direction, Δsl is ground displacement in slant range and θ is the incidence angle which is assumed to be 34.3° for ALOS PALSAR and 29.1 for ALOS 2 PALSAR 2 which is as same as the sensors off-nadir angle.

In this study, DInSAR technique was performed using the SARSCAPE module in ENVI software to detect land subsidence in Kathmandu Valley. The methodology flowchart of DInSAR processing is shown in **Figure 3.1**.

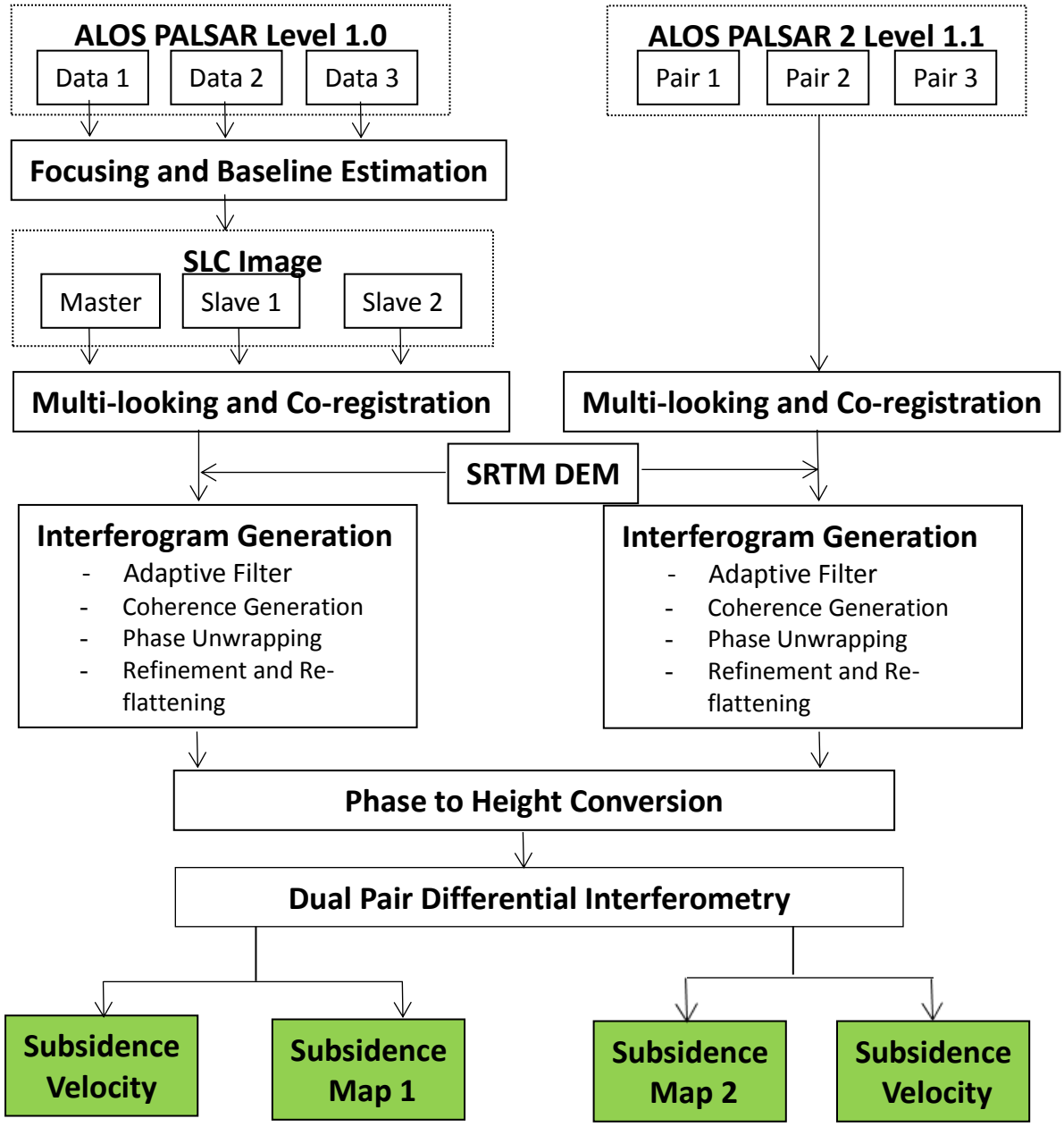

Figure 3.1 Methodology Flowchart for DInSAR processing

The detailed step wise methodology for DInSAR is explained as follows.

Focusing:

The purpose of this first step is to collect the energy dispersed along both azimuth and range direction in the raw (level 1.0 product) ALOS PALSAR data into a single pixel (i.e. Single Look Complex (SLC) image) which can be used for further processing. ALOS PALSAR 2 data provided by AUIG JAXA was already focused and the SLC image was available, therefore this step was not performed for PALSAR 2 data. The product of this step for one of ALOS PALSAR data is shown in **Figure 3.2 (A).**

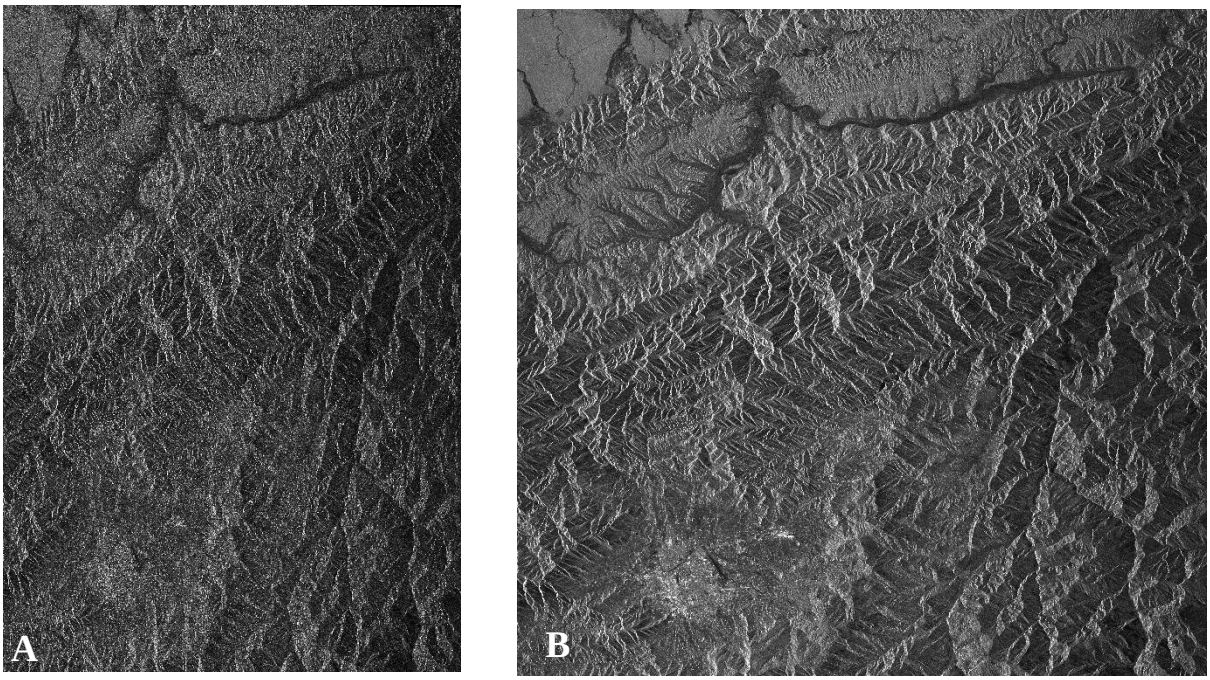

Figure 3.2 . (A) Focused ALOS PALSAR data. (B) Multilooked ALOS PALSAR data

Multilooking and Co-registration:

In this step, the SLC images are divided in different looks characterized by different frequencies in order to reduce the speckle due to constructive and destructive interferences between the different backscattered signals from the different ground targets (Exelis, 2007). The number of looks is a function of three factors, pixel spacing in azimuth, pixel spacing in slant range

and the incidence angle. The objective of this step is to produce a multilooked image that has approximately squared pixel with ground range resolution and the pixel spacing in azimuth. The produced multilooked image is of approximately the same spatial resolution of the predicted geocoded product in order to avoid under or over sampling effect. An example of a multilooked image is shown in **Figure 3.2 (B)**. In this study, the azimuth look and range look for ALOS PALSAR data was computed to be 8 and 3 respectively and in case of ALOS PALSAR 2 it was 14 and 9 respectively.

Image co-registration is the process of superimposing two or more SAR images with same orbit and acquisition mode in the slant range geometry (SAR guidebook, 2009). The basic steps involved in SAR image co-registration are evaluation and modeling of the geometric difference between master and slave image and the resampling of slave image into the master image geometry (Massonnet et al., 1998).

Interferogram Generation and Flattening:

After image co-registration where the master and slave images are precisely overlaid within an accuracy of fractions of a pixel to compute the phase difference between them, an interferometric phase is generated by multiplying master image by the complex conjugate of the slave image. The product of this processing is shown in **Figure 3.3.** The variable viewing angles of the terrain can cause range spectra shift and the different Doppler can cause azimuth spectra shift. An azimuth filter is applied during the interferogram generation to fully capture the scenes potential coherence (SAR guidebook, 2009). The constant height of the terrain results in parallel (flat earth) fringes along the range direction in the generated interferogram. A pre-existing DEM of 30m resolution from SRTM was applied to simulate the topographic phase to obtain a flattened interferogram. An example of flattened interferogram is shown in **Figure 3.4.**

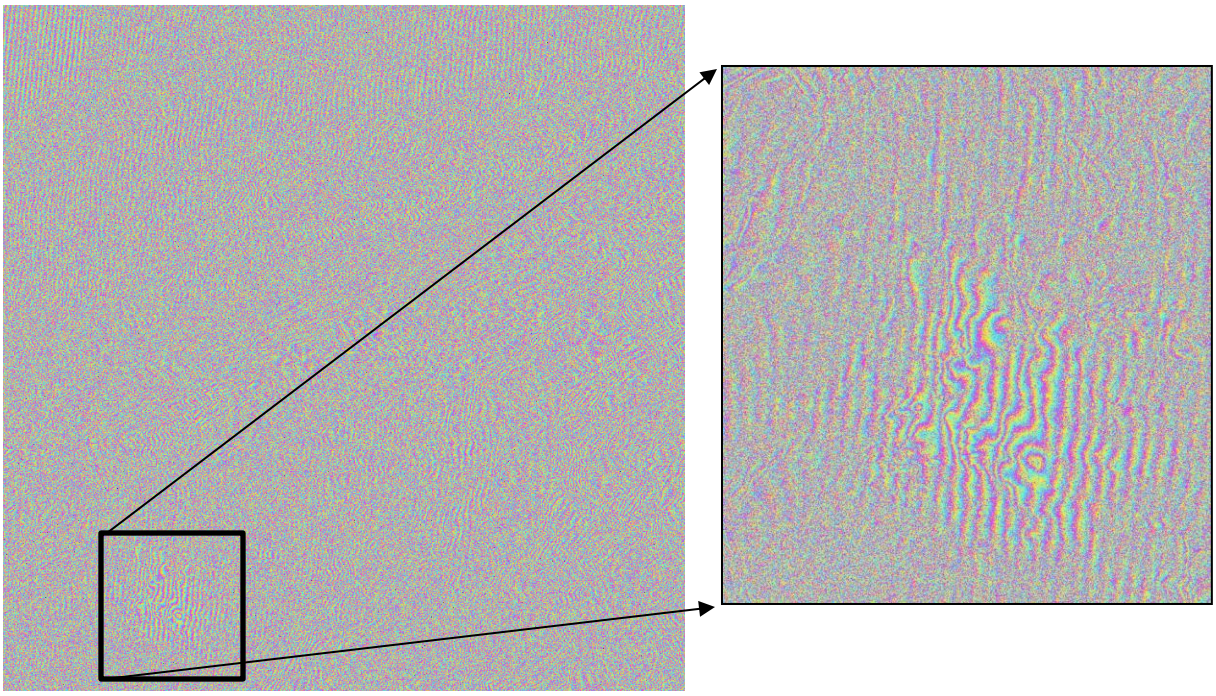

Figure 3.3. Interferogram generated from ALOS PALSAR data

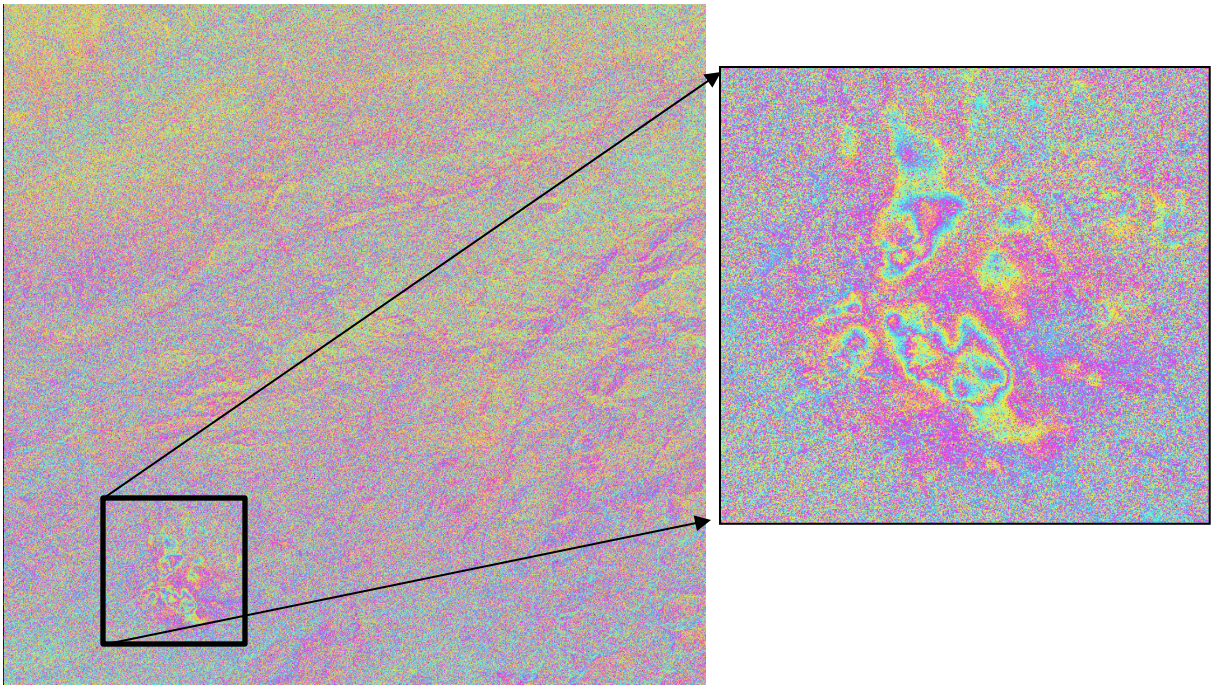

Figure 3.4. Flattened Interferogram generated from ALOS PALSAR data

Adaptive Filtering and Coherence generation:

The noise from radar instrument and the temporal deceleration was removed by applying the Goldstein-Werner filtering process to the noisy interferogram (Goldstein and Werner, 1998). An example of a filtered interferogram is shown in **Figure 3.5 (A).** Coherence is a measure of the interferogram quality. It is calculated as the ratio between coherent and incoherent summations of two co-registered SAR images. Coherence value approaching to 1 refers that the two pixels are correlated and there is no phase noise whereas a coherence value of 0 (black = 0) refers that the two pixels are decorrelated and there is phase noise and should not be considered for further processing.

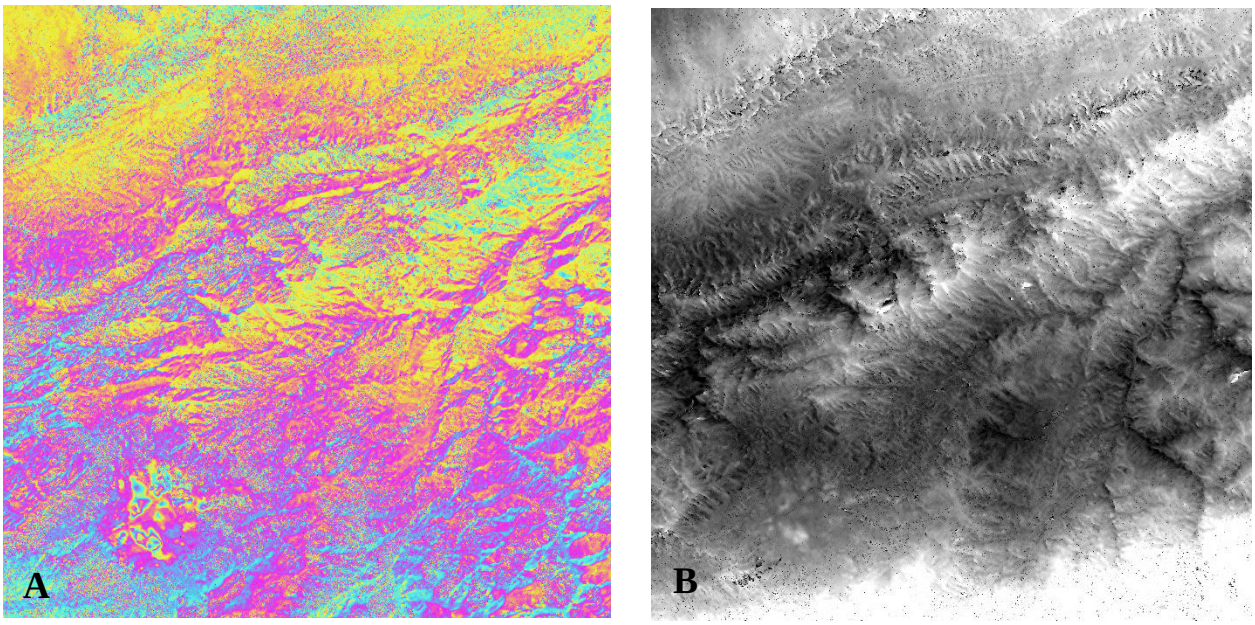

Figure 3.5. (A) Filtered Interferogram (B) Unwrapped Phase Image

Phase Unwrapping:

The flattened and filtered interferogram obtained from the earlier processing always has a phase value within the range of 0 and 2π which means that every time the phase change exceeds 2π, the phase value starts with 0 again and the cycle repeats itself. This is called 2π ambiguity and phase unwrapping resolves this problem. An example of unwrapped phase image is shown in **Figure 3.5 (B).** The pictorial representation of the phase unwrapping process in shown in **Figure**

3.6. The height and the amount of deformation of a terrain can be computed after the absolute phase of each pixel of the interferogram is known.

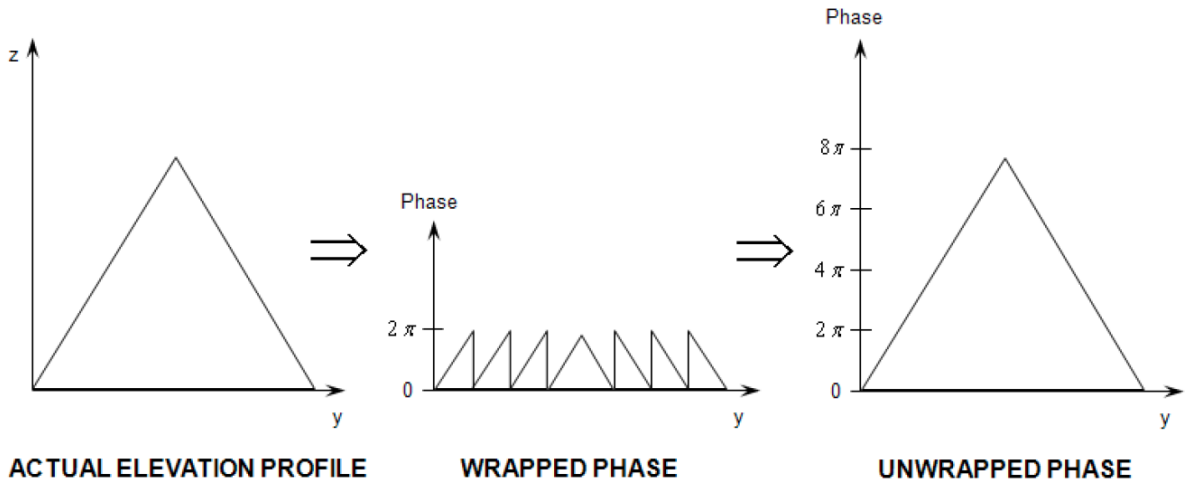

Figure 3.6. Phase unwrapping process (Source: Bayuaji, 2010)

Refinement and Reflattening:

Orbital correction has a great significance for an accurate transformation of the phase information to height information. Therefore, Ground Control Points appointed on 30m SRTM DEM were used to calculate the absolute phase and refine the orbits. An example of a product of this process is shown in **Figure 3.7 (A)**.

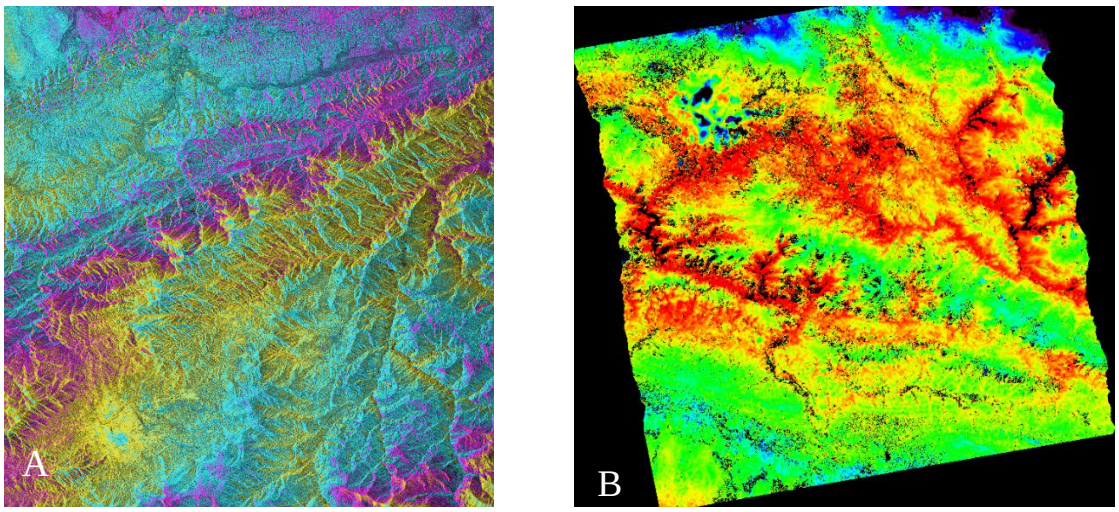

Figure 3.7. (A) Refined Interferogram (B) Geocoded Phase to Displacement Image

Phase to Displacement Conversion and Geocoding:

The obtained phase information was converted into displacement using equation (1) and (2) and was finally projected into a standard geographic coordinate system, thus generating a displacement map. The phase to displacement conversion process is similar to the geocoding process, the basic difference being that the process is applied to the two antennae which makes it possible to obtain the height of each pixel along with the location in a cartographic and geodetic reference system. An example of a product from this step is shown in **Figure 3.7 (B).**

Dual Pair Differential Interferometry:

This process extends the phase to displacement conversion case and was further performed in case of ALOS PALSAR data. Displacement, displacement velocity and height map were derived from this process. The process is expressed in a flowchart below.

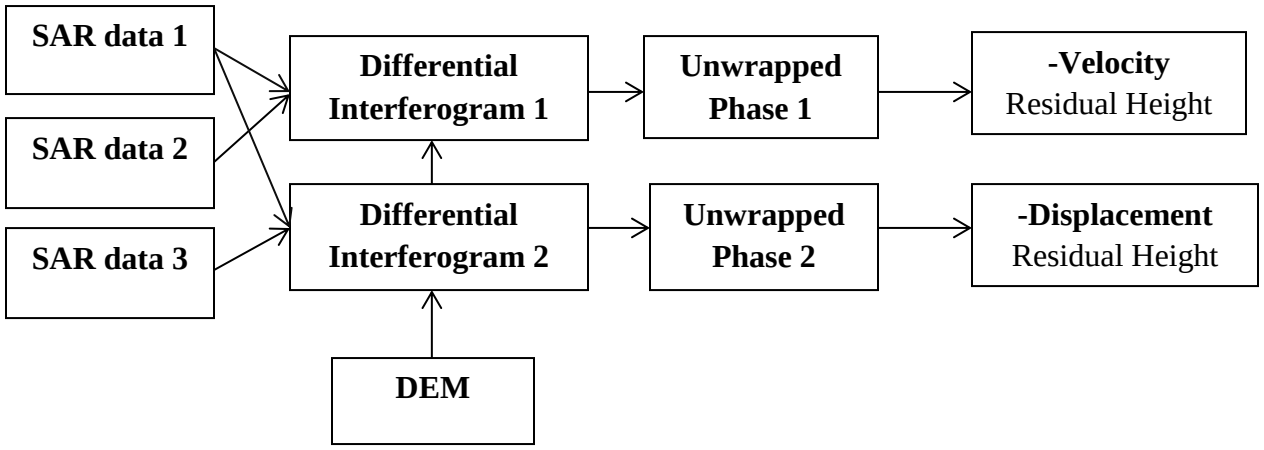

Figure 3.8 Dual Pair Differential Interferometry Flowchart. (SAR guidebook, 2009)

3.2.1 Methodology for Volume Estimation

Through various literature review it was found that in most of the cases the shape of subsidence is very similar to a cone shape. Also, in this study the generated subsidence shape somewhat resembled to a cone shape. Therefore, the subsidence volume of each subsidence zone can be estimated by an assumption that the border extremities of a subsidence zone is linearly moving at

a constant rate. A simple cone model designed by (Bayuaji, 2010) is used to estimate the land subsidence volume **Figure 3.9.**

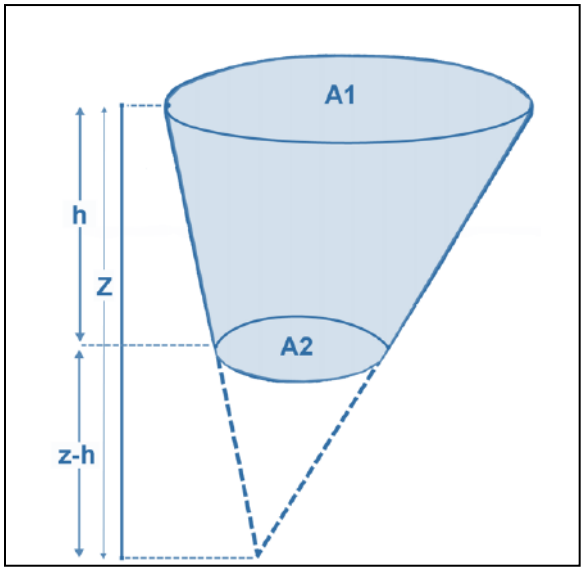

Where,

A1 = Upper Base Area
A2 = Lower Base Area
h = Subsidence depth

Figure 3.9 Cone model for volume estimation of land subsidence

Subsidence volume represented by the shaded portion in **Figure 3.9** can be estimated by applying the formula of a volume of a cone which is shown in Equation 3 (Gibilisco, 2006).

$$V = \frac{1}{3}\left[A1 + \sqrt{A1A2} + A2 \right]h \quad (3)$$

Where, V is the subsidence volume to be estimated, A1 is the upper base area, A2 is the lower base area and h is the height or the perpendicular distance between the surface A1 and A2. Area A1 and A2 will be calculated in ArcGIS (Version 10.4.1) by converting each subsidence zone into a shapefile. The subsidence depth (h) will be obtained from the DInSAR processing result.

3.3 Methodology for Risk Assessment

The main objective for assessing risk of land subsidence is to link the subsidence phenomenon with the damage it causes to the physical as well as social environment. The main factors that help to determine risk are hazard and vulnerability. Therefore, a hazard map and vulnerability map were generated and then combined to obtain the final risk map. The detailed methodology is explained as follows.

3.3.1 Disaster Risk Index Method

Risk assessment is an approach for evaluating risk, where risk is defined by the probability and frequency of occurrence of a negative consequence due to subsidence, exposure of people and property to the subsidence and consequence of that exposure (Hu, et al., 2009). The degree of risk of land subsidence significantly depends on two factors; hazard and vulnerability (Liu et al., 2015). According to the disaster risk index method, quantitative risk can be estimated by using Equation 4 (Lirer et al., 1998).

$$DR = f(H, V, C) \quad (4)$$

where, DR is the disaster risk, H is the hazard, V is the vulnerability and C is the capability of disaster prevention and reduction.

The hazard of land subsidence is defined as the intensity and the probability that land subsidence will occur in a certain area in a certain period. As defined by the Asian Disaster Preparedness Center (ADPC), land subsidence hazard evaluation simply is the process of determining the degree of severity and the extent of the impact area. In this research, accumulative subsidence volume, land subsidence velocity and groundwater exploitation intensity was used as the indicators to evaluate hazard in the study area (Wang, 2006). The former two indicators were obtained from the DInSAR processing results of this study and the groundwater exploitation intensity data was obtained from the Kathmandu Valley Water Supply Management Board (KVWSMB), Ministry of Water Supply and Sanitation, Government of Nepal.

The vulnerability of land subsidence is defined as the measure of susceptibility to physical harm or damage caused due to land subsidence. Vulnerability includes the ability of the human society and the economic development level of the society to cope with the disaster caused by land subsidence. As per the ADPC definition, land subsidence vulnerability evaluation is the process of assessing the sensitivity of the economy, population and physical infrastructure to the land subsidence phenomenon. In this research, population density, gross domestic product (GDP) and construction land proportion data was used as the indicators to evaluate vulnerability of the study area (Zhou et al., 2000). Population density refers to the number of people per unit area and this data for the study area was obtained from the Kathmandu Valley Development Authority (KVDA), Government of Nepal. GDP is one of the primary indicators used to evaluate the economic condition of a country and this data for the study area was obtained from National Accounts Section, Central Bureau of Statistics, Government of Nepal. Construction land proportion data gives the information of the proportion of built-up space and open space. This data was obtained from the Ministry of Land Reform and Management, Nepal.

The capability of disaster prevention and reduction refers to ability of the country to prevent or reduce the effect of potential land subsidence on life, property and economy. However, the land subsidence monitoring of the study area being very poor it was assumed that the country has no ability to control land subsidence at present.

3.3.2 Analytic Hierarchy Process (AHP)

Analytic hierarchy process is a multi-criteria mathematical decision making process developed by Saaty, (1977). This process uses hierarchical structures to derive relative priorities for criteria (indicators) employing pair wise comparisons. In this research, this process was used to give weights to the indicators identified for evaluating hazard and vulnerability in MSExcel. The basic procedure includes the following steps:

Pair-wise comparison: Pair-wise comparison matrix for hazard and vulnerability was developed separately to establish priorities among the indicators. The result of comparison is derived in terms

of integer ranging from 1 to 9 where the higher number indicates that the factor chosen is more important than the other compared factor.

Normalization: The integers obtained from the above step is normalized to compute the priority vector which gives the relative weights among the indicators and ultimately helps to decide which indicator is relatively more important in determining land subsidence risk. Normalization generally means to average the values in each row in order to compute the corresponding weight. First, each value in the column is divided by the total of the column which gives the normalized score. Then, the sum of each row in the normalized matrix is averaged to obtain the priority vector. The higher the priority vector the more significant the factor.

Consistency Analysis: The main objective of this step is to check if the preference ratings made in the pair-wise comparison are consistent. This is measured in terms of Consistency Ratio (CR), which can be calculated using Equation 5 (Saaty, 1980).

$$\mathrm{CR} = \frac{\mathrm{CI}}{\mathrm{RI}} \tag{5}$$

Where, CI is the consistency index and RI is the random inconsistency indices. RI is provided for each order of matrix by (Saaty, 1980). In this research, since the order of matrix was 3, the corresponding RI value 0.58 was used. The CI value can be calculated using the Equation 6.

$$\mathrm{CI} = \frac{\lambda_{max} - n}{n-1} \tag{6}$$

Where, λ_{max} is the value obtained from the summation of product of each normalized weight and sum of columns of the reciprocal matrix, n is the number of indicators used. Saaty (1980) suggested that the CR value equal to 0.1 or below shows that the comparison is consistent and hence

acceptable. (For detail description of the methodology refer "The analytical hierarchy process" Saaty, 1980).

The AHP calculation sheet for hazard and vulnerability is attached in **Appendix 1** and **Appendix 2** respectively. After obtaining the weights (priority vector) for each indicator; Hazard map and Vulnerability map was generated in ArcGIS (Version 10.4.1).

The equation used for producing Hazard map is as follows

Hazard = 0.63 * Accumulated Subsidence Volume + 0.26 * Subsidence Velocity + 0.11 * Groundwater extraction intensity (7)

The equation used for producing Vulnerability map is as follows

Vulnerability = 0.67 * Population density + 0.24 * Gross Domestic Product + 0.09 * Construction Land Proportion (8)

Where, the number multiplied to each of the indicators are their respective weights obtained from the AHP calculation. These two maps were then utilized to obtain the final Risk map. As mentioned previously, Risk can be quantified by using hazard, vulnerability and capability of disaster reduction and prevention. The capability of disaster reduction and prevention was assumed not to exist in Kathmandu Valley. Since, the hazard and vulnerability level were classified into three classes, the final risk level can be obtained by using Equation 9.

Risk = (Hazard / 3) * (Vulnerability / 3) (9)

Risk level is obtained in an integer number ranging from 1 to 3; where, 1 indicates the lowest risk level and 3 indicates the maximum risk level. Once, the risk level is obtained, a risk map will be generated in GIS software.

The methodology flowchart for risk assessment is shown in **Figure 3. 10.**

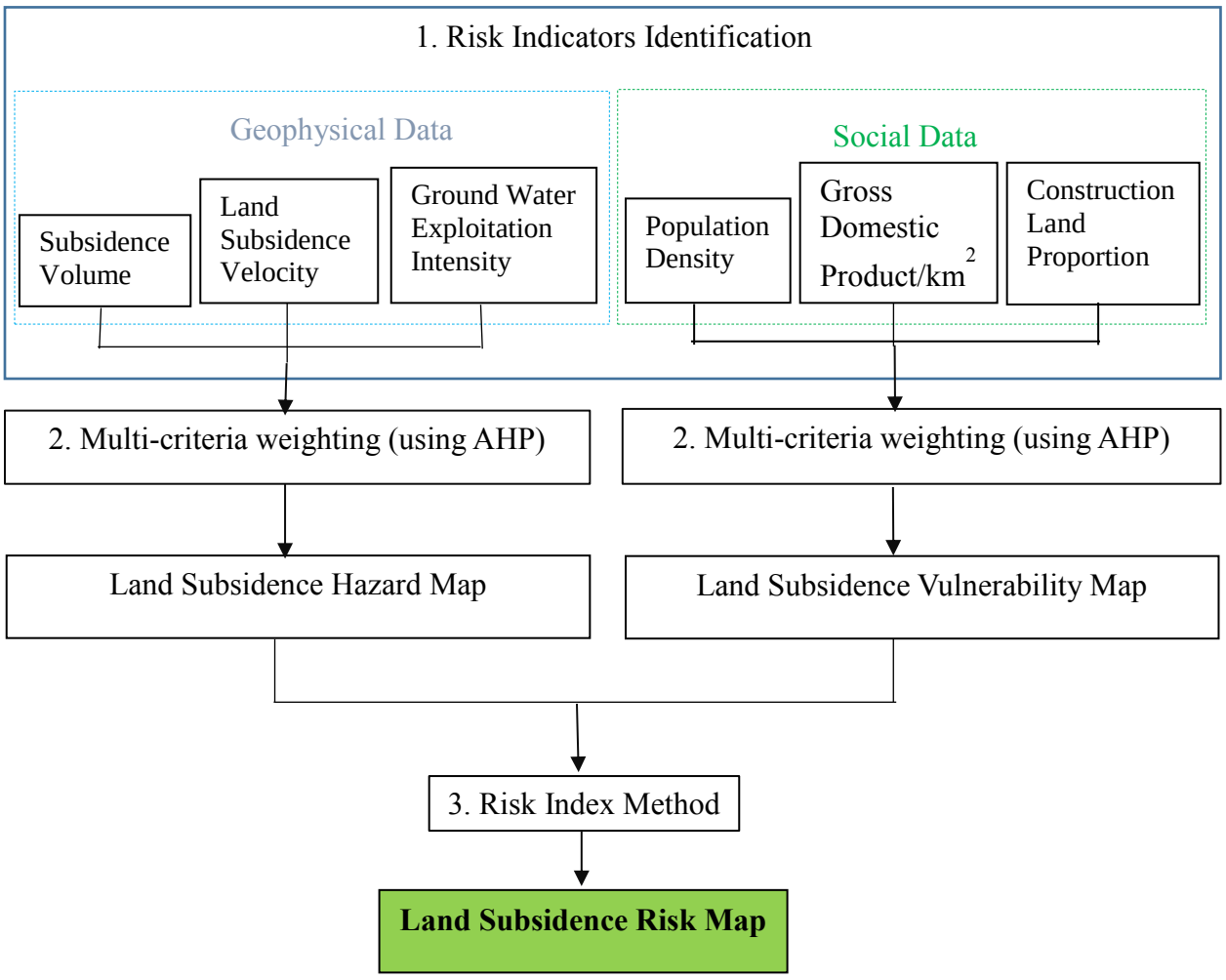

Figure 3.10. Methodology flowchart for Risk Assessment

4. RESULT AND DISCUSSION

4.1 Land Subsidence Mapping using ALOS PALSAR data

The coherence image of each pair for the study area is shown in **Figure 4.1**. The coherence value near to 1 (i.e. bright colour) indicates that there is no phase noise whereas a coherence value of 0 (i.e. dark colour) indicates that there is only phase noise. Areas with high coherence (coherence value 1) displays clear interferogram patterns in the interferogram image whereas areas with low coherence (coherence value 0) displays noisy interferogram patterns. Good coherence is seen in all our pairs; therefore, they can be considered for interferogram generation.

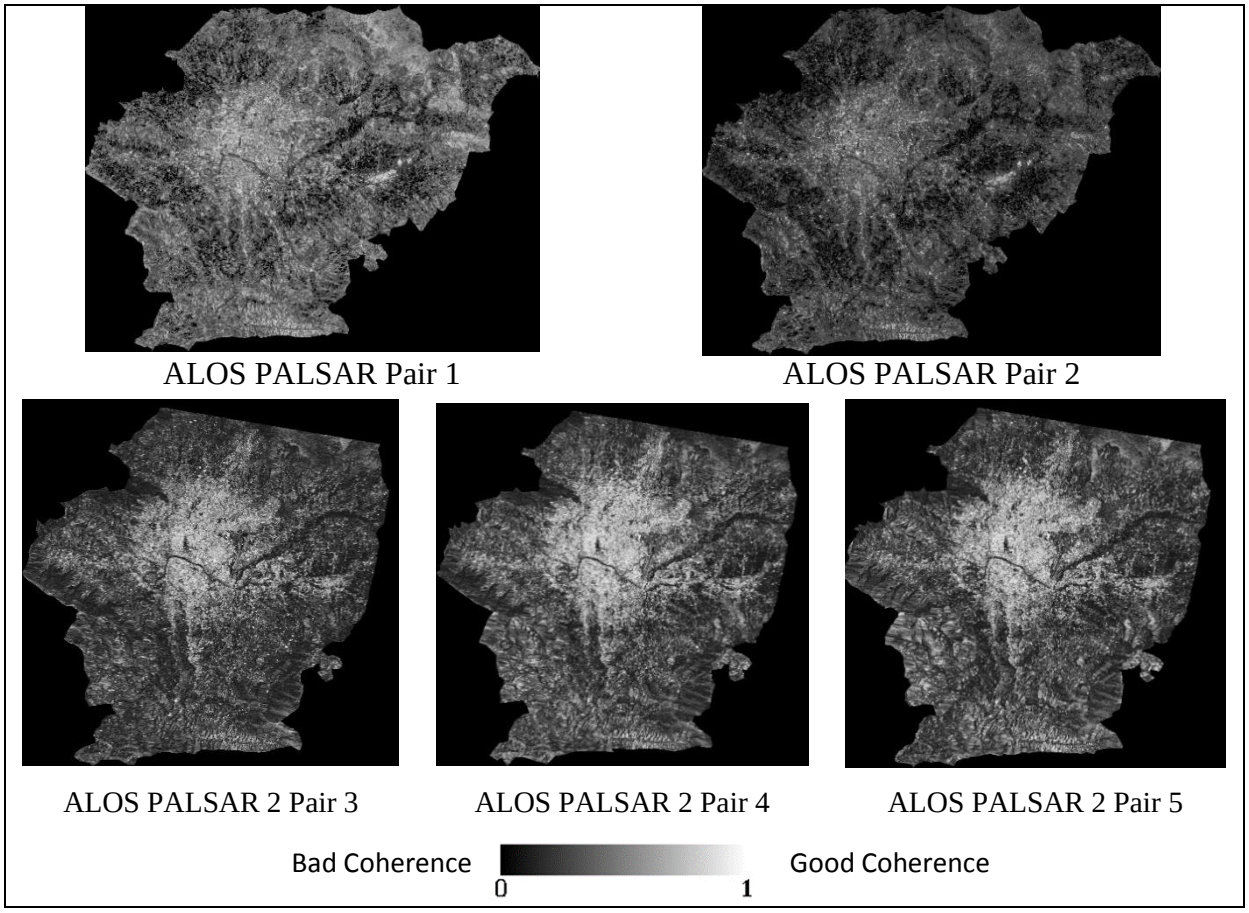

Figure 4.1. Coherence image of Pair 1 (2007/11/02 and 2008/03/19); Pair 2 (2007/11/02 and 2010/02/07); Pair 3 (2014/11/07 and 2015/05/08); Pair 4 (2015/05/08 and 2015/07/03) and Pair 5 (2015/07/03 and 2015/10/23).

The areas where dark values (black color) are seen are mostly result of no radar return because the study area is a valley surrounded by complex terrain (hills and slopes). Also, dark values are seen where the surface is changing regularly, water bodies and rivers in this case.

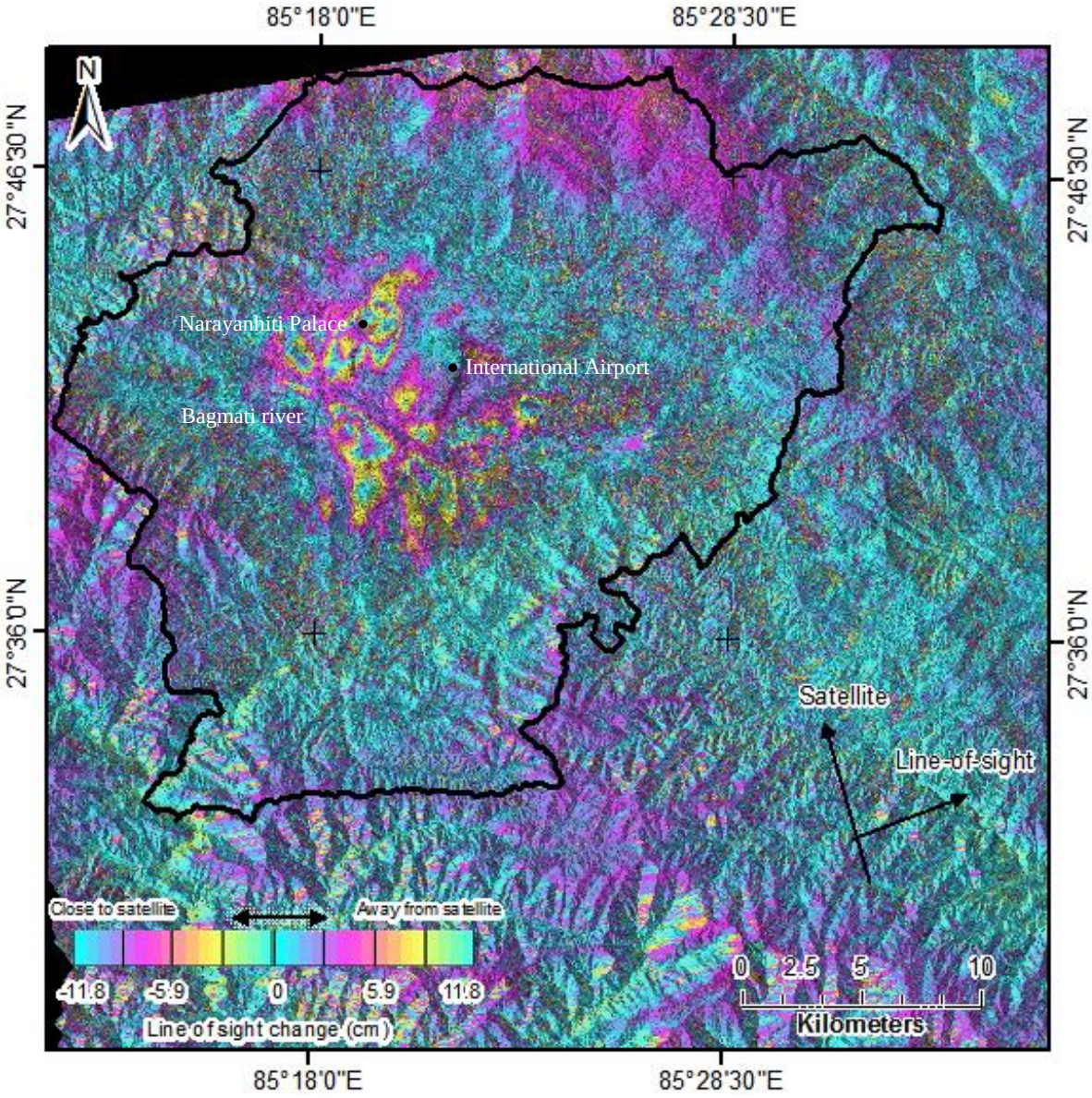

Figure 4.2 Differential Interferogram for Kathmandu Valley from 2007/11/02 to 2010/02/07 with the administrative boundary of Kathmandu valley indicated by black line.

The D-InSAR interferogram of Kathmandu valley for the observation interval 2007/11/02 to 2010/02/07 is shown in **Figure 4.2**. Interferogram fringes can be seen in various areas which indicates the occurrence of land subsidence. An area where the color turns from blue to red to

yellow to green is deformed. It is noticeable that some fringes on the south-eastern part does not display clear patterns. This is because interference cannot easily occur in inclined ground surfaces and this part of the study area is a hilly region.

Figure 4.3 shows the subsidence contour with displacement values in centimeter for the land subsidence affected areas which are indicated by points L1-L8. A significant linear feature striking NW-SE can be seen in **Figure 4.3.** The pattern displayed by ground deformation may depict the underlying structural arrangement of a location (Anderssohn et al., 2008). Referring to **Figure 1.2** and **Figure 4.6** it can be said that the subsidence pattern obtained here is modulated by the underlying sediments. Clear linear feature can be observed parallel to the fluvio-deltaic facies and lacustrine facies boundary.

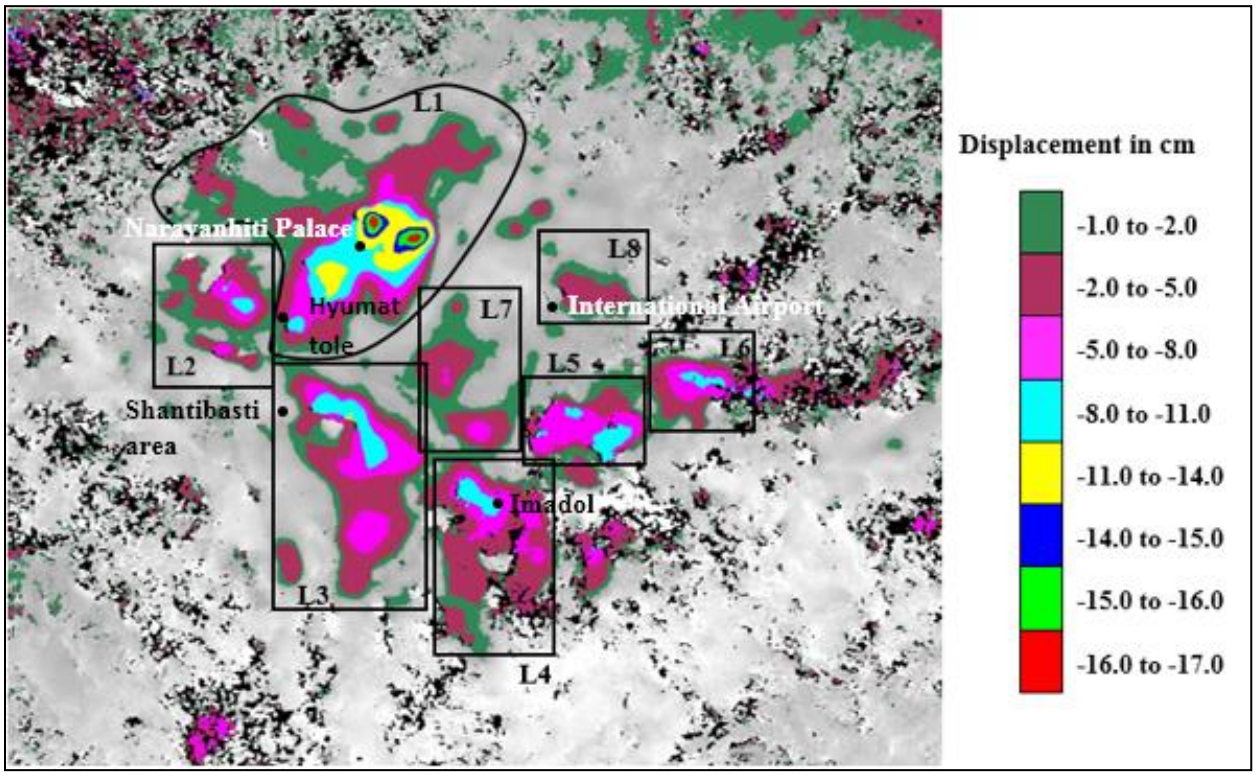

Figure 4.3 Subsidence contour with displacement values in centimeter for the land subsidence affected areas from 2007 Nov 02 to 2010 Feb 07 which are indicated by boxes L1-L8, along with three sites (Shantibasti area, Hyumat tole and Imadol; indicated by black dots) of localized subsidence reported in the past by Rana et al., 2007.

Location L1, central Kathmandu shows the maximum amount of subsidence (17 cm). It is a mixed-use development area. [A type of urban development that constitutes an amalgamation of residential, commercial, cultural, institutional, and /or industrial uses, along with their physical and functional integration, including pedestrian connections is called Mixed use development (Thrall, 2002)]. Location L2, Chauni and periphery is an old settlement area with an army camp and ancient museum covering most of the subsidence zone. Location L3, Lalitpur is also an old mixed use settlement area. Location L4, Imadol and periphery is a location on the outskirts of the Kathmandu city urban center which is gradually changing from farmland/cropland into urban landuse. This location also has a few number of brick kilns, that might be affecting the ground surface elevation. Location L5, Thimi and periphery is a mixed-use settlement area with croplands on the north-eastern side of the subsidence zone. Location L6, Madhyapur Thimi is mostly cropland with a few residential areas (spots) but is gradually being urbanized by land plotting. Location L7, New Baneshwor and Koteshwor are also mixed use settlement areas with the majority being commercial buildings. Location L8, Gothatar mostly consists of croplands with a few residential buildings along with a small northern portion of the international airport runway. The outskirts of the valley are mostly rural but urbanization is slowly spreading from the center of the valley towards the periphery.

The three sites of localized subsidence reported in the past by Rana et al, 2007 is represented by black dots in **Figure 4.3.** Land subsidence occurrence can be seen in Hyumat tole (-2cm to -5cm) and Imadol (-8cm to -11 cm) whereas in Shantibasti area there is no subsidence seen. Due to lack of data and proper description of the reported subsidence sites, this result cannot be validated.

The google earth image of portions of each location is shown in **Figure 4.4.** The subsidence coverage area and maximum subsidence depth of each location is shown in **Table 4.1**. Subsidence depths less than 2 cm has not been considered while calculating the coverage area.

Table 4.1 Detail information of the Land subsidence affected area.

Location Point	**Location Name**	**Location Specification**	**Subsidence Coverage area (km^2)**	**Maximum Subsidence depth (cm)**
L1	Central Kathmandu	Mixed use development	9.9	17
L2	Chauni	Old Army Camp	2.5	11
L3	Lalitpur	Mixed use development	7.7	14
L4	Imadol	Residential and cropland with few brick kilns	5.7	11
L5	Thimi	Mixed use development	3.0	11
L6	Madhyapur Thimi	Mixed use development	2.0	11
L7	New Baneshwor and Koteshwor	Mixed use development	2.1	8
L8	Gothatar	Residential and cropland with portion of runway	1.0	5

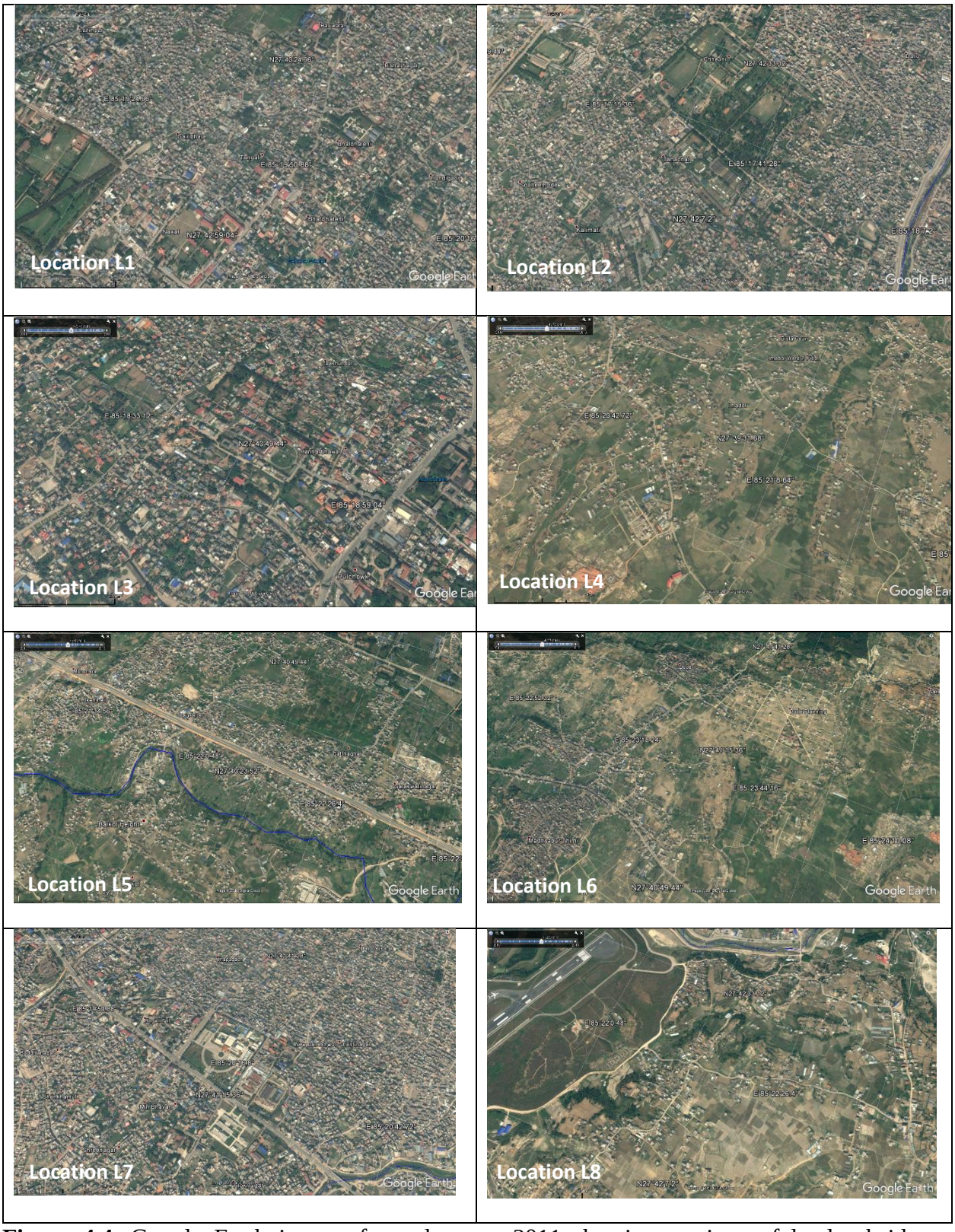

Figure 4.4. Google Earth images from the year 2011 showing portions of land subsidence locations L1 to L8.

The subsidence rates (velocity) of the occurred land subsidence was also obtained from the Dual Pair DInSAR processing. The subsidence rates for Locations L1 to L8 in the period from 2007/11/02 to 2010/02/07 was found to be 4.8, 2.6, 3.3, 3.0, 3.5, 2.9, 1.8 and 1.1 cm/year respectively. The velocity of land subsidence may depend on various factors like the amount groundwater extraction, recharge ability of the aquifer and the speed of the consolidation process of the sediments. Therefore, land subsidence may not proceed at the same rates for other time periods. This makes it difficult to predict the future estimate of subsidence without detailed study of the geologic setting and hydrogeology of the location.

The subsidence volume for each location was also estimated using **Equation 3.** The subsidence volume estimation for each location is shown in **Table 4.2.** These values were further used for hazard mapping of land subsidence in this research.

Table 4.2 Volume estimation of land subsidence locations.

Location	**Area 1 (m^2)**	**Area 2 (m^2)**	**Height (m)**	**Volume (m^3)**
Cone 1	124000	41000	0.04	3151
Cone 2	162000	44000	0.04	3872
Upper part	5179000	380000	0.12	278474
Location L1			Total	**285498**
Location L2	1369000	12000	0.11	55336
Location L3	4290000	900000	0.11	262348
Location L4	3696000	399000	0.11	194677
Location L5	536000	424000	0.11	52680
Location L6	1092000	194000	0.11	64030
Cone 1	1079000	211000	0.05	29452
Cone 2	784000	52000	0.05	17299
Location L7			Total	**46751**
Location L8	1000000	1000000	0.02	20000

Comparison with groundwater extraction data:

Kathmandu valley generally consists of three hydrogeologic layers namely, shallow aquifer, aquitard and deep aquifer. The shallow aquifer is thicker towards the north of the valleys groundwater basin whereas the deep aquifer is thicker towards the central and south part. The aquitard layer is thinnest at the northern part of the valley therefore, there is a connection between the shallow and deep aquifer here. The main natural recharge area is towards the northern part and a small area contributing to recharge is located towards the southern part (Pandey et al., 2012). Location L1, L7 and L8 lie on the northern part of the groundwater basin where the shallow aquifer is thicker whereas Location L3, L4, L5 and L6 lie on the central and southern part of the groundwater basin where the deep aquifer is thicker. As mentioned in the background earlier Kathmandu valley mainly relies on groundwater as the main source of water. According to the Kathmandu Valley Water Supply Management Board, the use of deep tube-well pumps for water extraction from deep aquifer is dominant throughout the valley. The depth of deep tube well mainly lies in a range of 30 meters to 300 meters and the daily discharge ranges from 3000 liters per day to 400000 liters per day (KVWSMB data).

Figure 4.5 shows the locations of registered deep tube wells in the subsidence locations of Kathmandu valley. We can see that the concentration of wells is denser in Location L1 where the subsidence is highest (17 cm) and sparse in other locations where the subsidence amount is lower. However, there are many unregistered wells throughout the valley without information on their depth and discharge which makes it difficult find an exact relation. Nonetheless, considering the density of urban built up (refer to **Figure 4.4**) it can be assumed that the concentration of deep tube wells will be higher in Locations L1, L2, L3 and L7. Also, the occurrence of land subsidence is a combined effect of groundwater extraction and vulnerable hydrogeology which might result in subsidence at places other than the site of extraction (Sato et al., 2003). Therefore, comprehensive study of the groundwater extraction and recharge ability of the aquifer which has not been included in this research should be done in order to find the exact relationship.

However, it has been found through various literature review that extensive water extraction is one of the main causes of land subsidence. From the results obtained from this research, we can

consider that water extraction does have a relation with the land subsidence. But, detailed study needs to be done to find the exact cause as land subsidence is a very complex phenomenon affected by various factors.

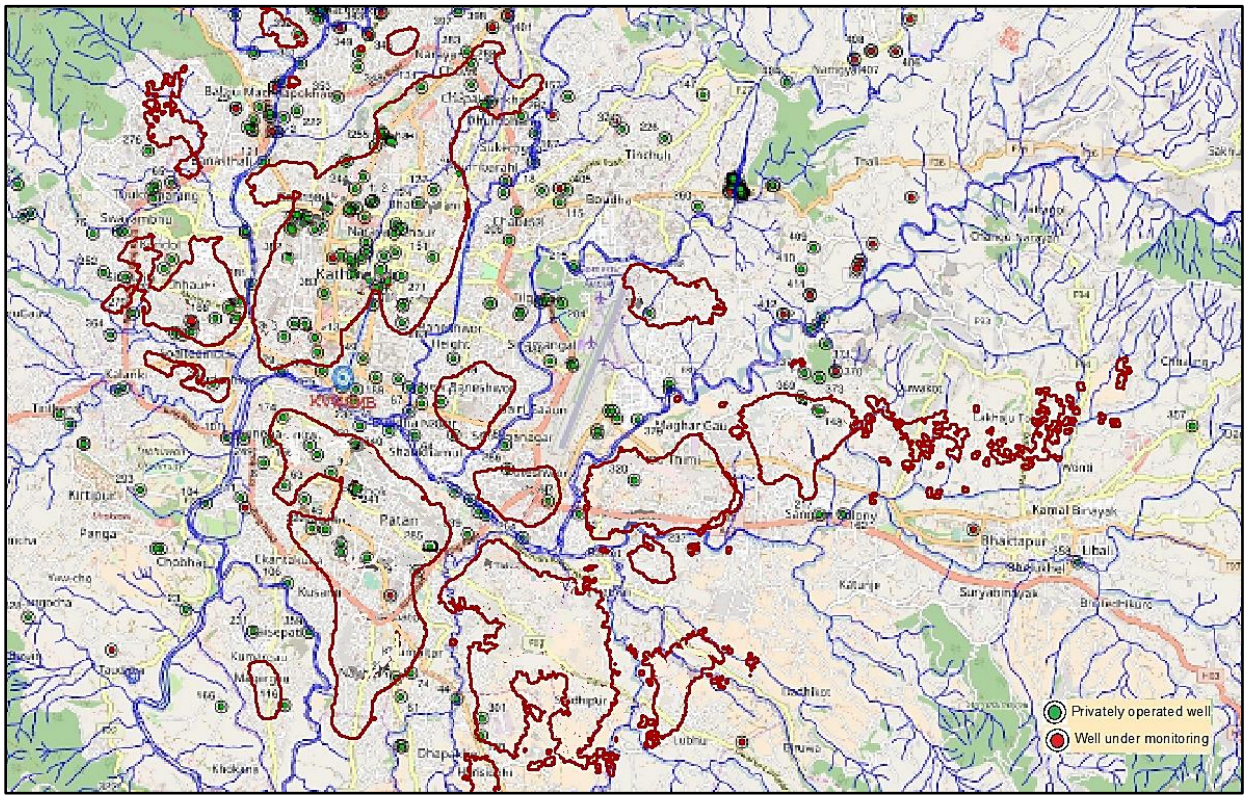

Figure 4.5 Location of registered deep-well pumps in land subsidence locations (indicated by maroon line boundary) in Kathmandu Valley. (Source for location of pumps: Kathmandu Valley Water Supply Management Board).

Comparison with geology:

Land subsidence map generated by DInSAR processing in this research was briefly compared with the geological map of Kathmandu valley. **Figure 4.6** shows the subsidence contour map overlaid on the geological map of Kathmandu valley. The maximum amount of subsidence (indicated by red color in **Figure 4.3**) can be seen over the Gokarna Formation. This formation is mainly composed of sands terrace from fluvio-lacustrine origins (Piya, 2004). Also, a spread of thick array

of sandy and silty sediments without clay content was observed from the extensive borehole data of this formation (Sakai, 2001). Similarly, Locations L5, L7 and L8 are also situated over the Gokarna Formation. Locations L2, L4, L6 and small portion of Locations L3 and L7 are situated over the Kalimati Formation. Kalimati is a local name for black clay. According to Sakai, 2001; the predominant constituent of this formation is dark grey carbonaceous and diatomaceous (naturally occurring, soft siliceous sedimentary rock that is easily crumbled into a fine white to off-white powder) beds of open lacustrine rocks that is vastly distributed underneath the surface of central portion of the Kathmandu Valley.

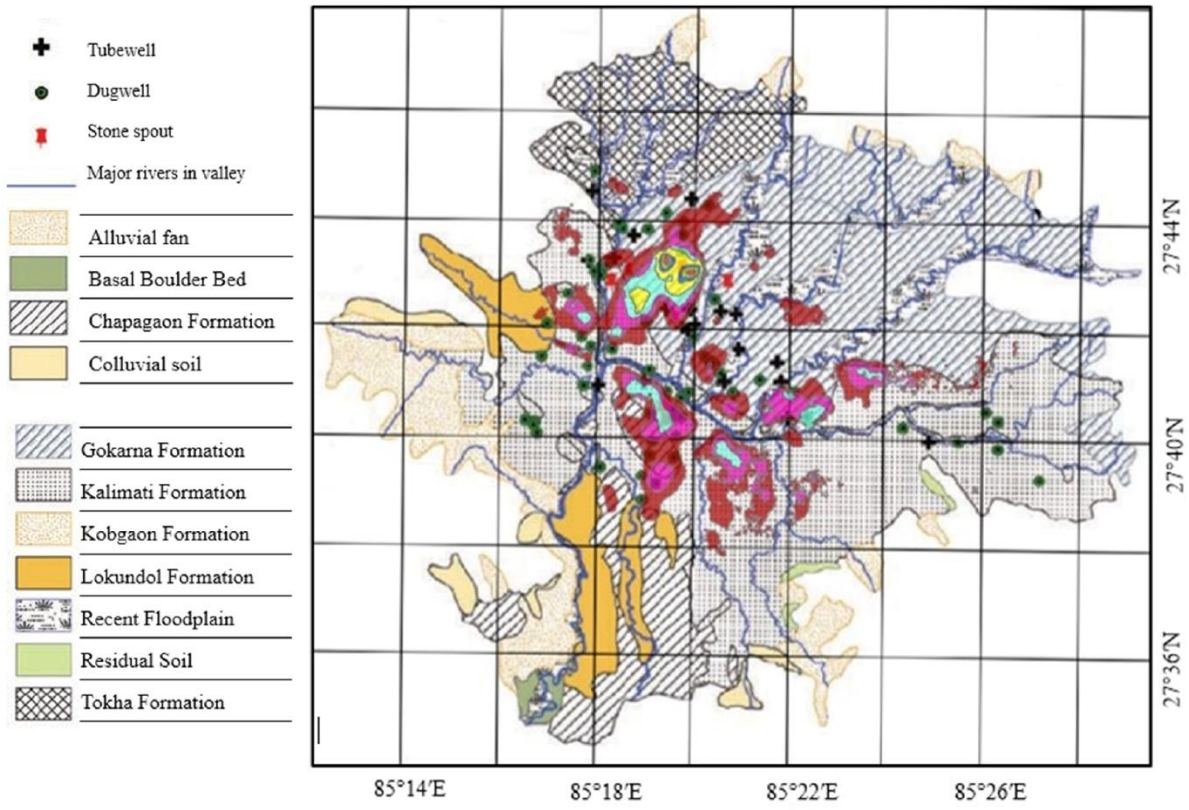

Figure 4.6 Subsidence contour overlaid on geological map of Kathmandu valley. (Geological map adapted from engineering and environmental geological map of Kathmandu valley, Department of Mines and Geology, Government of Nepal by Pathak et al., 2010)

It can also be seen in **Figure 4.6** that a larger portion of Location L3 is situated over the Chapagaon Formation. This formation consists of somewhat rounded silty sandy gravel, sporadically with boulder bed covered with less than 1 m thin clayey silt and silty sand (Shrestha and Shah, 2014).

From the above description, it can be summarized that land subsidence was observed mainly over three kinds of geological formations namely Kalimati, Gokarna and Chapagaon Formation. The main constituents of these formations are silica, sand, silt, clay and silty sandy gravel. As mentioned in the mechanism of land subsidence earlier, the major factor in occurrence of land subsidence due to ground water extraction is the presence of unconsolidated fine-grained sediments mainly clay and silt in an aquifer system. Hence, the relationship between geology and land subsidence occurrence can be established in this study.

These constituents are the main contents of the geology of Kathmandu valley and are spread throughout the valley, concluding that the primary factor (i.e. geology) for subsidence occurrence is prevalent. Therefore, it can be said that the triggering/immediate factor (i.e. groundwater characteristics) for subsidence occurrence is the major factor that determines the occurrence of land subsidence in the study area.

Furthermore, land subsidence is a complex phenomenon and this research is just a preliminary study that intends to provide basic evidence of land subsidence in the study area. This study can serve as a base for more comprehensive study in the future.

Also, due to the non-existence of previous land subsidence measurement data and difficulty in obtaining the GPS measurement data, the subsidence results were not able to be validated. In spite of this, the results can be considered acceptable owing to the fact that D-InSAR is a well-established methodology known to give accurate results for land deformation in urban areas.

4.2 Land Subsidence Mapping using ALOS 2 PALSAR 2 data

The D-InSAR interferogram of Kathmandu valley for the observation interval 2014/11/07 to 2015/05/08 is shown in **Figure 4.7**. Interferogram fringes can be seen throughout the scene, this is because on April 25, 2015, a devastating earthquake of magnitude Mw 7.8 (US Geological Survey, 2015) struck central Nepal. The epicenter was approximately 80 km northwest to Kathmandu main city core. Liner interferogram fringes seen in the northern and southern part of the Kathmandu valley (indicated by **A** in **Figure 4.7)** show color change from blue to yellow to

red to blue which indicates that land uplift has occurred in that area. Similarly, fringes in the center part of the valley (indicated by **B** in **Figure 4.7**) display the color change from blue to red to yellow which implies that land subsidence has occurred. The amount of subsidence and uplift occurred are discussed later in this section.

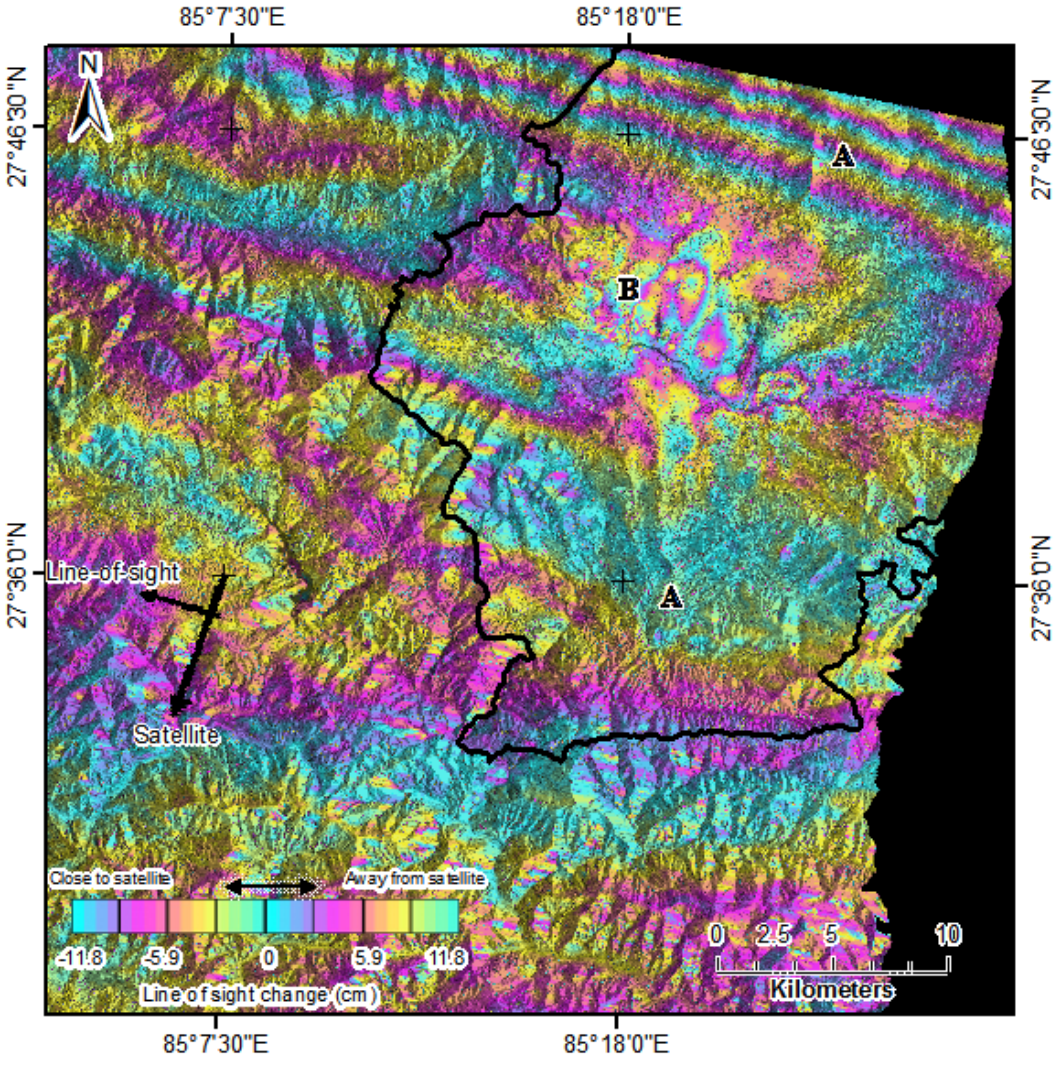

Figure 4.7. Differential Interferogram for Kathmandu valley from 2014/11/07 to 2015/05/08 where A indicates areas of uplift occurrence and B indicates area of subsidence occurrence.

The D-InSAR interferogram of Kathmandu valley for the observation interval 2015/05/08 to 2015/07/03 is shown in **Figure 4.8**. This interferogram shows the deformation caused by a strong aftershock of Mw 7.3 that followed the major earthquake on 12 May 2015 whose epicenter was approximately 65 km northeast to Kathmandu main city core. Little amount of subsidence (where the color has changed from blue to red) and uplift (where the color has changed from blue to yellow) can be observed in the valley. The amount of subsidence and uplift occurred are discussed altogether later in this section.

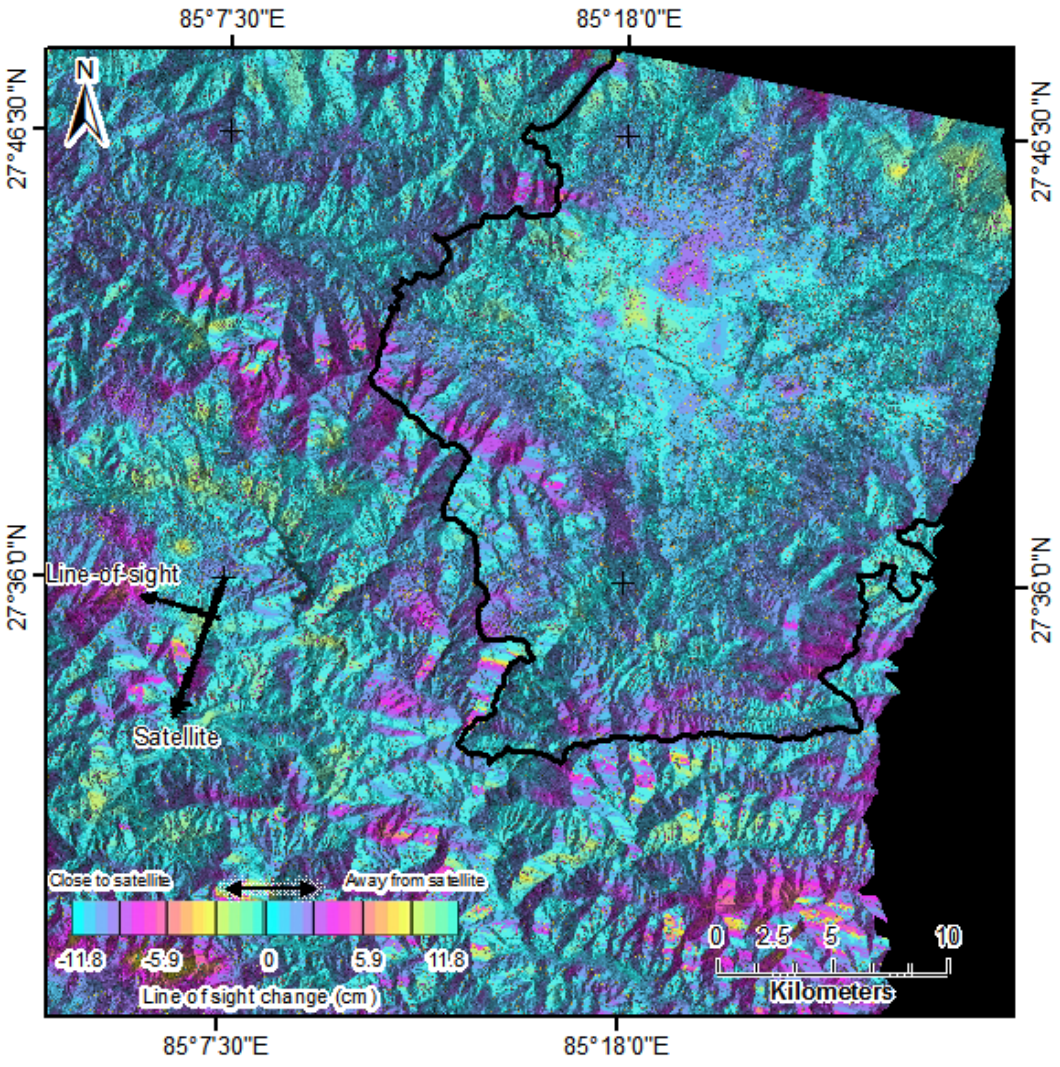

Figure 4.8. Differential Interferogram for Kathmandu valley from 2015/05/08 to 2015/07/03.

The D-InSAR interferogram of Kathmandu valley for the observation interval 2015/07/03 to 2015/10/23 is shown in **Figure 4.9.** This interferogram shows the deformation caused by minor aftershock (< Mw 6) events after all the major earthquake had ceased. Subsidence occurrence can be seen in places where the interferogram fringe color has changed from blue to red.

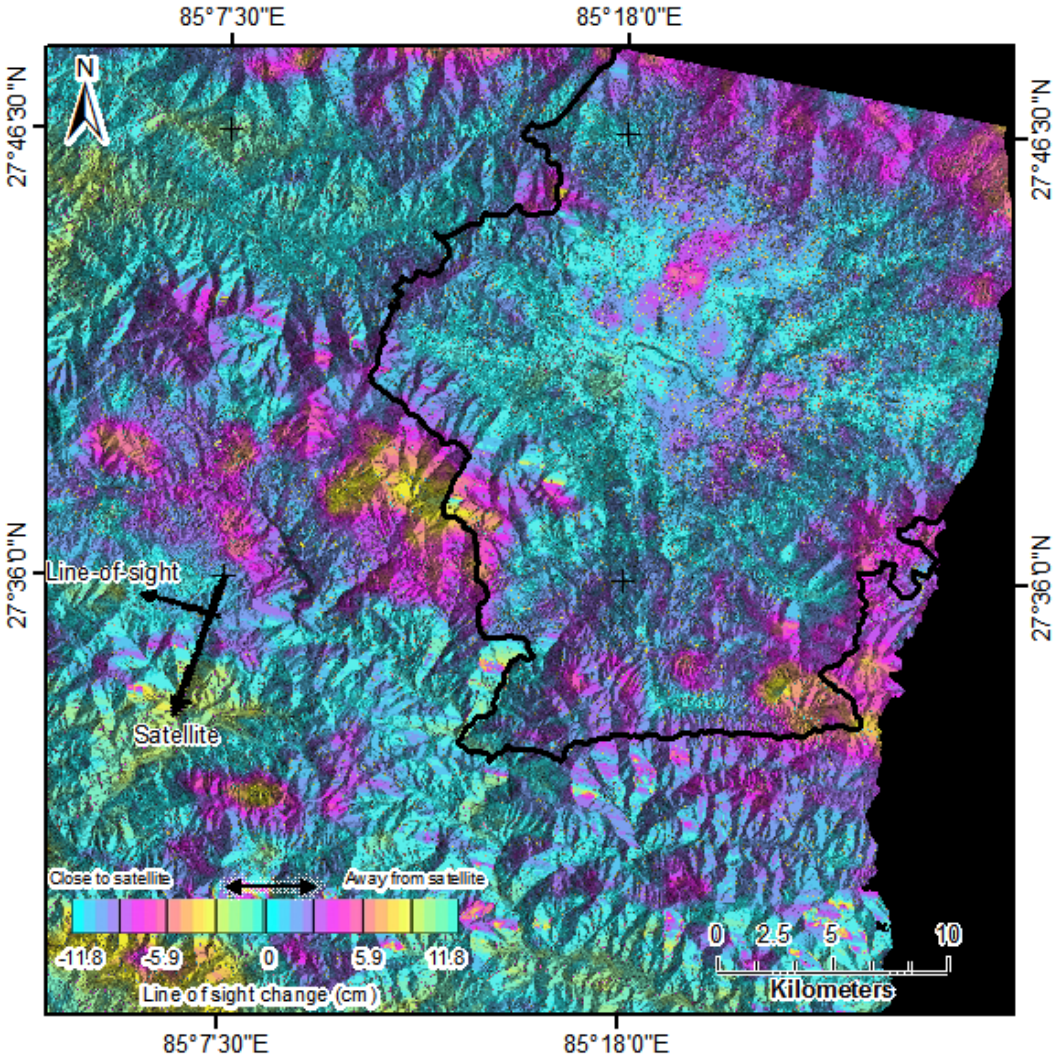

Figure 4.9. Differential Interferogram for Kathmandu valley from 2015/07/03 to 2015/10/23.

The overall D-InSAR interferogram generated by dual pair differential interferometry of Kathmandu valley for the observation interval 2014/11/07 to 2015/10/23 is shown in **Figure 4.10**. Interferogram fringes can be seen throughout the scene. Interferogram fringes seen in the northern and parts surrounding the valley center (indicated by **A** in **Figure 4.10**) show signs of uplift whereas the center and the southern part of the Kathmandu valley (indicated by **B** in **Figure 4.10**) show subsidence occurrence.

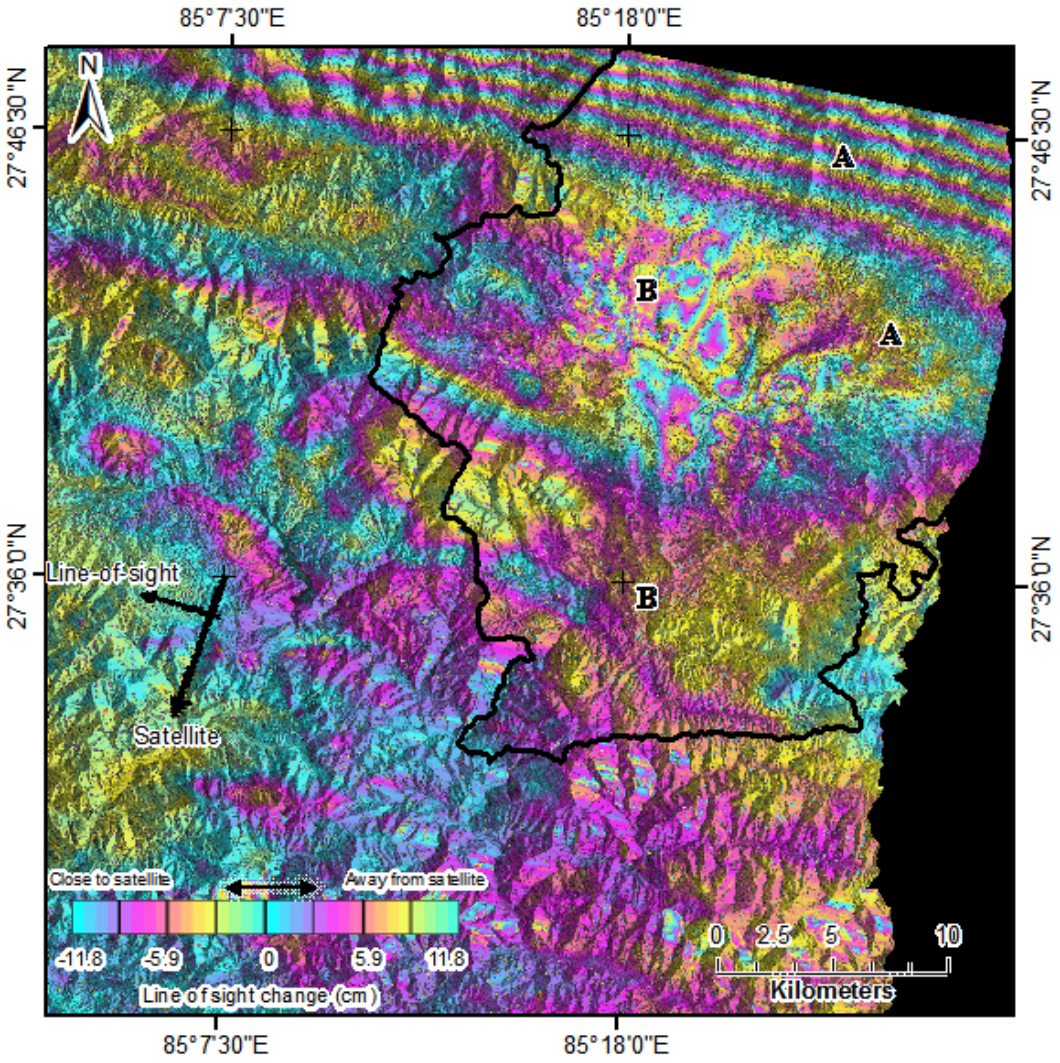

Figure 4.10 Differential Interferogram of Kathmandu valley for the observation interval 2014/11/07 to 2015/10/23 generated by ALOS 2 PALSAR 2 data.

Comparing the interferogram generated from ALOS PALSAR data (2007/11/02 – 2010/02/07) and ALOS 2 PALSAR 2 data (2014/11/07 – 2015/10/23) shown in **Figure 4.11 A** and **B** respectively, it is visible that the locations of subsidence occurrence is similar. This indicates that despite the earthquake event, the subsidence pattern and location are similar.

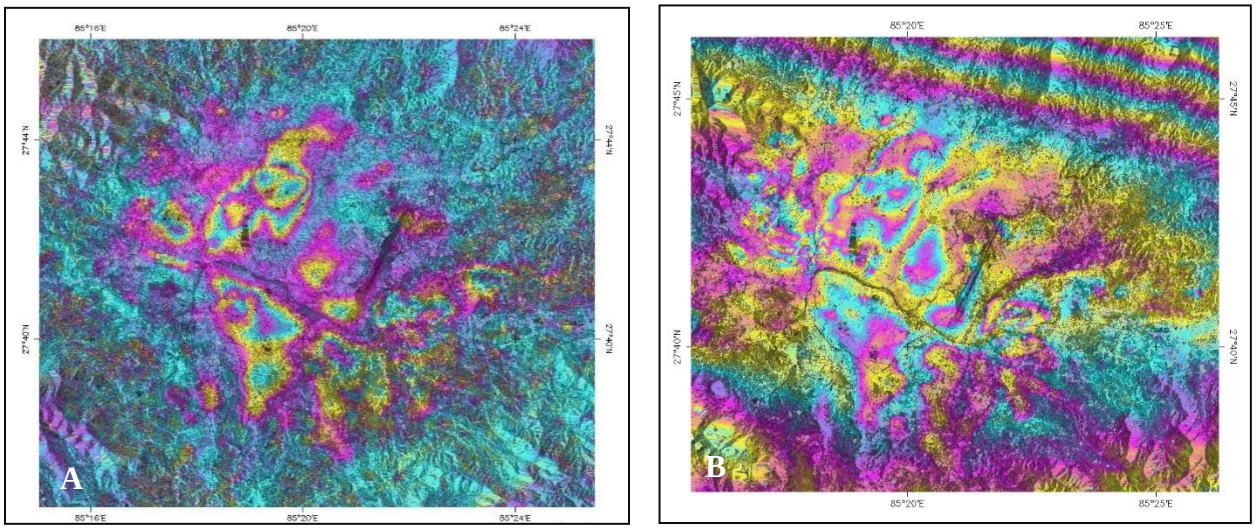

Figure 4.11 (A) Differential Interferogram generated from ALOS PALSAR data (2007/11/02 – 2010/02/07) and (B) Differential Interferogram generated from ALOS 2 PALSAR 2 data (2014/11/07 – 2015/10/23).

The subsidence contour with its displacement values in centimeters for the land subsidence affected area (from 2014 to 2015) similar to that generated from ALOS PALSAR (from 2007 to 2010) indicated by L1 – L7 is shown in **Figure 4.12.** The subsidence location identified for 2007 to 2010 resembles the subsidence locations identified for 2014 to 2015. The details of these locations are presented in **Table 4.3.**

Location L1, central Kathmandu shows a maximum amount of subsidence corresponding to 25 centimeters. The same location had experience 17 cm subsidence within 2007 to 2010. There is not much difference in the area affected by subsidence in the two observed time periods (refer to **Figure 4.3**). All the other location show an amount of 10 cm subsidence expect for Location L5

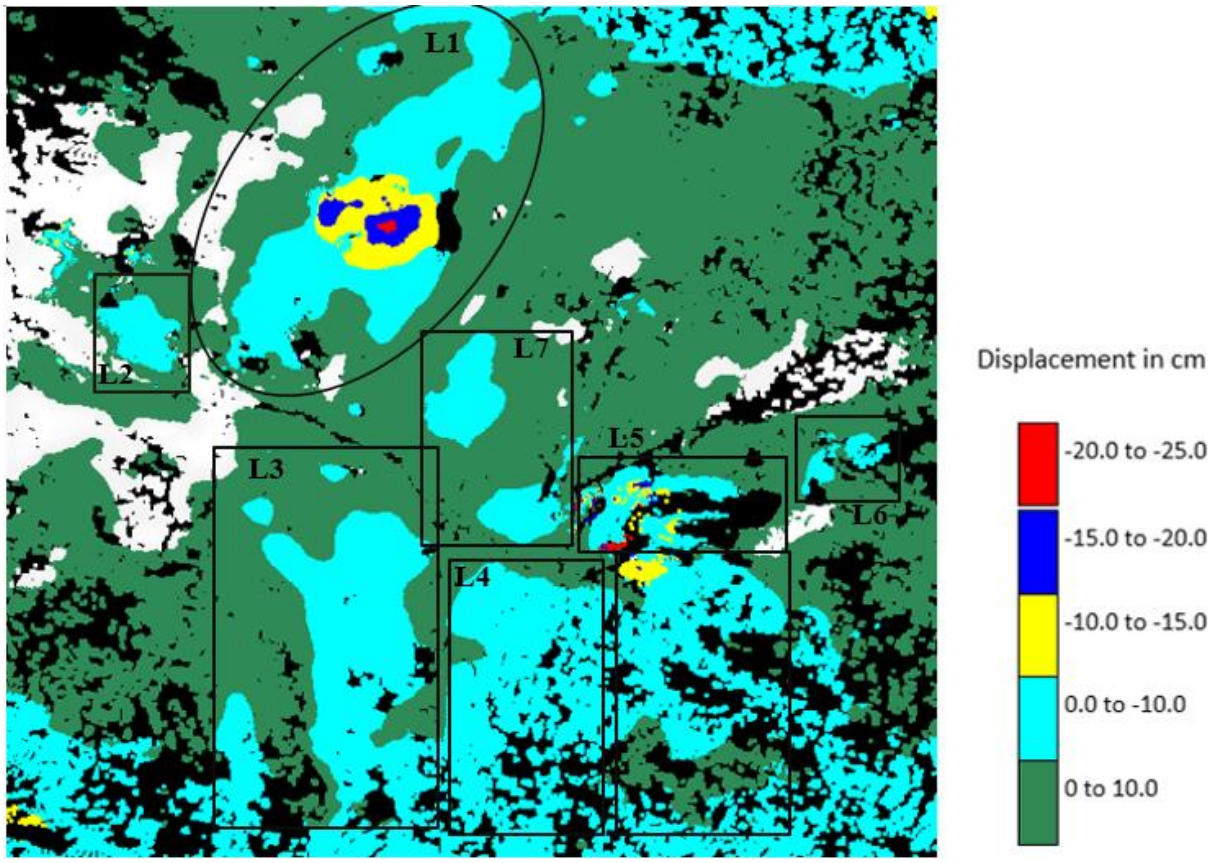

Figure 4.12 Subsidence contour showing displacement values in centimeter for land subsidence affected area for 2014/11/07 – 2015/10/23.

where a small area (near Lokanthali) shows a subsidence of 25cm and Balkot area shows a subsidence of 15 cm. A visible decrease in Location L3, L6 area and increase in Location L4 and L5 area is evident. Also, subsidence was not detected in Gothatar (Location L8; refer to **Figure 4.3)** which showed subsidence occurrence previously.

It is evident that the rate of subsidence has increased drastically. There might be two factors contributing to this increase. First and most significant being the increase in groundwater extraction. As mentioned by the Central Bureau of Statistics, the population of the valley has tripled in the last thirty years and this increase in bound to be continue in future as well (CBS, 2012).

Since, no change has been made to the condition regarding groundwater resources use in the valley, the population increase will have a direct effect on groundwater extraction that ultimately affects

the subsidence rate. The second factor that might have contributed to this increase in the rate of subsidence can be the effect of 2015 Earthquake event. As mentioned in the 'Literature Review' chapter earlier, Kathmandu valley was rocked by the earthquake in such a way that some parts experienced uplift and some parts experienced subsidence (refer to **Figure 2.3**). Also, after the 2011 Tohoku earthquake, Chiba prefecture had experienced a similar change in the velocity of land subsidence; the trend was regained after the earthquake. However comprehensive study is required to find the relationship between earthquake occurrence and land subsidence.

Table 4.3 Detail information of the land subsidence affected area (2014-2015).

Location Point	**Location Name**	**Location Specification**	**Subsidence Velocity (cm/yr. *)**	**Maximum Subsidence depth (cm)**
L1	Central Kathmandu	Mixed use development	15	25
L2	Chauni	Old Army Camp	8.0	10
L3	Lalitpur	Mixed use development	7.6	10
L4	Imadol	Residential and cropland with few brick kilns	6.5	10
L5	Thimi	Mixed use development	15	25
L6	Madhyapur Thimi	Mixed use development	4.0	10
L7	New Baneshwor and Koteshwor	Mixed use development	4.5	10

*350 days and earthquake event

4.3 Risk Assessment of Land Subsidence

An indicator framework based on the Disaster Risk Index method was prepared with two significant factors for risk assessment along with three indicators for each factor. The indicators were weighted by its significance to govern land subsidence risk using the AHP multi-criteria decision making process. The values of each indicator were classified into three classes Low, Medium and High where low indicates the lowest hazard / vulnerability level and high indicates the highest hazard / vulnerability level. **Table 4.4** shows the weighted values and grade and values for the respective indicators.

Table 4.4 Weighted values and grade and value for indicators of land subsidence risk assessment.

Index			**Grade and value**		
			Low	**Medium**	**High**
Factor	**Indicator**	**Weighted value**	[1]	[2]	[3]
Hazard	Accumulated Subsidence volume (mm)	0.63	0-10000	10000-100000	>100000
	Subsidence velocity (mm/yr.)	0.26	0-30	30-50	>50
	Groundwater exploitation intensity (10 ^4 m^3/yr.)	0.11	0-8	8-16	>16
Vulnerability	Population density (person/km^2)	0.67	0-1000	1000-10000	>10000
	GDP per km^2 (10^4 $)	0.24	0-99	100-499	>500
	Construction land proportion (%)	0.09	0-49	50-79	>80

4.3.1 Land Subsidence Hazard Evaluation

Kathmandu valley was divided into three zones corresponding to the major cities Kathmandu, Bhaktapur and Lalitpur along with the subsidence locations obtained from previous processing for hazard evaluation. The data values of indicator for each zone and location is shown in **Table 4.5**. The volume and maximum subsidence velocity for the three zones were considered to be nil as no subsidence was detected in these areas.

Table 4.5 Data values of indicators used for land subsidence hazard evaluation of Kathmandu valley.

Location	**Volume (m^3)**	**Maximum subsidence velocity(mm/yr.)**	**Average Discharge (10^4 m^3/yr.)**
Location L1	285498	48	32
Location L2	55336	26	4
Location L3	262348	33	3
Location L4	194677	30	2
Location L5	52680	35	4
Location L6	64030	29	1
Location L7	46751	18	3
Location L8	20000	11	2
Kathmandu zone	-	-	4
Lalitpur zone	-	-	4
Bhaktapur zone	-	-	3

The land subsidence hazard map of Kathmandu valley is shown in **Figure 4.13**. Land subsidence in Kathmandu valley mainly situates in low hazard area (indicated by yellow colour in **Figure 4.13**). High hazard areas can be seen scattered in the subsidence locations L1, L3 and L4 (indicated by red colour in **Figure 4.13**) whereas medium hazard areas can be seen scattered in the subsidence locations L2, L5, L6, L7 and L8 (indicated by green colour in **Figure 4.13**).

This indicates that there is a high probability that land subsidence occurrence is bound to intensify in locations L1, L3 and L4 considering there is no reduction in the average groundwater discharge.

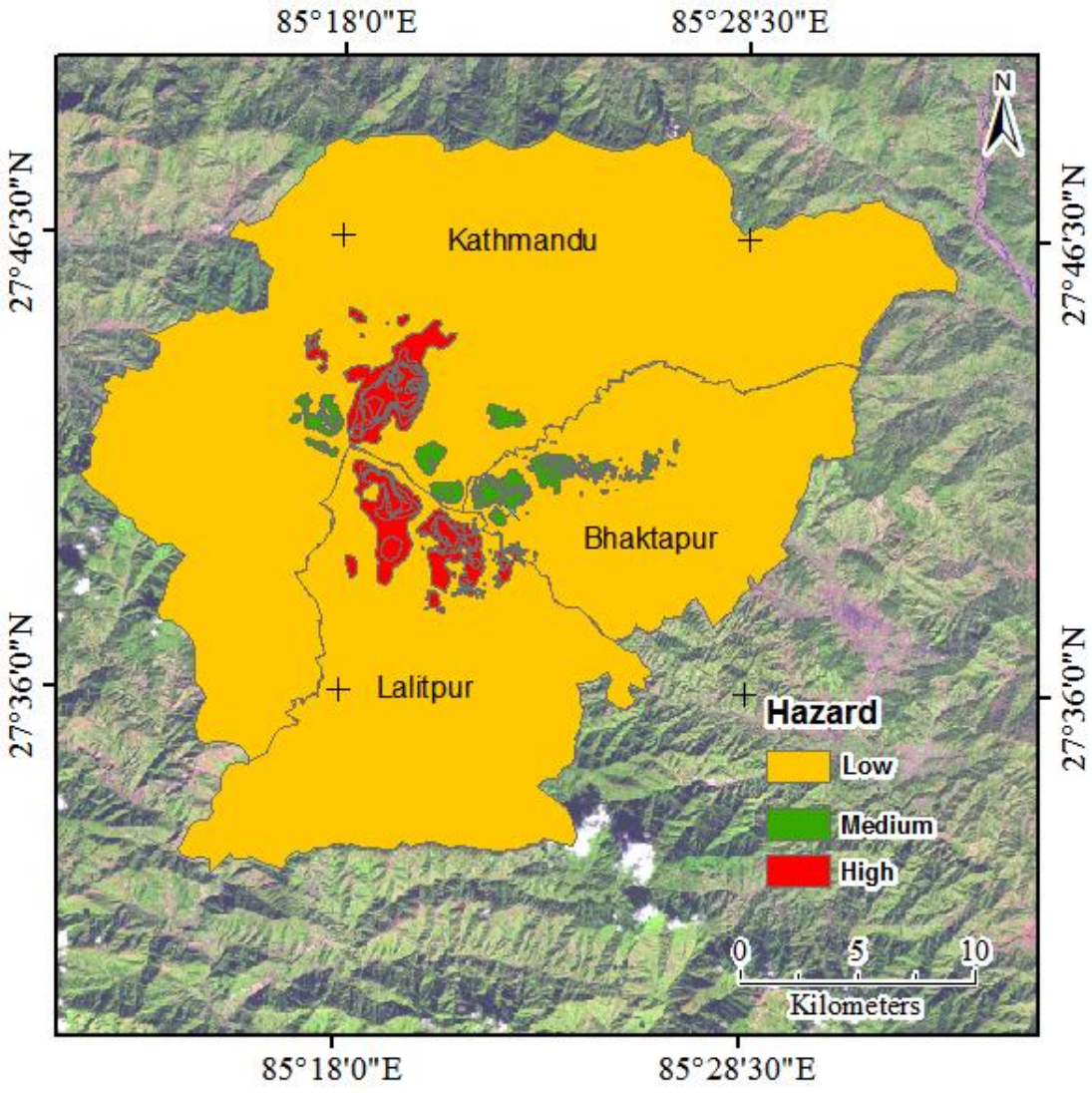

Figure 4.13 Land subsidence hazard map of Kathmandu valley generated through GIS processing for the period of 2007 Nov 02 to 2010 Feb 07.

4.3.2 Land Subsidence Vulnerability Evaluation

In the same manner to hazard evaluation, Kathmandu valley was also divided into three zones corresponding to the major cities Kathmandu, Bhaktapur and Lalitpur along with the subsidence locations obtained from previous processing. The data values of indicator for each zone and location is shown in **Table 4.6**. The individual subsidence locations were categorized into their respective municipality owing to the fact that it is difficult to acquire social and economic data (i.e. population density and GDP) for such small zones.

Table 4.6. Data values of indicators used for land subsidence vulnerability evaluation of Kathmandu valley.

Location	Municipality	Population density	GDP ($)	Construction land Proportion (%)
Location L1	Kathmandu	19726	749582	80
Location L2	Kathmandu	19726	749582	95
Location L3	Lalitpur	14574	1014539	80
Location L4	Lalitpur District	3241	4562750	30
Location L5	Madhyapur Thimi	7717	1916042	60
Location L6	Madhyapur Thimi	7717	1916042	20
Location L7	Kathmandu	19726	749582	70
Location L8	Kathmandu	19726	749582	50
Kathmandu zone		2382	6	60
Lalitpur zone		1197	12	40
Bhaktapur zone		680	22	30

(Data sources: KVDA; National Accounts Section, CBS and Ministry of Land Reform and Management, Government of Nepal) *refer to section "3.4 Methodology of Risk Assessment" for details.

The land subsidence vulnerability map for Kathmandu valley is shown in **Figure 4.14.** The evaluation results show that subsidence location L1, L2, L3 L7 and L8 (indicated by red colour in **Figure 4.14**) are highly vulnerable areas. These locations are situated in the main urban core of the Kathmandu valley where the population density is the highest and the economy is the most developed. Kathmandu zone, Lalitpur zone and subsidence locations L4, L5 and L6 are found to be in medium vulnerable zone (indicated by green colour in **Figure 4.14**). Lowest vulnerability is seen in Bhaktapur zone as the population density and economic activity is lowest in this area. The result indicates that Location L1, L2, L3 L7 and L8 are most sensitive to damage caused by land subsidence.

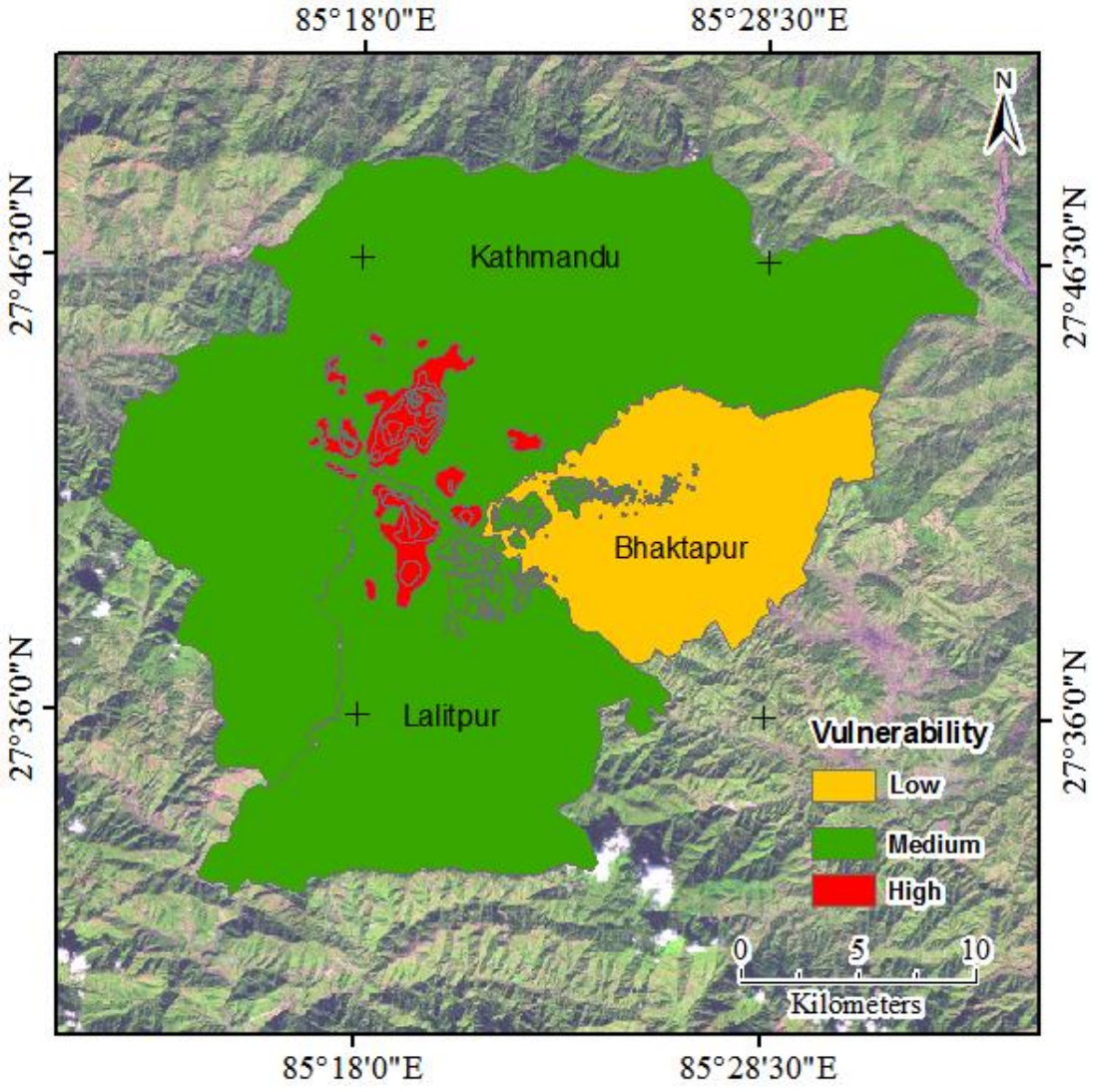

Figure 4.14 Land subsidence vulnerability map of Kathmandu valley generated through GIS processing for the period of 2007 Nov 02 to 2010 Feb 07.

4.3.3 Land Subsidence Risk Evaluation

Land subsidence risk map of Kathmandu valley was generated based on the hazard and vulnerability evaluation in GIS using Equation 4 (**Figure 4.15).** The areas where land subsidence was detected through DInSAR processing were found to be in high (Location L1 and L3; indicated by red colour in **Figure 4.15**) and medium (Location L2, L4, L5, L6, L7 and L8; indicated by green colour in **Figure 4.15**) risk areas. However, rest of the Kathmandu valley was found to be at low risk of land subsidence (indicated by yellow colour in **Figure 4.15).**

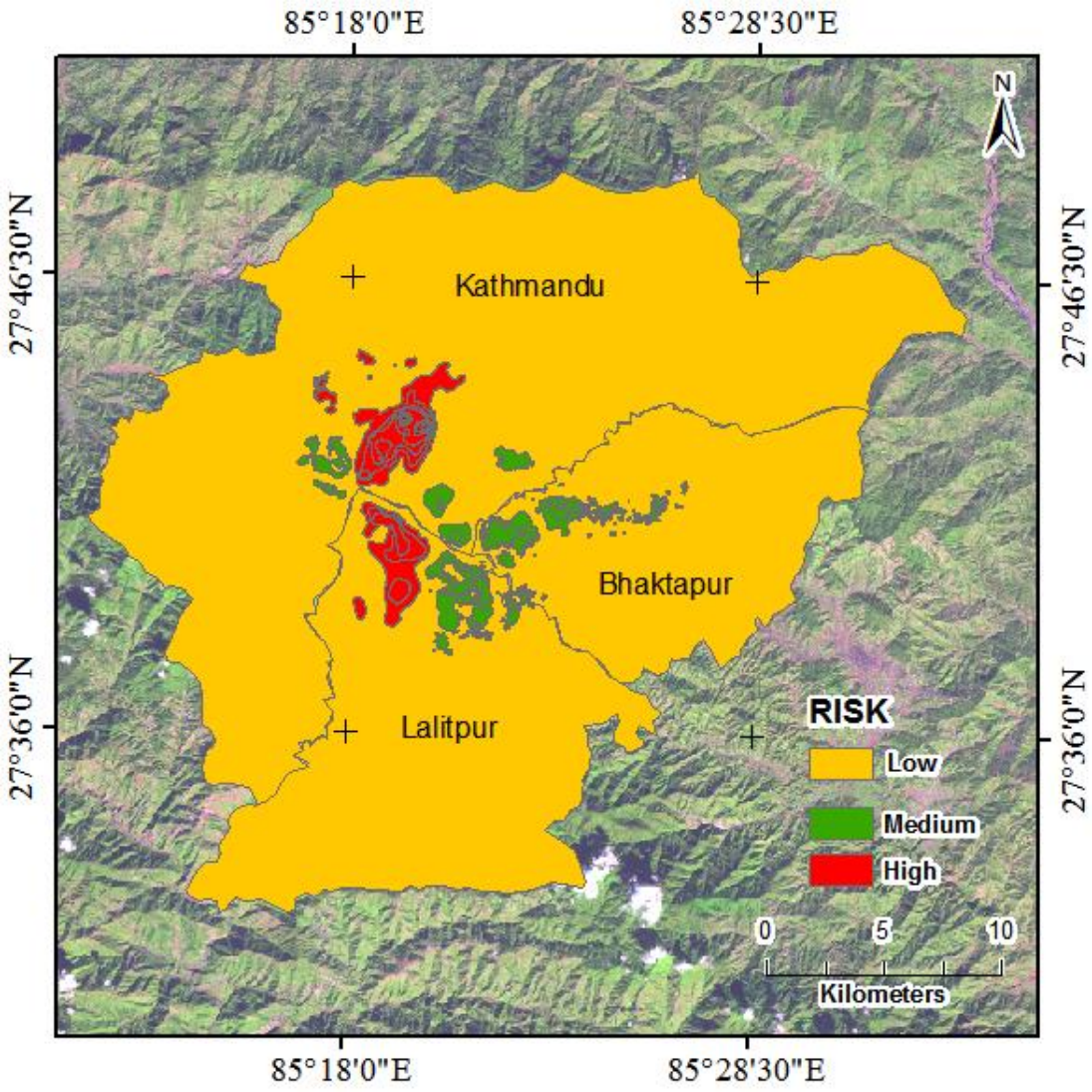

Figure 4.15 Land subsidence risk map of Kathmandu valley generated through GIS processing for the period of 2007 Nov 02 to 2010 Feb 07.

Since, the surface covered by basement rock is not susceptible to land subsidence, the obtained risk map was further modified by overlaying the basement rock boundary. **Figure 4.16** shows the risk map with no risk areas (indicated by light yellow colour), Low risk areas (indicated by yellow colour), Medium risk areas (indicated by green colour) and High risk areas (indicated by red colour). This obtained risk map is not the future prediction of risk that could arise from land subsidence as it uses the present data from 2007 to 2015.

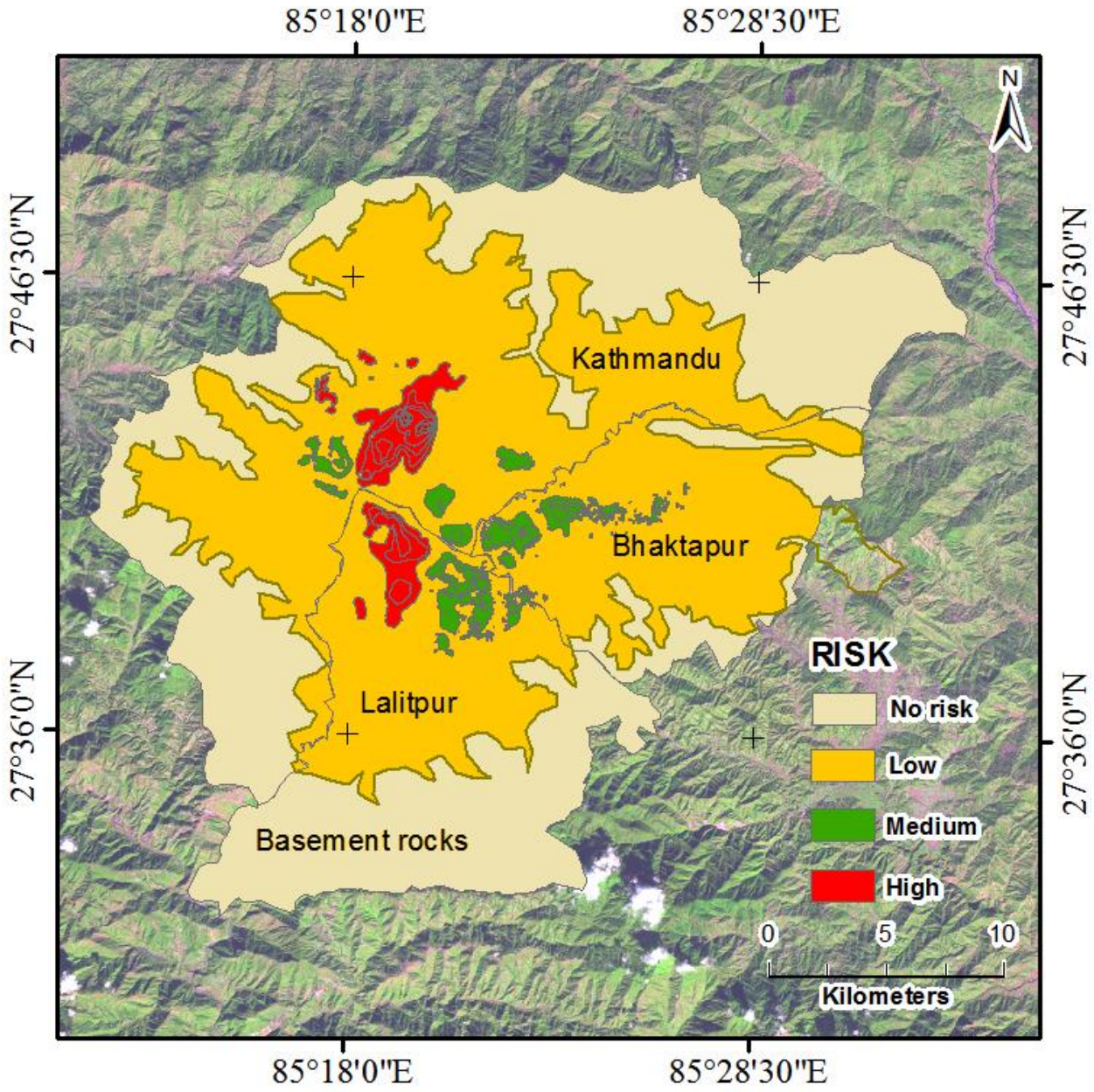

Figure 4.16 Land subsidence risk map of Kathmandu valley along with the basement rock boundary generated through GIS processing for the period of 2007 Nov 02 to 2010 Feb 07.

This risk map is purely a representation of areas that are liable to damage induced by the current scenario of land subsidence. Regular monitoring of the subsidence and the other affecting factors will be required to obtain an updated risk map.

Shrestha, et al., (2017), also predicted that Kathmandu valley is at low risk through a model-based estimation of land subsidence. Even though the prediction has not been validated, it resembles the result of this study.

Kathmandu valley is pristine in terms of land subsidence related research. Due to lack of proper scientific data and research, evidence of damage caused by land subsidence has not been reported in Kathmandu valley till date. Case studies from around the world can be referred to utilize the knowledge and experience in planning and policy making to reduce if not prevent the disastrous effect of land subsidence. The location of Kathmandu valley has a very close resemblance with the location of Mexico City where land subsidence has been documented very well. Hence, case study of land subsidence in Mexico City is discussed here.

Comparison with case study of Mexico City:

Mexico City is the capital city of Mexico located in the valley of Mexico Basin. It is surrounded by volcanic chain and mountains with elevations reaching up to 5000 m (NRC staff, 1995). Like the origin of Kathmandu Valley, Mexico City emerged where there was once Lake Texcoco, therefore the geology consists of highly saturated clay (Maricela et al., 2002). The geology is classified into three zones namely Foothill zone, Transition zone and Lake zone. The Foothill zone comprises heterogeneous volcanic deposits and lava. The Transition zone mainly comprises of sand and gravel alluvial deposits along with volcanic materials. The lake zone comprises of highly compressible lacustrine clays (Yan et al., 2012).

The city has been suffering from groundwater extraction related subsidence since decades (Cabral-Cano et al., 2012). The city has been reported with subsidence reaching up to 38 cm/yr. (Yan et al., 2012). The main cause has been identified to be the drying and compaction of soft clay layers which has less permeable capacity and is mainly triggered by excessive groundwater exploitation from the aquifers (Lapez-Quiroz et al., 2012).

The main problems reported relating to land subsidence in Mexico City are

- decrease in runoff and wastewater drainage ability, that ultimately results in flooding during rainy season (Maricela et al., 2002).
- Disruption to the water transportation structures (i.e. pipelines, canals) resulting in interference with water supply (Yan et al., 2012)
- Damage to the stability of manmade infrastructure (Buildings, transportation facilities like highways, roads and bridges) due to changes in surface gradients (Yan et al., 2012)

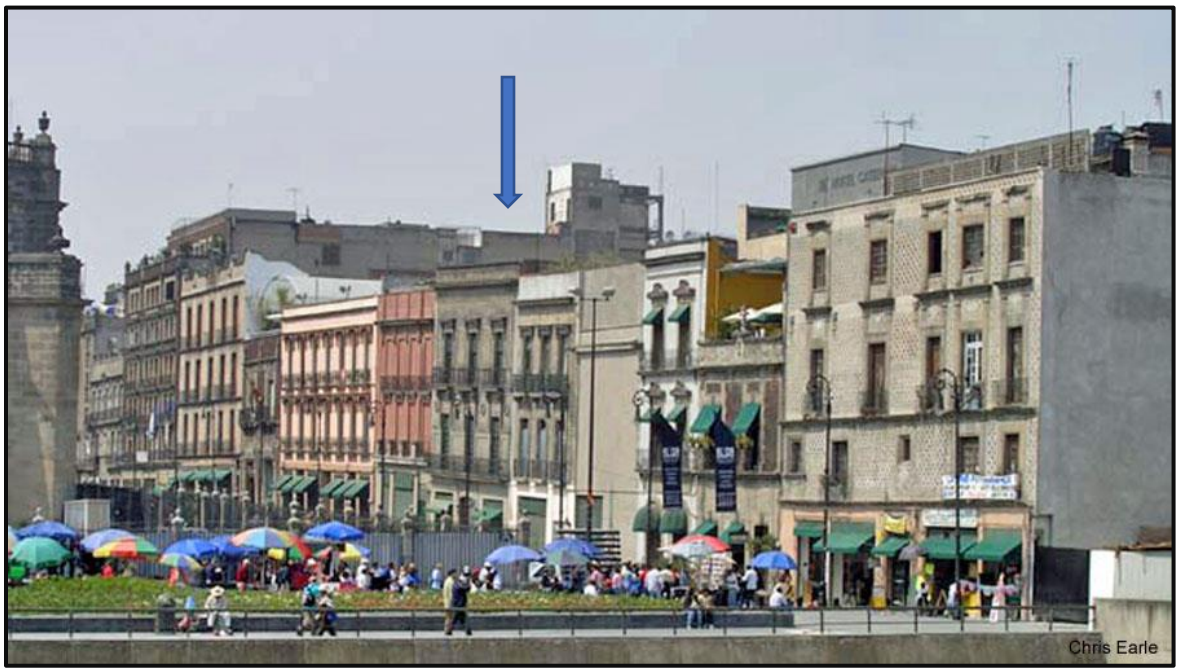

Figure 4.17 Buildings in Mexico City displaying wave pattern from left to right as a result of long term groundwater extraction induced land subsidence. (Source: Conifer-Hunting in Mexico, USGS, 2016)

Since, there is a close resemblance in Kathmandu Valley and Mexico City, it can be expected that these problems may be encountered in Kathmandu Valley in near future if current situations prevail. The high-risk areas indicated by red color in **Figure 4.15**, Central Kathmandu and Lalitpur which are the main urban core of the valley has the highest probability to suffer from such damages. Other locations that are at medium risk to such damages are Chauni, Imadol, Thimi, Madhyapur Thimi, New Baneshwor and Koteshwor and Gothatar. Since, these damages are not limited to a point location, the periphery areas are also bound to suffer. **Figure 4.18** shows inundated roads in some of the parts of Kathmandu valley, the actual cause of which are unknown. However, this

research has detected subsidence in the site of the pictures taken and comparing with the case of Mexico City, this reduction in rainwater drainage ability could be a result of land subsidence. Further detailed study might be able to find the actual cause of this inundation.

Figure 4.18 Pictures published in the Nepalese national newspapers showing **(a)** Inundated road in Putalisadak, Kathmandu **(Location L1),** on June 28th, 2016. **(b)** Inundated road in Jamal, Kathmandu **(Location L1). (c)** A waterlogged road in Jawalakhel, Lalitpur district **(Location L3),** on August 1st, 2016.

Comparison with case study of Japan:

Japan has a very long history of Land subsidence. From the beginning of the 20th century, land subsidence has damaged buildings and public property like open channels, levees and bridges (Sato et al., 2003). The main cause of land subsidence in Japan has been identified to be excessive

groundwater pumping in areas where soft ground is present (Hirono and Wadati, 1939). Ever since the problem was identified many surveys and research were done to investigate the situation and find the exact cause. Repeated precise levelling were done in various locations; observation wells that could also record the compaction were constructed; soil tests were conducted; a series of 5-year land subsidence explorations were carried out; industrial groundwater extraction amounts were surveyed; regional hydrogeological surveys were conducted; geological and hydrogeological maps were constructed (Inaba et al., 1969). All these surveys and research results made Japan data rich in terms of land subsidence issues. Therefore, they were able to the reduce and prevent land subsidence in some of the areas by enacting the "Industrial Water Law (1956)" and "Law concerning the regulation of pumping up of underground water for use in buildings (1962)". Additionally, counter measures like development of surface water resource and voluntary saving of ground water were also implemented (Sato, 2001). Even though, subsidence is reduced to some extent, it increases temporarily during dry years when the surface water is in short supply and the ground water demand is high. Currently, the Basic Environment Law of Japan has categorized land subsidence as a public nuisance and is treating it as a social problem.

Although, Japan has been successful to reduce land subsidence and gather enough information; continuous monitoring is still being done employing new technologies for increased efficiency.

On the other hand, Nepal is very new to the issue of land subsidence and lags in terms of data availability to address this issue. However, utilizing the learnings and experiences of Japan can be beneficial for Nepal not only to monitor the subsidence but also to reduce and prevent the problem.

5. CONCLUSION AND RECOMMENDATION

5.1 Conclusion

This study is the first to detect the current situation of land subsidence in Kathmandu Valley, Nepal by the application of Differential Synthetic Aperture Radar Interferometry (D-InSAR) technique to Advanced Land Observation Satellite Phased L-band SAR (ALOS- PALSAR) data along with risk assessment of land subsidence using Geographic Information System (GIS).

Most of the subsidence was found to have occurred in the center of the valley where the population density is relatively higher than the surrounding. Majority of the subsidence region comprised of mixed used development areas, where ground water extractions can be assumed to be in higher levels. Also, the locations where land subsidence is identified are the locations where rapid urbanization is taking place. Subsidence volume for each location was also derived by application of a simple mathematical formula which was further used for assessing the subsidence risk.

The generated subsidence map was further studied on the basis of groundwater extraction and geology of Kathmandu valley. It was found that the concentration of groundwater discharge units was higher in locations detected with high amounts of subsidence. However, in order to get a precise relationship between groundwater extraction and subsidence a more exquisitely detailed study including the recharge ability of the aquifer should also be conducted. Analysis of subsidence based on geology revealed that subsidence occurred in locations mostly comprising of unconsolidated fine-grained sediments (silica, sand, silt, clay and silty sandy gravel).

Land subsidence was also mapped after the devastating 2015 Gorkha Earthquake event using ALOS 2 PALSAR 2 data to see if it had any effect in the subsidence observed before the event. No difference was found in the location of subsidence occurrence. However, a little change in velocity and area covered were observed.

Land subsidence risk assessment based on current data revealed that the identified subsidence areas are at high and medium risk of suffering from subsidence induced damages like decrease in runoff

and wastewater drainage ability, disruption to water transportation structures and damage artificial infrastructure stability whereas the rest of the Kathmandu valley is at low risk under the circumstance that similar conditions prevail.

The outcomes of this research exhibit the advantage of DInSAR technique in detecting land subsidence and further utilizing the results for risk assessment. It was found that applying DInSAR technique over conventional ground measurement methods to complex terrain with difficult accessibility provides effective and inexpensive method for disaster identification and monitoring. Also, it was found that analyzing the results using AHP and GIS tools gave a much better perspective.

Land subsidence is a very complex phenomenon affected by various factors and very little study has been done in Nepal as of now. Therefore, the outcomes of this research even though it is not directly validated and produced with limited data; can be used as a base for further detailed study. The results could also serve beneficial for developing disaster prevention policy.

5.2 Recommendation for future research

DInSAR was applied to ALOS PALSAR data to detect land subsidence in Kathmandu valley because ALOS PALSAR covers a large area and since no study relating to land subsidence was conducted previously in the study area, it would serve as a best option to identify subsidence zones. Now, that this study reveals the areas affected by subsidence, Persistent Scatterer InSAR technique can be used to obtain subsidence values in the affected areas with millimetre accuracy. Also, other SAR data with fewer wavelengths like X- band or C- band can be used to focus on the area most affected.

Also, in this study, only a few pairs of SAR data were used, using more pairs of SAR data would provide better coherence resulting in more accurate outcomes.

Using detailed groundwater extraction data along with recharge ability of the aquifer, thickness and speed of the consolidation process of the sediments would provide precise information about subsidence.

In addition, a more comprehensive risk assessment of land subsidence can be done by considering other indicators like the geological characteristics and land use type of the location. This would give a more detailed outlook on factors that can be controlled to reduce if not prevent a huge disaster. Also, in this study, it was assumed that the study area had no capacity for disaster prevention and reduction for risk assessment. However, different case scenarios like with government action to reduce groundwater exploitation and with government action to reduce or prevent construction land proportion can be employed to judge the situation in a different perspective.

PUBLISHED PAPERS

International Journal

1. **Richa Bhattarai**, Haireti Alifu, Aikebaier Maitiniyazi and Akihiko Kondoh (2017) "Detection of Land Subsidence in Kathmandu Valley, Nepal, using DInSAR Technique". Land, Volume 6(2):39. doi:10.3390/land6020039

2. **Richa Bhattarai,** Akihiko Kondoh, (2017) "Risk Assessment of Land Subsidence in Kathmandu Valley, Nepal using Remote Sensing and GIS", Advances in Remote Sensing, 6, 132-146. Doi: 10.4236/ars.2017.62010

3. Toshiyuki Kobayashi, Ryutaro Tateishi, Bayan Alsaaideh, Ram C. Sharma, Takuma Wakaizumi, Daichi Miyamoto, Xiulian Bai, Bui D. Long, Gegentana Gegentana, Aikebaier Maitiniyazi, Destika Cahyana, Alifu Haireti, Yohei Morifuji, Gulijianati Abake, Rendy Pratama, Naijia Zhang, Zilaitigu Alifu, Tomohiro Shirahata, Lan Mi, Kotaro Iizuka, Aimaiti Yusupujiang, Fedri R. Rinawan, **Richa Bhattarai**, Dong X. Phong (2017) " Production of Global Land Cover Data- GLCNMO2013" Journal of Geography and Geology, Volume 9, No. 3 DOI: https://doi.org/10.5539/jgg.v9n3p1

Symposium and Conference

1. Nikhil R. Poudyal, Ryutaro Tateishi and **Richa Bhattarai**, "Monitoring glacier flow velocity by SAR Interferometry using ALOS PALSAR data around Mt. Everest Region", Proc. the 55th RSSJ conference, pp. 99-100, Koriyama, Japan, November 21-22, 2013

2. **Richa Bhattarai**, Ryutaro Tateishi and Nikhil Raj Poudyal, " Land Subsidence Mapping and Risk Assessment in Nepal Using D-InSAR Technique", Proceeding of the International Symposium on Remote Sensing (ISRS), pp. 674-677, Busan, Korea, April 16-18, 2014.

3. **Richa Bhattarai** and Ryutaro Tateishi, "Remote Sensing Application to Map Land Subsidence in Kathmandu Valley, Nepal", Proceeding of International Symposium on Remote Sensing (ISRS), Tainan, Taiwan, April 22-24, 2015. (**Winner of the "Best Student Paper Award")**

4. Bai Xiulian, Ryutaro Tateishi, Bayan Alsaaideh and **Richa Bhattarai**, "Bare Area Mapping for Continental Scale by using MODIS Data", Proceeding of International Symposium on Remote Sensing (ISRS), Tainan, Taiwan, April 22-24, 2015.

5. **Richa Bhattarai**, Haireti Alifu, Akihiko Kondoh, Ryutaro Tateishi, "Risk Assessment of Land Subsidence in Kathmandu Valley, Nepal", Proceeding of the 7th Indonesia Japan Joint Scientific Symposium (IJJSS), pp. 467- 472, Chiba, Japan. November 20-24, 2016. (**Winner of "Best Presenter Award**")

References:

Abidin, H.Z., Djaja, R., Darmawan, D., Hadi, S., Akbar, A., Rajiyowiryono, H., Sudibyo, Y., Meilano, I., Kasuma, M.A., Kahar, J., Subarya, C. (2001). *Land subsidence of Jakarta (Indonesia) and its geodetic monitoring system*. Nat Hazards 23(2–3):365–387.

ADPC. *Introduction to Hazards, Vulnerability and Risk.* Asian Disaster Preparedness Center, Training and Education Division. Retrieved on May 19, 2017 from www.adpc.net/casita/Bangkok.../Introduction_to_Hazard_Vulnerability_and_Risk.pdf

Adrian, O.G., Rudolph, L.D., Cherry, A.J. (1999). *Analysis of long-term land subsidence near Mexico City: field investigations and predictive modelling*. Water Resource Res 35(11):3327–3341.

Anderssohn, J., Wetzel, H-U., Walter, T.R., Motagh, M., Djamour, Y., Kaufmann, H. (2008). *Land Subsidence Pattern Controlled by Old Alpine Basement Faults in the Kashmar Valley, Northeast Iran: Results from InSAR and Levelling.* Geophysical Journal International. Vol. 174(1): pp. 287-294.

Ardiansyah (2013). *Tutorial Insar Menggunakan Sarscape.* Department of Geography, University of Indonesia (In Indonesian Language), pp. 8.

Autin, W. J. (2002). Landscape evolution of the five islands of south Louisiana: scientific policy and salt dome utilization and management. Geomorphology 47(2-4), pp. 227-244.

Bamler, R. (2000). *Principles of Synthetic Aperture Radar*. Surveys in Geophysics 21, pp 147-157.

Bankher, K. A. and Al-Harthi, A. A. (1999). *Earth fissuring and land subsidence in Western Saudi Arabia.* Natural Hazards, 20(1), pp. 21-42.

Bayuaji, L., Josaphat, T.S.S. and Kuze, H. (2010). *ALOS PALSAR D-InSAR for land subsidence mapping in Jakarta, Indonesia.* Can. J. Remote Sensing, Vol. 36, No.1, pp. 1-8.

Bergado, D. T., Nutalaya, P., Balasubramaniam, A. S., Apaipong, W., Chang, C. C. and Khaw, L.G. (1987). *Causes, effects and predictions of land subsidence in AIT campus Chao Phraya Plain, Bangkok, Thailand*. Bull Assoc Eng Geol 25(1):57-81.

Bell, F. G., Cripps, J. C., Culshaw, M. G. (1986). *A review of the engineering behavior of soils and rocks with respect to groundwater.* In: Groundwater in engineering geology. Geol Soc Eng Geol Spec, 3, pp. 1-23

Bolotin, V. V. (1993). *Sesmic risk assessment for structures with the Monte Carlo simulation. Probabilistic Engineering Mechanics*, vol. 8, issues 3-4, pp. 169-177.

Bonì, R., Herrera, G., Meisina, C., Notti, D., Béjar-Pizarro, M., Zucca, F., González, P. J., Palano, M., Tomás, R., Fernández, J., Fernández-Merodo, J. A., Mulas, J., Aragon, R., Guardiola-Albert, C. and Mora, O. (2015). *Twenty-year advanced DInSAR analysis of severe land subsidence: The Alto Guadalentín Basin (Spain) case study.* Engineering Geology, Vol. 198, pp. 40-52

Brabb, E. E. (1984). *Innovation approaches to landslide hazard and risk mapping.* Proceedings of 4th ISL, Torronto, pp. 307-323.

Budhu, M., Adiyaman, I. B. (2010). *Mechanics of land subsidence due to groundwater pumping.* Int. J. Numer. Anal. Methods Geomech, 34, 1459–1478.

Burgmann, R., Rosen, P. A. and Fielding, E. J. (2000). *Synthetic Aperture Radar Interferometry to measure Earth's surface topography and its deformation.* Annual Review of Earth and Planetary Sciences, 28, pp. 41.

Cabral-Cano, E., Solano-Rojas, D., HernÃ¡ndez-Espriu, J., Cigna, F., Wdowinski, S., Osmanoglu, B., Falorni, G., Bohane, A. and Colombo, D. (2012). *Subsidence Induced Faulting Hazard risk maps in Mexico City and Morelia, central Mexico.* NASA Astrophysics Data System (ADS).

CBS (2012). *National population and housing census*. National Report. Kathmandu: Central Bureau of Statistics.

Chatterjee, R. S., Fruneau, B., Rudant, J. P., Roy, P. S., Frison, P., Lakhera, R. C., Dadhwal, V. K., Saha, R. (2006). *Subsidence of Kolkata (Calcutta) City, India during the 1990s as observed from space by Differential Synthetic Aperture Radar Interferometry (D-InSAR) technique.* Remote Sensing of Environment 102, pp. 176-185

Chen, Y., Shu, L., Burbey, T. J. (2013). *Composite subsidence vulnerability assessment based on an index model and index decomposition method.* Human and Ecological Risk Assessment: An International Journal, 19:3, 674-698, DOI: 10.1080/10807039.2012.691405.

Chen, Y., Shu, L., Burbey, T. J. (2014). *An Integrated Risk Assessment Model of Township-Scaled Land Subsidence Based on an Evidential Reasoning Algorithm and Fuzzy Set Theory*. Risk Analysis, Vol. 34, No. 4.

CNES/ESA/ ESRIN study (2000). *The Izmit Earthquake of 17 August 1999 in Turkey.* Journal of Technical and Environmental Geology, issue no. 3

Colesanti, C., Ferretti, A., Prati, C., Rocca, F. (2003). *Monitoring landslides and tectonic motions with the permanent scatterers technique.* Eng. Geol. 68:3-14.

Colesanti, C., Wasowski, J. (2006). *Investigating landslides with space-borne Synthetic Aperture Radar (SAR) interferometry*. Eng. Geol. 88(3-4), pp. 173-199.

Corapcioglu, M. Y. (1989). Land subsidence: a state of art review. Fundamentals of transport phenomena in porous media. ASI series. Martinus Nijhott Publishers, Dordrecht, pp. 369-444.

Crosetto, M., CRippa, B., Biescas, E., Monserrat, O., Agudo, M., Fernandez, P. (2005). *Land deformation monitoring using SAR interferometry: state-of-the-art.* Photogramm Fernerkundung, Geoinformation, 6:497-510.

Curlander, J.C., McDonough, R.N. (1991). *Synthetic aperture radar: systems and signal processing.* Wiley- Interscience, Toronto, Ont.

Diao, F., Walter, T. R., Motagh, M., Prats-Iraola, P., Wang, R., and Samsonov, S. V. (2015). *The 2015 Gorkha earthquake investigated from radar satellites: slip and stress modeling along the MHT.* Front. Earth Sci.. https://doi.org/10.3389/feart.2015.00065

DLR news (2015). *Disaster relief – DLR provides aerial image of Kathmandu*. German Aerospace Center. URL: http://www.dlr.de/dlr/en/desktopdefault.aspx/tabid-10081/151_read-13487/#/gallery/19391.

Elliott, J. R., Jolivet, R., Gonzalez, P.J., Avouac, J. P., Hollingswort, J., Searle, M. P. and Stevens, V. L. (2016). *Himalayan megathrust geometry and relation to topography revealed by the Gorkha earthquake.* Nature Geoscience, 9, pp.174–180. Doi:10.1038/ngeo2623

European Commission (2010). *Commission staff working paper: Risk assessment and mapping guidelines for disaster management.* Brussels, (21.12.2010). Retrieved on 14 June 2017 fromhttps://www.google.co.jp/search?q=Risk+Assessment+and+Mapping+Guidelines+for+Disaster+Management&oq=Risk+Assessment+and+Mapping+Guidelines+for+Disaster+Management&aqs=chrome..69i57j0l2.1125j0j7&sourceid=chrome&ie=UTF-8#

Exelis (2007). *Help article*: *Estimating the appropriate number of looks when multilooking images in SARSCAPE*.

URL: http://www.harrisgeospatial.com/Support/HelpArticles/TabId/185/ArtMID/800/ArticleID/4265/4265.aspx

Faunt, C. C., Sneed, M., Traum, J., Brandth, J. T. (2015). *Water availability and land subsidence in Central Valley, California, USA*. Hydrogeology Journal. DOI 10.1007/s10040-015-1339-x

Ferretti, A., Prati, C., Rocca, F. (2001) *Permanent scatterers in SAR interferometry*. IEEE Trans Geosci Remote Sensing 39(1), pp 8-20.

Gabriel, A. K., Goldstein, R. M. and Zebker, H. A. (1989). *Mapping small elevation changes over large areas: Differential Radar Interferometry*. J. Geophysics. Res., 94.

Gabrysch, R.K., Neighbors RJ. (2000). *Land-surface subsidence and its control in the Houston-Galveston region, TX, 1906–1995*. In: Proceedings 6th international symposium. Land Subsidence, Ravenna, Italy, September 2:81–92.

Galloway, D. L., Hudnut, K., W., Ingebritsen, S. E., Phillips, S., P., Peltzer, G., Rogez, F. and Rosen, P. A. (1998). *Detection of aquifer system compaction and land subsidence using interferometric synthetic aperture radar, Antelope Valley, Mojave Desert, California.* Water Resources Research, Vol. 34, No. 10, pp. 2573-2585.

Galloway, D. L., Burbey, T. J. (2011). *Review: Regional land subsidence accompanying groundwater extraction*. Hydrogeol. J. 19, 1459–1486.

Gautam, D., Prajapati, R. N. (2014). *Drawdown and Dynamics of Groundwater Table in Kathmandu Valley, Nepal*. The Open Hydrology Journal, 8, pp. 17-26.

Gens, R. and Van Genderen, J. L. (1996). *Review Article SAR interferometry issues, techniques, applications*. International Journal of Remote Sensing, 17, pp. 1803-1835.

Gibilisco, S. (2006). *Technical Math Demystified*, United Sates of America, McGraw-Hill Professional, 1st edition, pp.191-196

Goldstein, R. M., Engelhardt, H., Kamb, B., Frolich, R. M. (1993). *Satellite radar interferometry for monitoring ice sheet motion: application to an Antarctic ice streamy*. Science, 262 (5139), pp. 1525–1530, doi:10.1126/science.262.5139.1525, PMID 17829380

Goldstein, R.M., Werner, C.L. (1998). *Radar interferogram filtering for geophysical applications*. Geophysical research letters, Vol. 25, pp. 4035-4038

Graham, L. C. (1974). *Synthetic Interferometer Radar for Topographic Mapping.* Proceedings of the IEEE, Vol. 62, No. 6, pp. 763.

Guzzetti, F., Manunta M., Ardizzone, F., Pepe, A., Cardinali, M., Zeni, G., Reichenbach, P., Lanari, R. (2009). *Analysis of ground deformation detected using the SBAS-DInSAR technique in Umbria, Central Italy*. Pure Appl Geophys. 166:1425-1459

Hanssen, R. F. (2002). *Radar Interferometry: Data Interpretation and Error Analysis*. Kluwer Academic Publishers, New York. Vol 2. pp 43

Heath, R.C. and Spruill, R.K. (2003). *Cretaceous aquifers in North Carolina: analysis of safe yields based on historical data.* Hydrogeol J. 11:249-258

Herrera, G., Tomás, R., Vicente, F., Lopez-Sanchez, J. M., Mallorquí, J. J., Mulas, J. (2010). *Mapping ground movements in open pit mining areas using differential SAR interferometry*. International Journal of Rock Mechanics and Mining Sciences. 47 (7): 1114–1125. Doi: 10.1016/j.ijrmms.2010.07.006.

Hirono, T. and Wadati, K. (1939). *On the land subsidence in western Osaka (1*). Report of the Research Institute for Disaster Prevention. Osaka, Japan. (In Japanese)

Holzer, T. L. (1984). *Ground failure induced by ground-water withdrawal from unconsolidated sediments.* Geol. Soc. Am. Rev. Eng. Geol. VI, 67–105.

Holzer, T. L. and Galloway, D.L. (2005). *Impacts of land subsidence caused by withdrawal of underground fluids in the United States.* Rev. Engineering Geology., XVI, pp. 87–99.

Hooper, A., Bekaert, D., Spaans, K., Arikan, M. (2012). *Recent advances in SAR interferometry time series analysis for measuring crustal deformation.* Tectonophysics 514-517:1-13.

Hu, B., Jiang, Y., Zhou, J. (2008). *Assessment and zonation of land subsidence disaster risk of Tianjin Binhai area.* Sci. Geogr. Sin., Vol. 28, pp. 693-697.

Hu, B., Wang, J., Chen, Z., Wang, D., Xu, S. (2009). *Risk assessment of land subsidence at Tianjin coastal area in China*. Environ Earth Sci 59, pp. 269-276.

Hu, J.C., Chu, H.T., Hou, C.S., Lai, T.H., Chen, R.F., Nien, P.F. (2006). *The contribution to tectonic subsidence by groundwater abstraction in the Pingtung area, southwestern Taiwan as determined by GPS measurements*. Quatern Int 147:62-69.

Hu, J., Li, Z-W., Li, J., Zhang, L., Ding, X-L., Zhu, J-J., Sun, Q. (2014). *3-D movement mapping of the alpine glacier in Qinghai-Tibetan Plateau by integrating D-InSAR, MAI and Offset-Tracking: Case study of the Dongkemadi Glacier*. Global and Planetary Change, Volume 118, Pp. 62-68

ICIMOD (2007). Kathmandu valley environmental outlook. ISBN 9789291150199.

Inaba, Y., Abe, I., Iwasaki, S., Aoki, S., Endo, T. and Kaido R. (1969). *Review of Land Subsidence Researches in Tokyo*. Land Subsidence, Proceeding of Tokyo Symposium, Vol. 1, pp. 87-98.

Jackson, J. A. (1997). Glossary of geology, 4th edition, American Geological Institute, Alexandria.

Jebur, M. N., Pradhan, B. and Tehrany, M. S. (2013). *Using ALOS PALSAR derived high-resolution DInSAR to detect slow-moving landslides in tropical forests: Cameron Highlands, Malaysia*. Geomatics, Natural Hazards and Risk. http://dx.doi.org/10.1080/19475705.2013.860407.

Kampes, B. M. (2006). Radar Interferometry: Persistent Scatterrer Technique. Remote Sensing and Digital Image Processing. Springer, Vol. 12

Kappel, W.M., Yager, R.M., Todd, M.S. (1999). The Retsof Salt Mine Collapse. In: Galloway, D.L., Jones, D. R., Ingebritsen, S.E. (eds) Land Subsidence in United States, vol. 1182., US Geological Survey, Reston, pp. 111-120.

Katel, T.P., Upreti, B.N., Pokharel, G.S., (1996). *Engineering properties of fine grained soils of Kathmandu Valley Nepal*. Journal of Nepal Geological Society 13, 121– 138

Kayastha, P., Dhital, M. R., Smedt, F. D. (2013). *Application of the analytical hierarchy process (AHP) for landslide susceptibility mapping: A case study from the Tinau watershed, west Nepal.* Computers and Geosciences, Vol. 52, pp. 398-408.

Kobayashi, T., Morishita, Y. and Yarai, H. (2015). *Detailed crustal deformation and fault rupture of 2015 Gorkha earthquake, Nepal, revealed from ScanSAR-based interferograms of ALOS-2*. Earth, Planets and Space, 67:201

Lagios, E., Sakkas, V., Parcharidis, I. S., Dietrich, V. (2005). *Ground deformation of Nisyros Volcano (Greece) for the period 1995-2002: results from DInSAR and DGPS observations.* Bull Volcanol. 68.201-214.

Lanari, R., Casu, F., Manzo, M., Zeni, G. Berardino, P., Manunta, M., Pepe, A. (2007*). An overview of the small baseline subset algorithm: A DInSAR technique for surface deformation analysis.* Pageoph Topical Volumes. Pp. 637-661.

Lapez-Quiroz, P., Doin, M., Carreon-Freyre, D. and Cerca, M. (2012). *Analysis of nonlinear and subsidence in Mexico city lacustrine plain.* NASA Astrophysics Data System (ADS)

Lirer, L. and Vitelli, L. (1998) *Volcanic risk assessment and mapping in the Vesuvian area using GIS*. Nat Hazards 17:1-15

Liu, J., Wang, H. and Yan, X. (2015). *Risk evaluation of land subsidence and its application to metro safety operation in Shanghai.* Proc. International Association of Hydrological Sciences (IAHS), 372, 543–553, doi:10.5194/piahs-372-543-2015

Maricela, Y., Pierre, M. (2002). *Air Pollution in Mexico City*. Project study paper, University of Salzburg, Austria. URL: http://biophysics.sbg.ac.at/mexico/air.htm

Martínez, J. P., Cabral-Cano, E., Wdowinski, S., Marín, M. H., Ortiz-Lozano, J. A., and Zermeño-de-León, M. E. (2015). *Application of InSAR and Gravimetry for Land Subsidence Hazard Zoning in Aguascalientes, Mexico.* Remote Sensing, 7, pp. 17035-17050

Massonnet, D., Briole, P., Arnaud, A. (1995), "*Deflation of Mount Etna monitored by spaceborne radar interferometry"*, Nature, 375 (6532), pp. 567–570, doi:10.1038/375567a0

Massonnet, D., Rossi, M., Carmona, C., Adragna, F., Peltzer, G., Feigl, K., Rabaute, T. (1993). *The displacement field of the Landers earthquake mapped by radar interferometry.* Nature, 364:138-142

Massonnet, D. and Feigl, K. L. (1998). *Radar Interferometry and its Application to Changes in the Earth's Surface*. Reviews of Geophysics, 36, pp.60.

Meizner, O.E. (1928). *Compressibility and elasticity of artesian aquifers*. Economic Geology. 23 (3): 263-291.

Metcalf and Eddy (2000). *Urban water supply reforms in the Kathmandu valley (ADB TA Number 2998-NEP),* Completion report. Volume I and II. Metcalf and Eddy, Inc with CEMAT Consultants Ltd., Monitoring and Evaluation Studies. *Disaster Risk Assessment Process.*

Retrieved on June 14, 2017, from http://www.mnestudies.com/disaster-management/disaster-risk-assessment-process.

Moribayashi, S. and Maruo, Y. (1980). *Basement Topography of Kathmandu Valley, Nepal -An application of gravitational method to the survey of a tectonic basin in the Himalayas*. Journal of the Japan Society of Engineering Geology 21-2, pp. 30-37.

Motagh, M., Walter, T. R., Sharifi, M. A., Fielding, E., Schenk, A., Anderssohn, J. and Zschau, J. (2008). *Land Subsidence in Iran caused by widespread water reservoir overexploitation.* Geophysical Research Letters, Vol. 35, LI6403

National Research Council Staff (1995). *Mexico City's Water Supply: Improving the Outlook for Sustainability*. Washington, D.C., USA: National Academies Press. ISBN 978-0-309-05245-0.

Nakagawa, H., Murakami, M., Fujiwara, S. and Tobita, M. (1999). *Land subsidence of Northern Kanto Plains detected by JERS-1 SAR Interferometry*. Journal of the Geodetic Society of Japan, 45, 347-350 (In Japanese with English Abstract).

Nautiyal, S. P., Sharma, P.N. (1961). *A Geological Report on the Groundwater Investigation of Kathmandu Valley*. Unpublished work.

Palà, V., Mora, O., Arbiol, R., Marturià, J. (2006). *Products derived from an advanced DInSAR-GIS application for risk management*. In: ISPRS (ed) Geospatial database for sustainable development. Goa, pp. 5.

Pandey, M. R. (2016). *Ground response of Kathmandu valley on the basis of microtremors.* World Conference on Earthquake Engineering.
URL: http://www.iitk.ac.in/nicee/wcee/article/2106.pdf

Pandey, V. P. and Kazama, F. (2011). *Hydrogeologic characteristics of groundwater aquifers in Kathmandu Valley, Nepal.* Environmental Earth Sciences 62(8): 1723-1732

Pandey, V. P., Shrestha, S., Kazama, F. (2012). *Groundwater in the Kathmandu Valley: Development dynamics, consequences and prospects for sustainable management*. European Water 37, pp. 3-14.

Paudyal, Y. R., Yatabe, R., Bhandary, N. P. and Dahal, R. K. (2013). *Basement topography of the Kathmandu Basin using microtremor observation.* Journal of Asian Earth Sciences. Vol. 62, pp. 627-637.

Perlman, H. (2016) *Land Subsidence.* United States Geological Survey. URL: http://water.usgs.gov/edu/earthgwlandsubside.html

Pezzo, G., Boncori, J. P. M., Atzori, S., Antonioli, D. P. A., Salvi, S. (2014). *The 2013 Lunigiana (Central Italy) earthquake: Seismic source analysis from DInSAR and seismological data, and geodynamical implications for the northern Apennines*. Tectonophysics, Volume 636, pp. 315-324

Phien-wej, N., Giao, P. H. and Nutalaya, P. (2006) *Land subsidence in Bangkok, Thailand*. Eng Geol 82:187-201.

Piya, B. K. (2004). *Generation of a Geological Database for the Liquefaction hazard assessment in Kathmandu Valley*. Master of Science thesis submitted to International Institute for Geo-Information Science and Earth Observation. The Netherlands.

Poland, J. F., Davis, G. H. (1969). *Land subsidence due to withdrawal of fluids*. In: Reviews in engineering geology, vol2. Geological Society of America, Boulder, pp 187-269

Pradhanang, S. M., Shrestha, S. D. and Steenhuis, T.S. (2012). *Comprehensive review of groundwater research in the Kathmandu valley, Nepal*. Kathmandu valley Groundwater Outlook, Kathmandu: AIT/SEN/CREEW/ICRE-UY, pp. 6-18.

Prati, C., Ferretti, A., Perissin, D. (2010). Recent advances on the surface ground deformation measurement by means of repeated space borne SAR observations. J Geodyn 49(3-4), pp. 161-170.

Pratt, W. E., Johnson, D. W. (1926). *Local subsidence of the Goose Creek oil field*. J. Geol 34:577-590

Rana, G., Murray, A., Maharjan, D., Thaku, A., (2007). *Kathmandu Valley environment outlook.* Kathmandu: International Centre for Integrated Mountain Development (ICIMOD). ISBN 9789291150199.

Raucoules, D., Colesanti, C. and Carnec, C. (2007). *Use of SAR Interferometry for detecting and assessing ground subsidence*. Comptes Rendus Geosciences, 339, pp. 289-302.

Remondo, J., Bonachea, J., Cendrero, A. (2008). *Quantitative landslide risk assessment and mapping on the basis of recent occurrences*. Geomorphology, vol. 94, issues 3-4, pp. 496-507.

Rocca, F., Prati, C., Monti Guarnieri, A. and Ferretti, A. (2000). *SAR Interferometry and its Applications*. Surveys in Geophysics, 21, pp. 159-176.

Rosen, P. A., Hensley, S., Zebker, H. A., Webb, F. H., Fielding, E. J. (1996), "*Surface deformation and coherence measurements of Kilauea Volcano, Hawaii, from SIR C radar interferometry*", J. Geophys. Res., 101 (E10), pp. 23,109–23,126, doi:10.1029/96JE01459

RSLUP Report (2015). *Support to develop Risk Sensitive Land Use Plan and Building Bye-Laws of Kathmandu Valley*. UNDP, Nepal. Comprehensive Disaster Risk Management Programme, pp. 6.

Saaty, T.L. (1980). *The analytic hierarchy process*. McGraw-Hill, New York.

Sakai, H., Fujii, R., Kuwahara, Y., Upreti, B. N. and Shrestha, S. (2001). *Core drilling of the basin-fill sediments in the Kathmandu Valley for paleoclimatic study: preliminary results*. J. Nepal Geol. Soc., 25, Special Issue, 9-18.

Sakai, H., Fujii, R., Kuwahara, Y., (2002). Changes in the depositional system of the Paleo-Kathmandu Lake caused by uplift of the Nepal Lesser Himalayas. Journal of Asian Earth Sciences 20, 267–276.

Sakai, H. (2015). *The tectonics of the 2015 Nepal earthquake and the extremely soft ground of Kathmandu*. Geological Society of Japan (Retrieved from www.eri.u-tokyo.ac.jp/ on 2017/5/16) (In Japanese)

SAR Guidebook. Available online: www.sarmap.ch/pdf/SAR-Guidebook.pdf

Sato, H.P. (2001). *Current status of land subsidence in Japan*. Bulletin of GSI, Vol 47, 5, pp. 35-45

Sato, H. P., Abe, K. and Ootaki, O. (2003). *GPS- measured land subsidence in Ojiya City, Niigata Prefecture, Japan.* Engineering Geology, 67, pp. 379-390.

Schlögel, R., Doubre, C., Malet, J-P., Masson, F. (2015). *Landslide deformation monitoring with ALOS/PALSAR imagery: A D-InSAR geomorphological interpretation method.* Geomorphology, Vol. 231, pp. 314-330

Shi, X. Q., Xue, Y. Q., Ye, S. J., Wu, J. C., Zhang, Y., Yu, J. (2007). *Characterization of land subsidence induced by groundwater withdrawals in Su-Xi -Chang area, China.* Environmental Geology 52:27-40

Shrestha, A. B., Eriksson, M., Mool, P., Ghimire, P., Mishra, B., Khanal, N. R. (2010). *Glacial lake outburst flood risk assessment of Sun Koshi basin, Nepal.* Geomatics, Natural Hazards and Risk, Vol. 1, Issue 2.

Shrestha, S. D., Karmacharya, R., Rao, G. K. (1996). Estimation of Groundwater Resources in Kathmandu Valley, Nepal- from the watertable fluctuation and the natural discharge-. Journal of the Japan Society of Underground Water, vol. 38, no. 1, pp. 29-40.

Shrestha, S. R. and Shah, S. (2014). *Shallow Aquifer Mapping of Kathmandu Valley*. Groundwater Resources Development Board, Babarmahal, Kathmandu. URL: http://www.academia.edu/27155659/Shallow_Aquifer_Mapping_of_Kathmandu_Valley.

Shrestha, P. K., Shakya, N. M., Pandey, V. P., Birkinshaw, S. J. and Shrestha, S. (2017). *Model-based estimation of land subsidence in Kathmandu Valley, Nepal.* Geomatics, Natural Hazards and Risk. URL: http://dx.doi.org/10.1080/19475705.2017.1289985

Shrestha, S., Semkuyu, D. J. and Pandey, V. P. (2016). *Assessment of groundwater vulnerability and risk to pollution in Kathmandu Valley, Nepal*. Science of the Total Environment 556, pp. 23-35

Shuchman, R., Schaub, D., Ruiter, J. (2005). *Radar Sensors for Transportation Applications of Restricted Use Technology Study*. Intelligent Transportation Systems. Interim Report.

Sneed, M., Ikeheara, M. E., Galloway, D.L. and Amelung, F. (2001). *Detection and Measurement of Land Subsidence Using Global Positioning System and Interferometric Synthetic Aperture Radar, Coachella Valley, California, 1996-98*. Water-Resources Investigations Report 01-4193

Stocklin, J. and Bhattarai, K. D. (1977). *Geology of Kathmandu Area and central Mahabharat Range, Nepal Himalaya*. HMG/UNDP Mineral Exploration Project, Kathmandu, Nepal.

Strozzi, T. and Wegmuller, U. (1999). *Land Subsidence in Mexico City mapped by ERS differential SAR interferometry*. Geoscience and Remote Sensing Symposium, 1999. IGARSS `99 Proceedings. IEEE 1999 International.

Teatini, P., Ferronato, M., Gambolati, G., Bertoni, W., Gonella, M. (2005). *A century of land subsidence in Ravenna, Italy*. Environ Geol 47:831–846.

Thrall, G.I. (2000). *Business Geography and New Real Estate Market Analysis*, Oxford University Press, pp. 216.

Tomás, R., García-Barba, J., Cano, M., Sanabria, M.P., Ivorra, S., Duro, J., Herrera, G. (2012). *Subsidence damage assessment of a gothic church using Differential Interferometry and field data.* Structural Health Monitoring. 11 (6): 751–762. doi:10.1177/1475921712451953.

Tomás, R., Li, Z., Liu, P., Singleton, A., Hoey, T., Cheng, X. (2014a). *Spatiotemporal characteristics of the Huangtupo landslide in the Three Gorges region (China) constrained by radar interferometry.* Geophysical Journal International. 197: pp. 213–232. Doi:10.1093/gji/ggu017.

Tomás, R., Romero, R., Mulas, J., Marturia, J. J., Mallorqui, J. J., Lopez-Sanchez, J. M., Herrera, G., Gutierrez, F., Gonzalez, P. J., Fernandez, J., Duque, S., Concha-Dimas, A., Coclsley, G., Castaneda, C., Carrasco, D., and Blanco, P. (2014b). *Radar interferometry techniques for the study of ground subsidence phenomena: a review of practical issues through cases in Spain.* Environ. Earth Sci., 71, pp. 163-181

Tsuji, T., Yamamoto, K., Matsuoka, T., Yamada, Y., Onishi, K., Bahar, A., Meilano, I. and Abidin, H. Z. (2009). *Earthquake fault of the 26 May 2006 Yogyakarta earthquake observed by SAR interferometry.* Earth Planets Space, 61, pp. e29-e32.

UNISDR (2009). UN International Strategy for Disaster Reduction Sec. Retrieved on June 14, 2017, from http://www.unisdr.org/we/inform/terminology

US Geological Survey (2015) M 7.8 - 36km E of Khudi, Nepal. (Retrieved on: 19 April, 2017) URL: https://earthquake.usgs.gov/earthquakes/eventpage/us20002926#executive

US Geological Survey (2017). *Land Subsidence: Cause and Effect.* (Retrieved on 21 April 2017). URL: https://ca.water.usgs.gov/land_subsidence/california-subsidence-cause-effect.html

Wang, G. L. (2006). Preliminary studies on dangerous grading standard of land subsidence. Shanghai Geol 4:39-43

Wang, J., Gao, W., Xu, S., Yu, L. (2012). *Evaluation of the combined risk of sea level rise, land subsidence and storm surges on the coastal areas of Shanghai, China*. Climatic Change 115:537-558

Wempen, J. M., McCarter, M. K. (2017). *Comparison of L-band and X-band differential interferometric synthetic aperture radar for mine subsidence monitoring in central Utah.* International Journal of Mining Science and Technology, Volume 27, Issue 1, pp. 159-163.

Westen, C. J., Montoya, L., Boerboom, L., Badilla E. C. (2002) *Multi-hazard risk assessment using GIS in urban areas: a case study for the city of Turrialba, Costa Rica*. In: Regional Workshop on Best Practices in Disaster Mitigation, 24-26 September 2002, Bali, Indonesia (pp. 120-136).

Westen, C. J., Alkema, D., Damen, M.C.J., Kerle, N. and Kingma, N.C. (2011) *Multi-hazard risk assessment*. Distance education course guide book, United Nations University – ITC School on Disaster Geo-Information Management (UNU-ITC DGIM).

Woodhouse, I. H. (2005). Introduction to Microwave Remote Sensing, The University of Edinburgh, Scotland, CRC press, pp. 281-282.

Xu, Y.S., Shen, S.L., Cai, Z.Y., Zhou, G.Y. (2008) *The state of land subsidence and prediction approaches due to groundwater withdrawal in China*. Nat Hazards 45:123-135.

Yamaguchi, R. (1969). *Water level change in the deep well of the University of Tokyo*. Bull Earthquake Res Inst No.47.

Yan, Y., Doin, M-P., Lopez-Quiroz, P., Tupin, F. (2012). *Mexico City subsidence measured by InSAR Time Series: Joint Analysis Using PS and SBAS Approaches*. IEEE Journal of Selected Topics in Applied Earth Observations and Remote Sensing, Vol. 5, No.4, pp. 1312-1326.

Yen, J. Y., Chen, K. S., Chang, C. P. and Boerner, W. M. (2008). *Evaluation of earthquake potential and surface deformation by Differential Interferometry*. Remote Sensing of Environment, 112, pp. 782-795.

Yerro, A., Corominas, J., Monells, D., Mallorqui, J.J. (2014). *Analysis of the evolution of ground movements in a low densely urban area by means of DInSAR technique*. Engineering Geology. Vol. 170, pp. 52-56.

Yu, B., Liu, G., Zhang, R., Jia, H., Li, T., Wang, X., Dai, K., Ma, D. (2013). *Monitoring subsidence rates along road network by persistent scatterer SAR interferometry with high-resolution TerraSAR-X imagery*. Journal of Modern Transportation. 21: 236–246. doi:10.1007/s40534-013-0030-y.

Yu, J., Wu, J., Wang, X. (2008). *Preliminary research on risk of land subsidence*. Geol. J. China University, 14, pp. 450-454.

Zebker, H. A., Goldstein, R. M. (1986). *Topographic Mapping from Interferometric Synthetic Aperture Radar Observations*. Journal of Geophysical Research. Vol. 91, No. B5, pp. 4993-4999

Zebker, H. A., Rosen, P. A. and Hensley, S. (1997). *Atmospheric effects in interferometric synthetic aperture radar surface deformation and topographic maps.* Journal of Geophysical Research, Vol. 102, pp. 7547-7563.

Zhang, W. R., Duan, Z. L., Zeng, Z. Q., Shi, H. P. (2003). Evaluation on economic losses resulted from land subsidence in Shanghai: 1921-2000. J. Tongji University 31(6), pp. 743-748.

Zhou, C. H., Wan, Q., Huang, S. F. (2000). *A GIS-based approach to flood risk zonation*. Acta Geogr sin 55(1):15-24

Zhu, L., Chen, Y., Gong, H.L., Liu, C. and Wang, R. (2013) *Spatial risk assessment on land subsidence in Beijing, China*. 20th International Congress on Modelling and Simulation, Adelaide, Australia, 1– 6 December 2013.

Annex

Appendix 1: Analytic Hierarchy Process calculation sheet for hazard mapping.

1. Pair wise comparison

Table: Pair wise comparison matrix which holds the preference values (**For Hazard**)

Criteria	C11	C12	C13
C11	1	3	5
C12	0.33	1	3
C13	0.20	0.33	1
Total	**1.53**	**4.33**	**9**

1/C12

1/C13

Factor	Factor weighting score							Factor	
	More importance than			Equal	Less importance than				
C11 (volume)	9 8 7	6 5 4	3 2	1	2 3 4	5 6 7	8 9	C12	
C12 (Velocity)	9 8 7	6 5 4	3 2	1	2 3 4	5 6 7	8 9	C13	
C13 (GWE Intensity)	9 8 7	6 5 4	3 2	1	2 3 4	5 6 7	8 9	C11	

Priority Vector

2. Normalization and 3. Consistency Analysis

Factor	C11	C12	C13	Total	**Average**	**Consistency Measure**			**π max**
C11	0.65	0.69	0.56	1.90	0.63	3.07			0.97
C12	0.22	0.23	0.33	0.78	0.26	3.03			1.13
C13	0.13	0.08	0.11	0.32	0.11	3.01			0.96
Total	1.00	1.00	1.00		1.00				**3.06**
					Consistency Index (CI)			0.03	
					Random Index (RI)			0.58	(Saaty,1980)
					C Ratio			0.05	

Appendix 2: Analytic Hierarchy Process calculation sheet for vulnerability mapping.

1. Pair wise comparison									
Table: Pair wise comparison matrix which holds the preference values (**For Vulnerability**)									
Criteria	C21	C22	C23						
C21	1	3	7						
C22	0.33	1	3						
C23	0.14	0.33	1						
Total1	**1.48**	**4.33**	**11**						
Factor	Factor weighting score							Factor	
	More importance than			Equal	Less importance than				
C21 (Popn density)	987	654	32	1	234	567	89	C22	
C22 (GDP/km2)	987	654	32	1	234	567	89	C23	
C23 (Constructionland propon)	987	654	32	1	234	567	89	C21	
					Priority Vector				
2. Normalization and 3. Consistency Analysis									
Factor	C21	C22	C23	Total	**Average**	**Consistency Measure**			**π max**
C21	0.68	0.69	0.64	2.01	0.67	3.01			0.99
C22	0.23	0.23	0.27	0.73	0.24	3.01			1.05
C23	0.10	0.08	0.09	0.26	0.09	3.00			0.97
Total	1.00	1.00	1.00		1.00				**3.01**
					Consistency Index (CI)			0.01	
					Random Index (RI)			0.58	(Saaty,1980)
					C Ratio			0.01	

Published Papers

land

MDPI

Article

Detection of Land Subsidence in Kathmandu Valley, Nepal, Using DInSAR Technique

Richa Bhattarai [1,*], Haireti Alifu [2], Aikebaier Maitiniyazi [1] and Akihiko Kondoh [2]

[1] Geosystem and Biological Sciences Division, Graduate School of Science, Chiba University, 1-33 Yayoi-cho, Inage-ku, Chiba-shi, Chiba 263-8522, Japan; akbar120311@gmail.com

[2] Center for Environmental Remote Sensing, Chiba University, 1-33 Yayoi-cho, Inage-ku, Chiba-shi, Chiba 263-8522, Japan; hairetialifu@outlook.com (H.A.); kondoh@faculty.chiba-u.jp (A.K.)

* Correspondence: richa_b5@hotmail.com

Academic Editor: Paul Aplin
Received: 17 April 2017; Accepted: 6 June 2017; Published: 11 June 2017

Abstract: Differential Synthetic Aperture Radar Interferometry (DInSAR) is a remote sensing technique that is capable of detecting land surface deformation with centimeter accuracy. In this research, this technique was applied to two pairs of Advanced Land Observing Satellite (ALOS) Phased Array L-band SAR (PALSAR) data to detect land subsidence in the Kathmandu valley from 2007 to 2010. The result revealed several subsidence areas towards the center of the valley ranging from a maximum of 9.9 km^2 to a minimum of 1 km^2 coverage with a maximum velocity of 4.8 cm/year, and a minimum velocity of 1.1 cm/year, respectively. The majority of the subsidence was observed in old settlement areas with mixed use development. The subsidence depth was found to gradually increase from the periphery towards the center in almost all detected subsidence areas. The subsidence depth was found to be in a range of 1 cm to 17 cm. It was found that the concentration of deep water extraction wells was higher in areas with higher subsidence rates. It was also found that the detected subsidence area was situated over geological formations mainly consisting of unconsolidated fine-grained sediments (silica, sand, silt, clay and silty sandy gravel), which is the major factor affecting the occurrence of land subsidence due to groundwater extraction.

Keywords: land subsidence; ALOS PALSAR; DInSAR; Kathmandu valley; urban

1. Introduction

1.1. Background

Land subsidence is defined as an environmental geological phenomenon that causes the slow lowering of ground surface elevation [1]. It is often a result of the natural compaction of sediments and extraction of ground water, geothermal fluids, oil, gas, coal and other solids through mining [2]. Land subsidence tends to change the topographic gradients, and thus causes infrastructure damage, ruptures in the land surface, aggravates flooding, causes inundation of land and reduces the capacity of aquifers to store water; ultimately posing a risk for society and the economy [3]. The occurrence of land subsidence has been studied in many places around the world, including Tokyo, Japan [4]; Mexico [5]; Saudi Arabia [6]; Texas, USA [7]; Jakarta, Indonesia [8]; Ravenna, Italy [9]; Bangkok, Thailand [10,11]; Pingtung Plain, Taiwan [12]; and China [13].

The driving force behind land subsidence is mainly a combination of a primary factor and an immediate factor; the primary factor being the existence of unconsolidated sediment deposits that comprise the aquifer system, and the immediate factor being the diminishing groundwater level [14–16]. An area is potentially prone to land subsidence if a thick sediment deposit prone to consolidation exists in the subsoil, along with water which is susceptible to being pumped. Lowering of the water

table due to groundwater harvesting is the triggering factor of subsidence [17]. Nonetheless, even if the water table is reduced, land subsidence will not occur if the aquifer system lacks the presence of unconsolidated sediments. It has been found that excessive groundwater exploitation can result in a slow, but eventually significant, land subsidence [1,18–21]. A close relationship between the amount of groundwater withdrawal for industrial activities and advancement of land subsidence was recognized early in Japan during observations made between 1954 and 1960 [22]. Additionally, geology also plays a vital role in the acceleration of land subsidence. Large amounts of groundwater extraction from certain types of underlying sediments, such as fine-grained sediments, result in compaction of these sediments, because the groundwater is partly responsible for the subsurface support. This ultimately triggers land subsidence [23].

Kathmandu is a bowl-shaped valley with two principle landforms-alluvial and flood plains-making it even more prone to subsidence. Groundwater has always been a significant source of the water supply in the Kathmandu valley since the early 1970s [24]. As the water demand started exceeding the supply, private and governmental institutions started to pump groundwater through private wells. Visible impacts on water levels were observed during the mid-eighties, when the Nepal Water Supply Corporation (NWSC) started including groundwater into its supply system [25]. During the nineties, the number of private wells increased so rapidly that the extraction exceeded the water recharge levels. The constantly increasing population, industrialization and urbanization have triggered the increase in groundwater consumption. Extraction of groundwater has increased from 2.3 million-liters-a-day (MLD) in 1979 to 80 MLD in 2011 [26]. Groundwater fulfills nearly 50% of the total water demand during the wet season and 60–70% during the dry season [27]. Consequently, annual extraction exceeds recharge, leading to tremendous depletion in groundwater levels. With an ever-increasing population, development activities and a lack of groundwater resource policy, the water demand is bound to exerting increasing pressure on the groundwater table. This, in turn, will result in aquifer compaction in areas consisting of highly compressible clay and silt layers, raising the risk of land subsidence [28]. Also, considering the relation of groundwater exploitation and land subsidence from the case studies of various countries, it can be assumed that the same may occur in the Kathmandu valley, as well. Nonetheless, no published research has been done, to the authors' knowledge, to determine if land subsidence is actually taking place to ground water extraction; therefore, no evidence of land subsidence in the Kathmandu valley is available [24].

Research has been done focusing on the land deformation caused by the crustal movements in the region. On 25 April 2015, a devastating earthquake of Mw 7.8 struck central Nepal. It was followed by a strong aftershock of Mw 7.3 on 12 May 2015, and many other aftershocks greater than Mw 6 thereafter. This earthquake was a result of stress released from the under thrust movement of the Indian tectonic plate beneath the Eurasian tectonic plate [29]. The earthquake ruptured the Main Himalayan Thrust fault (MHT), which stopped halfway at 11 km under the Kathmandu valley. Therefore, there are chances of a future fault rupture on the surface [30]. Uplift of approximately 1 m was observed 20 km northeast of Kathmandu city at longitude/latitude 27.74/85.50°, and local subsidence was observed to the north of the city [29,31]. The data inventory of the historical occurrence of great Himalayan earthquakes is sporadic, due to the complexity of evaluating these events [31–33]. Also, the rupture location identity and the return time is difficult to predict [34]. Therefore, it is difficult to conduct seismic hazard assessment in highly-populated regions near the Himalayas [35].

It was only after this event that a few works mentioned subsidence, with the sole cause being the earthquake [29,36]. A developing country, recently struck by a natural disaster, is rebuilding; and if subjects like land subsidence, which have been troubling the globe, are not addressed immediately, then the consequences could be unaffordable. Therefore, mapping, continuous monitoring and risk assessment of land subsidence is critical in a place like the Kathmandu valley.

Differential Synthetic Aperture Radar interferometry (DInSAR) is an advanced remote sensing tool that has the ability to map displacements over vast areas at a very high spatial resolution, at a lower cost than other conventional techniques, such as GPS, topographic measure and extensometers [37]. Previously, several researchers have applied this method to map and monitor groundwater

extraction-induced subsidence all around the world with successful results. For example, in Antelope Valley, California [38]; Coachella Valley, California [39]; Kolkata, India [40]; Iran [41]; Jakarta [42]; and Alto Guadalentin Basin, Spain [43].

1.2. Relevant Literature

Land subsidence has been a global problem for a very long time. Many studies have and are being conducted throughout the world by applying remote sensing techniques [2,37–40,42,44–48]. Reviewing case histories of geologically similar areas can give the impression of a possible land subsidence trend. Some similar studies are as follows:

A study conducted by Strozzi et al., 1999 [2] in a valley of Mexico City that is built on highly compressible lacustrine clays with high ground water extraction values showed results of land subsidence velocity of more than 30 cm/year in some areas. Seven ERS-1/2 SAR images pairs from December 1995 to September 1997 were processed using differential SAR interferometry to map land subsidence.

Amelung et al., 1999 detected land subsidence in Las Vegas, Nevada, United States between 1992 and 1997 by using InSAR technique. A maximum subsidence of 19 cm during the observation period was observed by utilizing two SAR images acquired by the ERS satellite. The study also concluded that the extent of the subsidence was dependent on the geological structure and sediment composition of the location [49].

Another study conducted by Boni et al. [43] in 2015 revealed that the Alto Gudalentin Basin in southern Spain had up to 2.5 m cumulated subsidence between 1992 and 2012. The DInSAR technique was applied to four datasets of SAR images obtained from ERS-1/2, ENVISAT, ALOS and COSMO-SkyMed satellites to obtain land subsidence evolution within a twenty-year period. It was found that the ground displacement was directly correlated with the thickness of the compressible alluvial deposits. The authors also suggest that the detected land subsidence over the past 20 years is a consequence of 100–200 m groundwater drop caused by overexploitation of the Alto Guadalentin aquifer system.

A study conducted by Calo et al., 2015 in Istanbul Megacity, Turkey, where the major geological constituents are mainly composed of clay, sand, gravel and silt, revealed subsidence occurrence over urbanized areas during the observation period of 2010–2012. The SBAS (Small Baseline Subset) DInSAR technique was applied to 43 TerraSAR-X data, which revealed an average subsidence velocity of 3 cm/year, with most of the detected subsidence found to be occurring in the Quaternary layers [50].

1.3. Scope

Little is known about land subsidence, and very few studies are being conducted, in Nepal. Therefore, the outcome of this research will help build our understanding of the current situation, allowing the development of prevention techniques and risk management. After verifying the accuracy of this result by comparing it with land measurement data and field survey, it is expected that it will be useful for the government and interested stakeholders for the promotion of a better understanding of the situation for sustainable development and policy-making for disaster prevention.

The results from this study could serve as a significant benchmark for the Kathmandu Valley, Nepal, as it is developing towards sustainable urbanization, but lacks proper data and research.

1.4. Objective

The main objective of this research is to detect land subsidence in the Kathmandu valley by the application of the Differential Synthetic Aperture Radar Interferometry (DInSAR) technique to Advanced Land Observing Satellite (ALOS) Phased Array L-band Synthetic Aperture Radar (PALSAR) data.

2. Materials and Methodology

2.1. Study Area

The Kathmandu valley, the largest urban agglomerate of Nepal, is located between 27°34'33" and 27°49'4" N latitudes and 85°11'19" and 85°34'57" E longitudes, covering an area of 654.7 km^2. The valley consists of three major cities: namely, Kathmandu, the capital city; Bhaktapur and Lalitpur, ancient cultural gem cities. The population density is 2793 people per square kilometer as of the 2011 census. The average elevation is approximately 1400 m above sea level. This bowl-shaped valley is filled with more than 550 m thick lacustrine and fluvial deposits [51], which make it prone to land subsidence. The Landsat image of the Kathmandu valley is shown in Figure 1.

Geology of the Kathmandu valley: the Kathmandu valley is surrounded by the Shivapuri mountain range (2732 m) in the North, the Phulchauki mountain range (2762 m) in the south, the Nagarkot mountain range (1895 m) in the east and the Chandragiri mountain range (2356 m) in the west [52]. The main geological composition of the Kathmandu valley is quaternary sediment over basement rock [53]. The basement rock is formed by Precambrian to Devonian rocks, which mainly consist of limestone, dolomite, slate, metasandstone, phyllite, marble, schist, quartzite and garnet-schist [54]. The quaternary sediment consists of thick (more than 650 m deep), semi-consolidated fluvio-lacustrine sediments from the Pliocene to the Pleistocene age [54]. It is composed of fine-to coarse-grained sand, gravel, clay, silt, peat, lignite and diatomite [55]. The geological map of the Kathmandu valley is shown in Figure 2.

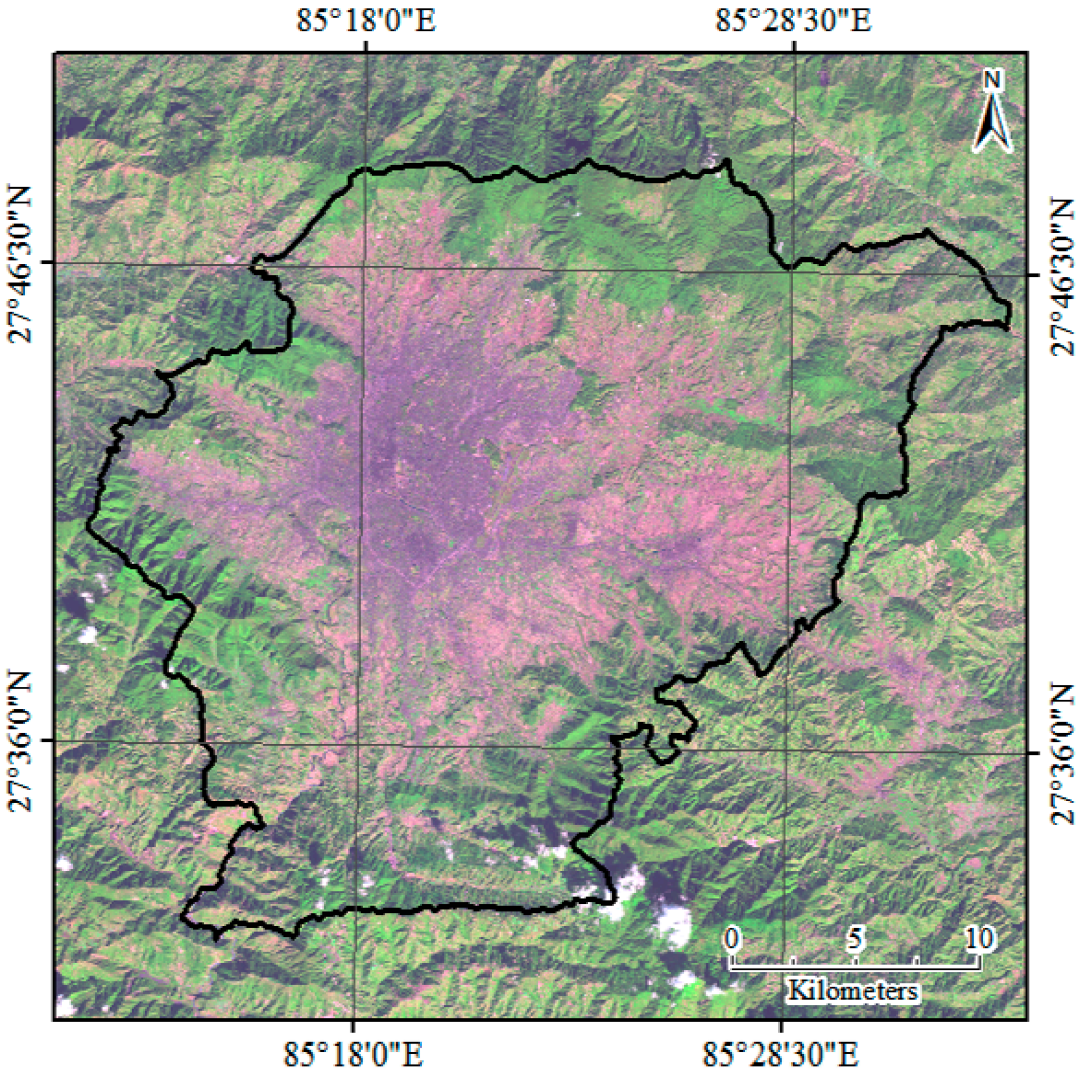

Figure 1. Landsat Image of the Kathmandu valley, observed on 10 November 2016.

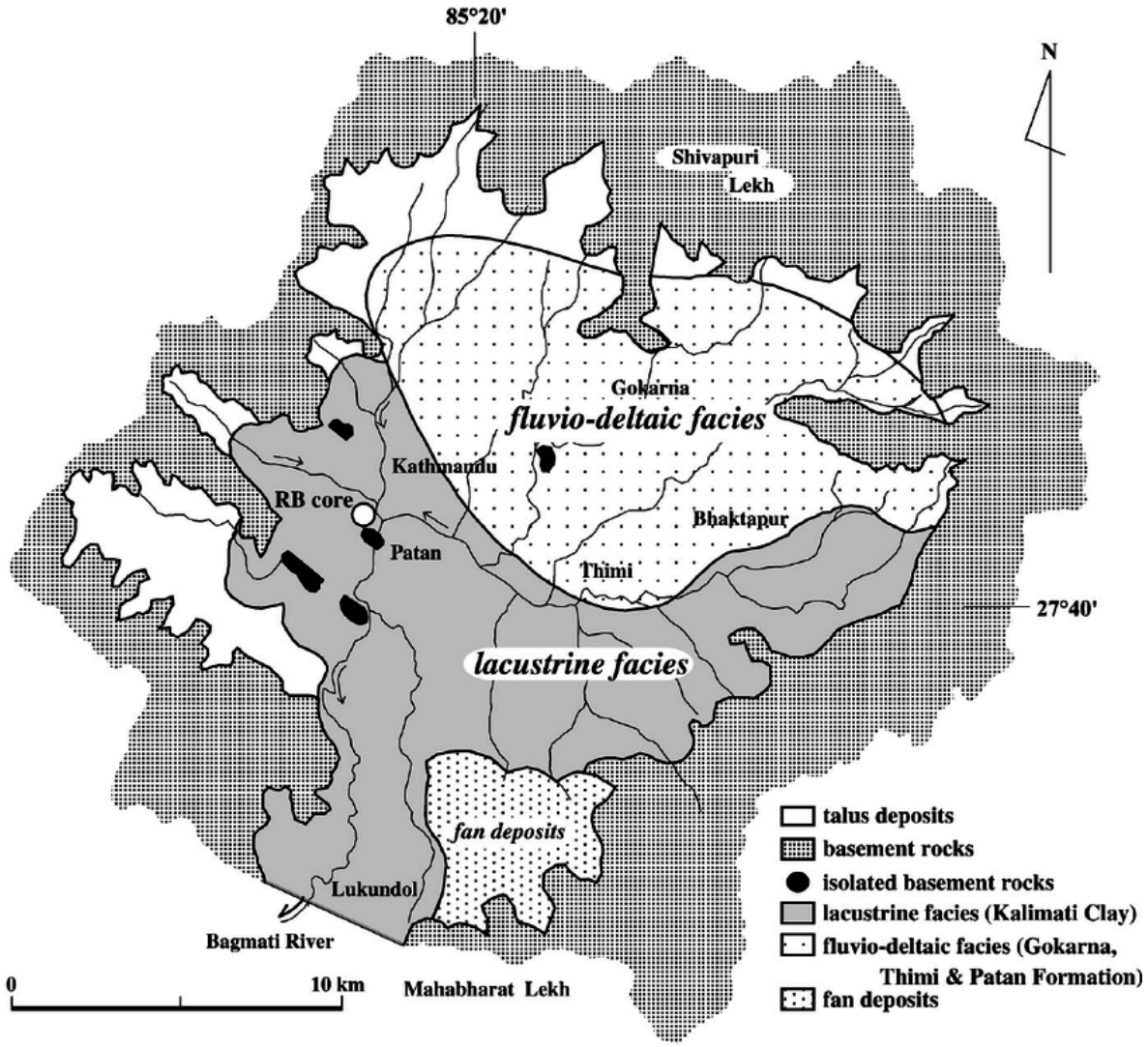

Figure 2. Geological map of the Kathmandu basin (Source: [56])

2.2. Data

Three ALOS PALSAR fine-mode, single-polarization data, acquired at different acquisition times between 2007 and 2010 with identical observation parameters—like path/row 510/54, off nadir angle 34.3°—were selected for this research. The details of the two pairs generated from this data are shown in Table 1, below. Since a perpendicular baseline value between 150 to 450 m gives the best interferogram result [57], this factor was also considered while selecting the pairs of images. The data used in this research was purchased from Japan Space Systems.

Also, a Digital Elevation Model (DEM) was extracted from Shuttle Radar Topography Mission (SRTM) 1 Arc second (resolution of 30 m) global elevation data. This data was downloaded from theEarth explorer data portal.

Table 1. ALOS PALSAR data pair information

InSAR Pair	Observation Date	Interval (Days)	Perpendicular Baseline (m)
Pair 1	2 November 2007 19 March 2008	138	417
Pair 2	2 November 2007 7 February 2010	828	257

2.3. Methodology

Synthetic Aperture Radar (SAR) is a system able to obtain high-resolution, complex images from wide areas of terrain, usually located on board an orbital or airborne platform, but also useable in ground based deployments [58]. DInSAR is a remote sensing technique useful for detecting land displacement or deformation accurately for a wide coverage area by utilizing the phase difference between two or more sets of SAR data taken at different acquisition times. The phase difference between an interferometry data pair can be expressed as follows:

$$\text{Int} = \varphi\text{disp} + \varphi\text{atm} + \varphi\text{noise} + \varphi\text{topo} + \varphi\text{flat} \quad (1)$$

where φdisp refers to the phase difference from ground displacement along the slant range; φatm refers to the atmospheric effect; φnoise refers to the noise from the radar instrument and temporal deceleration; φtopo refers to the topographic height information; and φflat refers to the assumption of an ideally flat earth terrain [42]. In the DInSAR technique, the ground displacement is estimated to be in a slant range direction; therefore, Equation (2) can be used to obtain ground displacement in a vertical direction [59].

$$\Delta z = \Delta sl \cos\theta \quad (2)$$

where Δz is ground displacement in a vertical direction; Δsl is ground displacement in a slant range; and θ is the incidence angle, which is assumed to be 34.3°, which is as same as the sensor's off-nadir angle.

In this study, the DInSAR technique was performed using the SARSCAPE module in ENVI software to detect land subsidence in the Kathmandu valley. The method of DInSAR processing is explained step by step as follows:

Focusing: The purpose of this first step is to collect the energy dispersed in both azimuth and range directions in the raw (level 1.0 product) ALOS PALSAR data into a single pixel (i.e. Single Look Complex (SLC) image), which can be used for further processing.

Multilooking and Co-registration: In this step, the SLC images are divided into different looks, characterized by different frequencies in order to reduce the speckle due to constructive and destructive interferences between the different backscattered signals from the different ground targets [60]. Image co-registration is the process of superimposing two or more SAR images in the slant range geometry. [61].

Interferogram Generation and Flattening: After image co-registration, where the master and slave images are precisely overlaid with an accuracy within fractions of a pixel to compute the phase difference between them, an interferometric phase is generated by multiplying the master image by the complex conjugate of the slave image. The variable viewing angles of the terrain can cause range spectra shifts, and the different Doppler can cause azimuth spectra shifts. An azimuth filter is applied during the interferogram generation to fully capture the scene's potential coherence [61]. The constant height of the terrain results in parallel (flat earth) fringes along the range direction in the generated interferogram. A pre-existing DEM of 30 m resolution from SRTM is applied to simulate the topographic phase to obtain a flattened interferogram.

Adaptive Filtering and Coherence Generation: The noise from radar instruments and temporal deceleration is removed by applying the Goldstein-Werner filtering process to the noisy interferogram [62]. Coherence is a measure of interferogram quality. It is calculated as the ratio between coherent and incoherent summations of two co-registered SAR images. A coherence value approaching 1 suggests that the two pixels are correlated and there is no phase noise; whereas a coherence value of 0 (black = 0) suggests that the two pixels are decorrelated and there is phase noise, and thus should not be considered for further processing.

Phase Unwrapping: The flattened and filtered interferogram obtained from the earlier processing always has a phase value within a range of 0 to 2π, which means that every time the phase change exceeds 2π, the phase value starts with 0 again and the cycle repeats itself. This is called 2π ambiguity and phase unwrapping resolves this problem.

Refinement and Reflattening: Orbital correction has great significance for the accurate transformation of phase information to height information. Therefore, Ground Control Points appointed on DEM are used to calculate the absolute phase, and refine the orbits.

Phase to Displacement Conversion and Geocoding: The obtained phase information is converted into displacement using Equations (1) and (2), and is finally projected onto a standard geographic coordinate system, thus generating a displacement map.

3. Result and Discussion

The coherence image of each pair for the study area is shown in Figure 3. A coherence value close to 1 (i.e., white color) indicates that there is no phase noise, whereas a coherence value of 0 (i.e., black color) indicates that there is only phase noise. Areas with high coherence (coherence value 1) display clear interferogram patterns in the interferogram image, whereas areas with low coherence (coherence value 0) displays noisy interferogram patterns. Good coherence is seen in both of our pairs; therefore, they can be considered for interferogram generation.

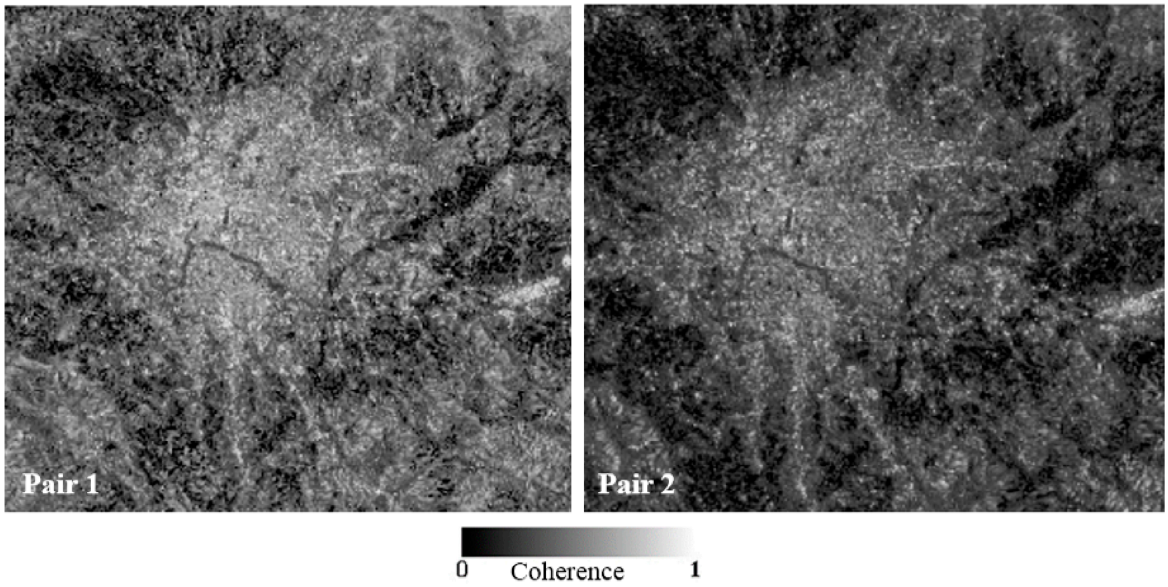

Figure 3. Coherence image of Pair 1 (2 November 2007and 19 March 2008) and Pair 2 (2 November 2007 and 7 February 2010) obtained from DInSAR processing.

The DInSAR interferogram of the Kathmandu valley for the observation interval 2 November 2007 to 7 February 2010 is shown in Figure 4. Interferogram fringes can be seen in various areas which indicates the occurrence of land deformation. An area where the color turns from blue to pink to yellow to green is considered to be affected by land subsidence, whereas the area where the color turns from blue to green to yellow to pink is considered to be affected by land uplift. Figure 4 clearly indicates the occurrence of land subsidence. It is noticeable that some fringes on the south-eastern part do not display clear patterns. This is because interference cannot easily occur in inclined ground surfaces, and this part of the study area is a hilly region.

Figure 5 shows the subsidence contour with displacement values in centimeters for the land subsidence-affected areas, which are indicated by points L1–L8. A significant linear feature striking NW-SE can be seen in Figure 5. The pattern displayed by ground deformations may depict the underlying structural arrangement of a location [63]. Referring to Figure 2 and Figure 9, it can be said that the subsidence pattern obtained here is modulated by the underlying sediments. Clear linear features can be observed parallel to the fluvio-deltaic facies and lacustrine facies boundary.

Location L1, in central Kathmandu, shows the maximum amount of subsidence (17 cm). It is a mixed-use development area (a type of urban development that comprises an amalgamation of residential, commercial, cultural, institutional, and/or industrial uses, along with their physical and functional integration, including pedestrian connections [64]). Location L2—Chauni and periphery—

is an old settlement area with an army camp and ancient museum covering most of the subsidence zone. Location L3—Lalitpur—is also an old mixed-use settlement area. Location L4—Imadol and periphery—is a location on the outskirts of the Kathmandu city urban center, which is gradually changing from farmland/cropland into urban land use. This location also has a small number of brick kilns, which might be affecting the ground surface elevation. Location L5—Thimi and periphery—is a mixed-use settlement area with croplands on the north-eastern side of the subsidence zone. Location L6—Madhyapur Thimi—is mostly cropland with a few residential areas (spots), but is gradually being urbanized by land plotting. Location L7—New Baneshwor and Koteshwor—are also mixed-use settlement areas, with the majority being commercial buildings. Location L8—Gothatar—mostly consists of croplands with a few residential buildings, along with a small northern portion of the international airport runway. The outskirts of the valley are mostly rural, but urbanization is slowly spreading from the center of the valley towards the periphery. A Google Earth image displaying portions of location is shown in Figure 6.

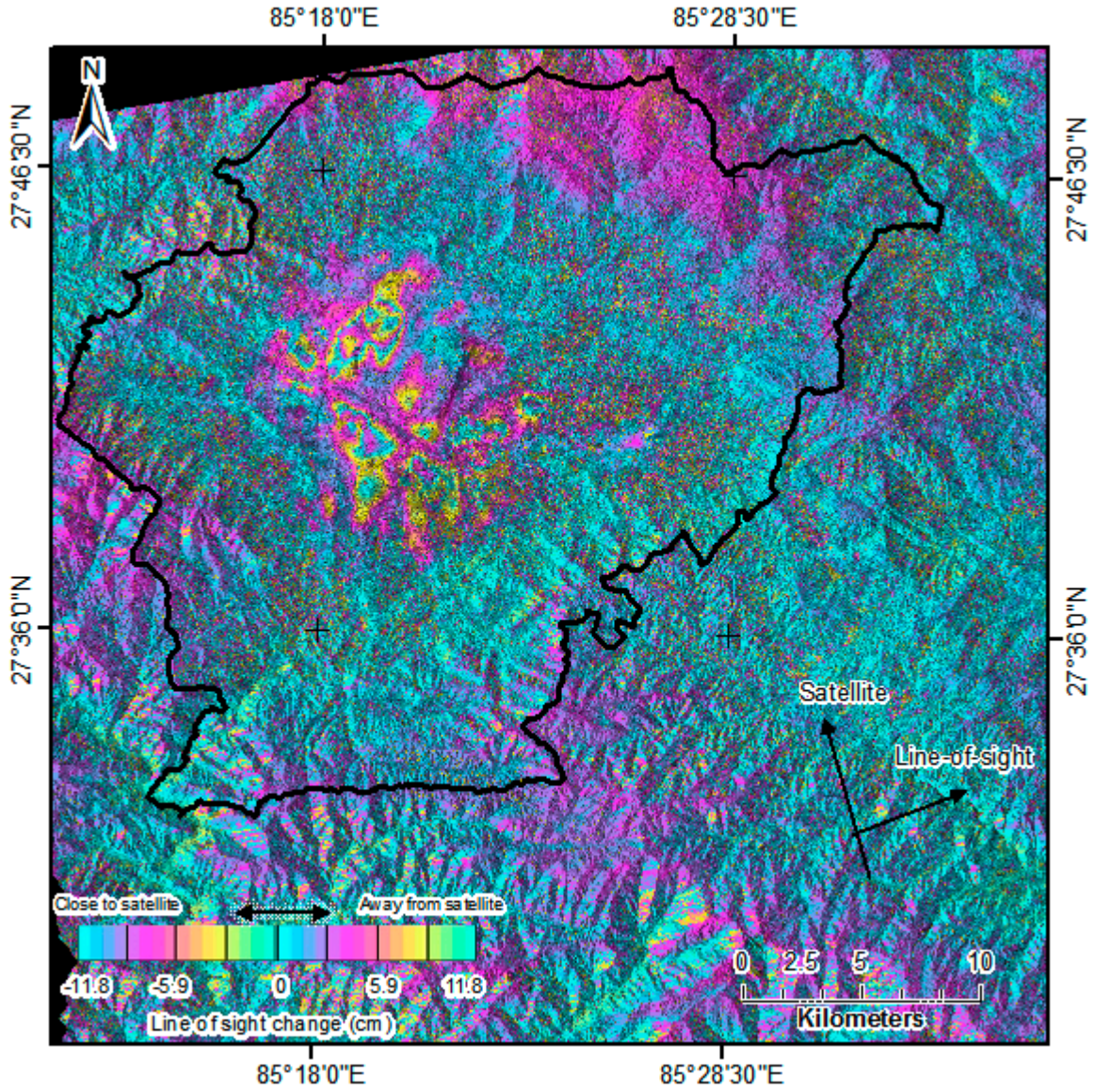

Figure 4. Differential interferogram for Kathmandu Valley from 2 November 2007 to 7 February 2010 obtained from DInSAR processing.

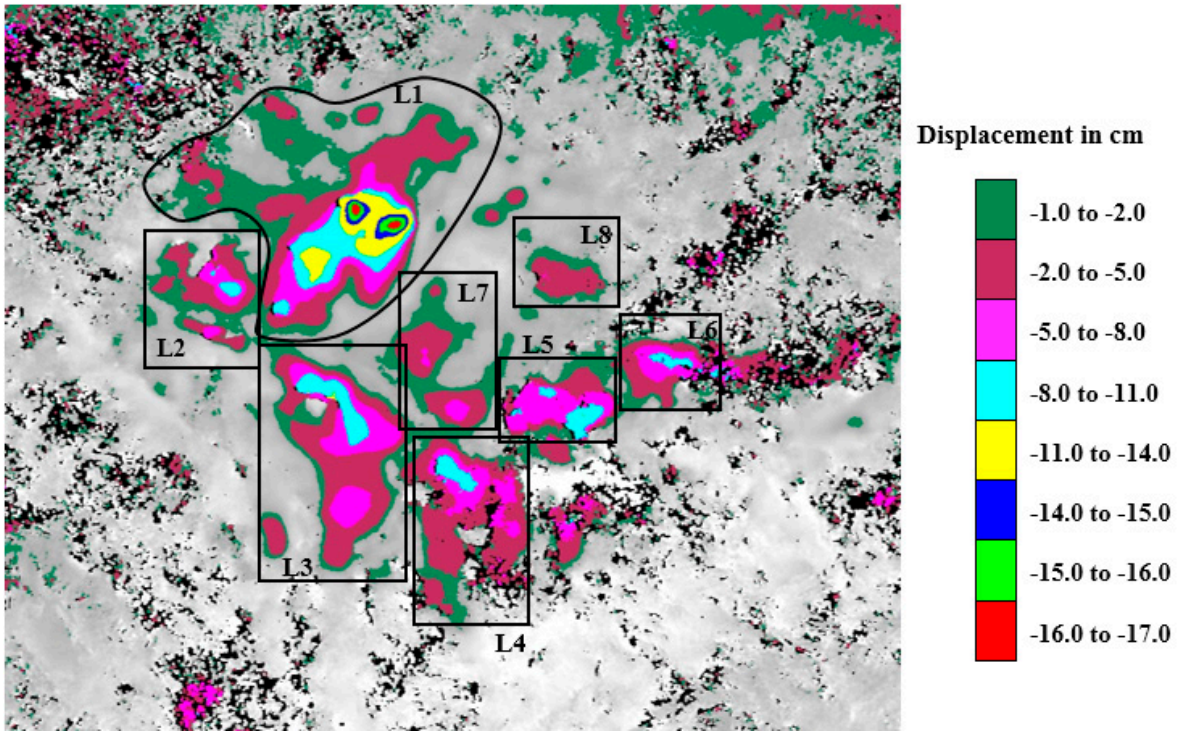

Figure 5. Subsidence contour showing displacement values in centimeters.

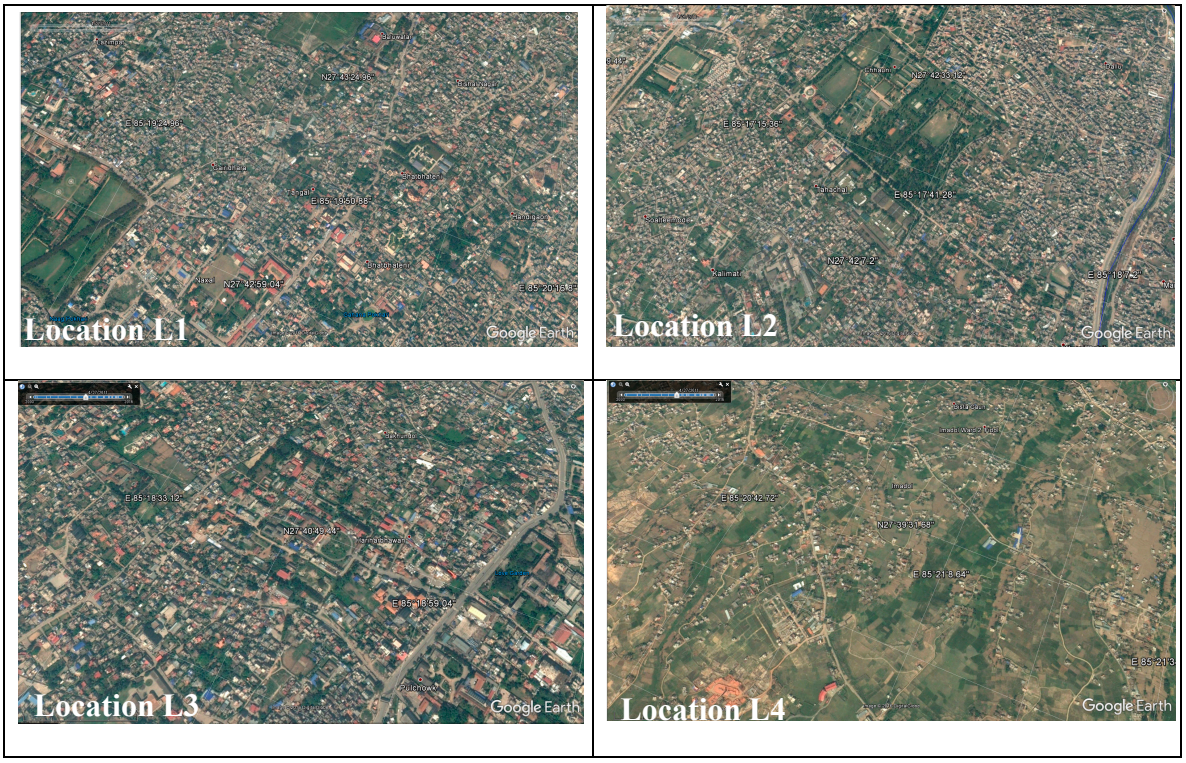

Figure 6. Google Earth images from the year 2011 showing portions of land subsidence Locations L1 to L8.

Figure 7 shows the location of destroyed structures as a result of the Mw 7.8 2015 Gorkha Earthquake. Maximum destruction can be observed in the location corresponding to the maximum subsidence (i.e., Location L1) whereas other locations show less destruction. The factor contributing to this might also be the fact that Location L1 consists of portions of very old settlement area where old, weak buildings were abundant.

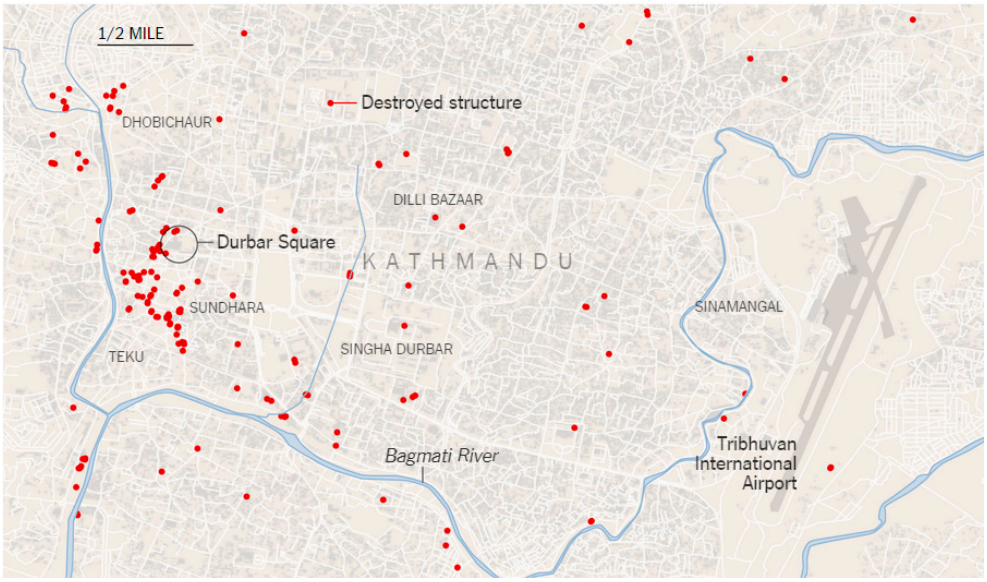

Figure 7. Grading map showing the location of destroyed structures due to 2015 Gorkha earthquake indicated by red dots. (Source: European Commission Copernicus Emergency Management Service).

The subsidence coverage area and maximum subsidence depth of each location is shown in Table 2. Subsidence depths less than 2 cm have not been considered when calculating the coverage area.

Table 2. Detailed information of areas affected by land subsidence.

Location Point	Location Name	Location Specification	Subsidence Coverage Area (km²)	Maximum Subsidence Depth (cm)
L1	Central Kathmandu	Mixed-use development	9.9	17
L2	Chauni	Old Army Camp	2.5	11
L3	Lalitpur	Mixed-use development	7.7	14
L4	Imadol	Residential and cropland with few brick kilns	5.7	11
L5	Thimi	Mixed-use development	3.0	11
L6	Madhyapur Thimi	Mixed-use development	2.0	11
L7	New Baneshwor and Koteshwor	Mixed-use development	2.1	8
L8	Gothatar	Residential and cropland with portion of airport runway	1.0	5

Comparison with groundwater: the Kathmandu valley generally consists of three hydrogeologic layers: namely, shallow aquifer, aquitard and deep aquifer. The shallow aquifer is thicker towards the north of the valley's groundwater basin, whereas the deep aquifer is thicker towards the central and southern part. The main natural recharge area is towards the northern part, and a small area contributing to recharge is located towards the southern part [24]. Locations L1, L7 and L8 lie on the northern part of the groundwater basin, where the shallow aquifer is thicker; whereas Locations L3, L4, L5 and L6 lie on the central and southern part of the groundwater basin, where the deep aquifer is thicker. As mentioned in the background, earlier, the Kathmandu valley mainly relies on groundwater as the main source of water. According to the Kathmandu Valley Water Supply Management Board, the use of deep tube-well pumps for water extraction from deep aquifers is dominant throughout the valley. The depth of deep tube wells mainly lies in a range of 30 to 300 m, and the daily discharge ranges from 3000 liters per day to 400,000 liters per day. Figure 8 shows the locations of registered deep tube wells in the Kathmandu valley. We can see that the concentration of wells is denser at Location L1 where the subsidence is highest, and sparse in other locations where the subsidence amount is lower. However, there are many unregistered wells throughout the valley with no information on their depth and discharge, which makes it difficult find an exact relation. Nonetheless, considering the density of urban build-up (refer to Figure 6), it can be assumed that the concentration of deep tube wells will be higher at Locations L1, L2, L3 and L7. Also, the occurrence of land subsidence is a combined effect of groundwater extraction and vulnerable hydrogeology, which might result in subsidence at places other than the site of extraction [65]. Therefore, comprehensive study of the groundwater extraction and recharge ability of the aquifer, which has not been included in this research, should be done in order to find the exact relationship.

However, it has been found through various literature reviews that extensive water extraction is one of the main causes of land subsidence. From the results obtained from this research, we can consider that water extraction does have a relation with land subsidence. But detailed study needs to be done to find the exact cause, as land subsidence is a very complex phenomenon, affected by various factors.

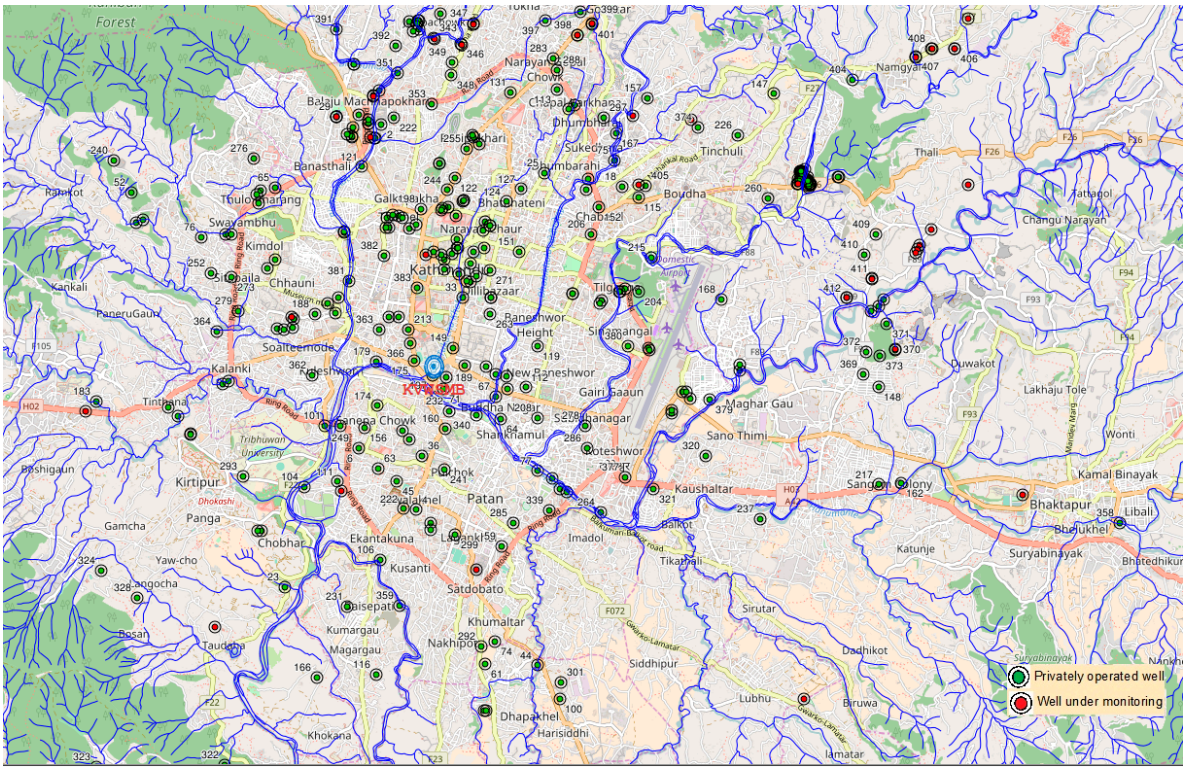

Figure 8: Location of registered deep well in Kathmandu Valley. (Source: Kathmandu valley water supply management board)

Comparison with geology: The land subsidence map generated by DInSAR processing in this research was compared briefly with the geological map of the Kathmandu valley. Figure 9 shows the subsidence contour map overlaid on the geological map of the Kathmandu valley. The maximum amount of subsidence (indicated by the red color in Figure 5) can be seen over the Gokarna Formation. This formation is mainly composed of a sands terrace from fluvio-lacustrine origins [55]. Also, a thick array of sandy and silty sediments without clay content was observed from the extensive borehole data of this formation [66]. Similarly, Locations L5, L7 and L8 are also situated over the Gokarna Formation. Locations L2, L4, L6 and small portions of Locations L3 and L7 are situated over the Kalimati Formation. Kalimati is a local name for black clay. According to Sakai (2001) [66], the predominant constituent of this formation is dark grey carbonaceous and diatomaceous (naturally occurring, soft siliceous sedimentary rock that is easily crumbled into a fine white to off-white powder) beds of open lacustrine rocks that are widely distributed underneath the surface of the central portion of the Kathmandu valley. It can also be seen in Figure 9 that a larger portion of Location L3 is situated over the Chapagaon Formation. This formation consists of somewhat rounded silty sandy gravel, occasionally with a boulder bed covered with a layer less than 1 m thick of clayey silt and silty sand [67].

From the above description, it can be summarized that land subsidence was observed mainly over three kinds of geological formations; namely, Kalimati, Gokarna and Chapagaon Formations. The main constituents of these formations are silica, sand, silt, clay and silty sandy gravel. As mentioned in relation to the mechanisms of land subsidence earlier, the major factor in occurrence of land subsidence due to ground water extraction is the presence of unconsolidated fine-grained sediments—mainly clay and silt—in an aquifer system. Hence, the relationship between geology and land subsidence occurrence can be established from this study.

These constituents are the main contents of the geology of the Kathmandu valley, and are spread throughout the valley, with the result being that the primary factor (i.e., geology) for subsidence occurrence is prevalent. Therefore, it can be said that the triggering/immediate factor (i.e.,

groundwater characteristics) for subsidence occurrence is the major factor that determines the occurrence of land subsidence in the study area.

Nevertheless, land subsidence is a complex phenomenon, and this research is just a preliminary study that intends to provide basic evidence of land subsidence in the study area. This study can serve as a base for more comprehensive study in the future.

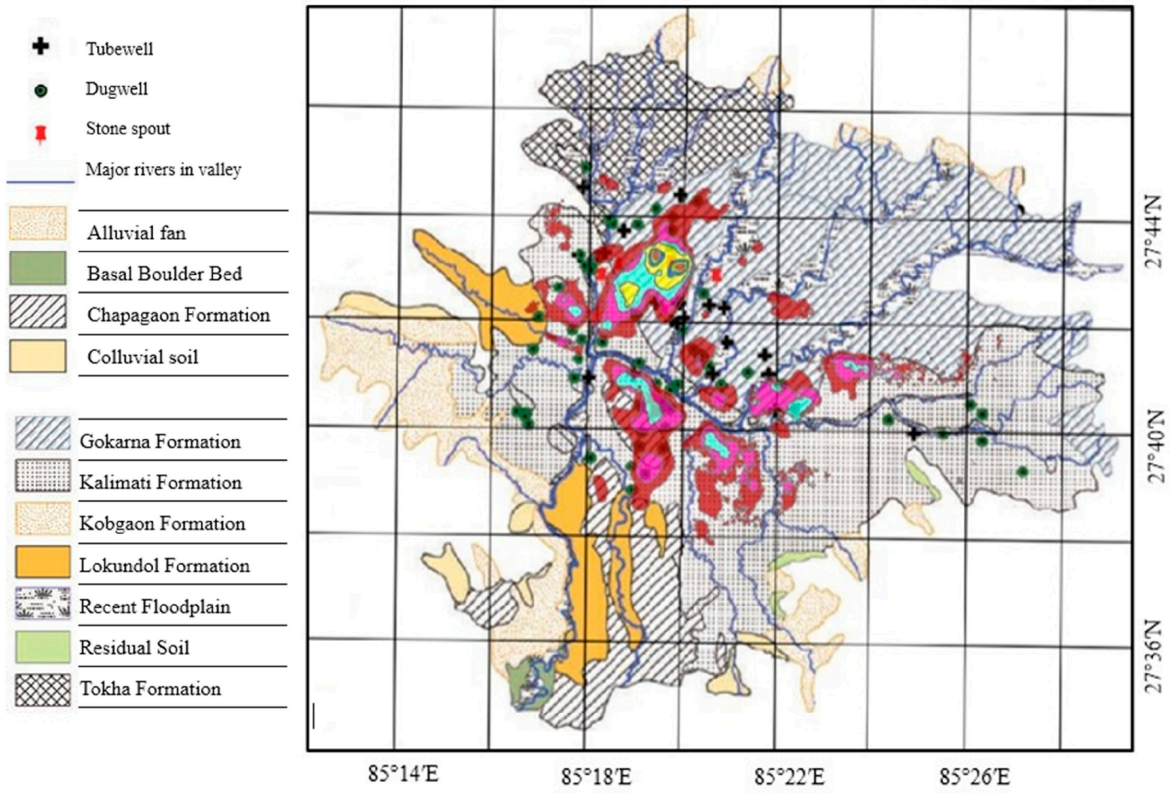

Figure 9. Subsidence contour overlaid on a geological map of the Kathmandu valley. (Geological map adapted from an engineering and environmental geological map of the Kathmandu valley, Department of Mines and Geology, Government of Nepal by [68].

4. Conclusion

Land subsidence occurrence in the urban Kathmandu valley was detected by the application of the Differential Synthetic Aperture Radar Interferometry (DInSAR) technique to Advanced Land Observation Satellite Phased L-band SAR (ALOS-PALSAR) data. Most of the subsidence was found to have occurred in the center of the valley, where the population density is relatively higher than the surroundings. Also, the majority of the subsidence region comprised mixed-used development areas, where ground water extractions can be assumed to be at higher levels. The generated subsidence map was further studied on the basis of groundwater extraction and the geology of the Kathmandu valley. It was found that the concentration of groundwater discharge units was higher in locations detected to have high amounts of subsidence. Due to the complex nature of subsidence occurrence, and the involvement of many factors in such phenomena, detailed study is required to find the exact cause. Also, due to the non-existence of previous land subsidence measurement data and the difficulty of obtaining the GPS measurement data, the subsidence results were not able to be validated. In spite of this, the results can be considered acceptable, owing to the fact that DInSAR is a well-established methodology known to give accurate results for land deformation in urban areas.

However, very little study has been done in Nepal as of now, so the result of this research can serve as a basis for many further detailed studies. DInSAR was applied to ALOS PALSAR data to detect land subsidence in the Kathmandu valley because ALOS PALSAR covers a large area, and since no study relating to land subsidence had previously been conducted in the study area, it would serve as the best option for identifying subsidence zones. Now that this study reveals the areas

affected by subsidence, Persistent Scatterer InSAR technique can be used to obtain subsidence values in the affected areas with millimeter accuracy. Also, other SAR data with shorter wavelengths, like X-band or C-band can be used to focus on the area most affected. Also, in this study, only a few pairs of SAR data were used; using more pairs of SAR data would provide better coherence, resulting in more accurate outcomes.

Acknowledgments: The first author would like to express sincere gratitude to the Ministry of Education, Culture, Sports, Science and Technology (MEXT)—Super Global University (SGU), Japanese government scholarship for financially supporting the educational expenses during the period of this research. A special thanks to Ryutaro Tateishi for his valuable guidance and supervision throughout and for purchasing the required data. The authors would also like to thank the Kathmandu Valley Water Supply Management Board for providing water extraction information. Also, a hearty thanks to Ayihumaier Halipu and all the members of Tateishi lab and Kondoh lab for their constant suggestions and help throughout.

Author Contributions: Richa Bhattarai conceived, designed and performed the research; Haireti Alifu and Aikebaier Maitiniyazi contributed in parts of analysis and helped with the analysis tools; Haireti Alifu and Aikebaier Maitiniyazi also gave valuable suggestions for improving the manuscript; Akihiko Kondoh supervised the research throughout and gave valuable suggestions for improving the results and manuscript; Richa Bhattarai wrote the paper.

Conflicts of Interest: The authors declare no conflict of interest.

References

1. Hu, B.; Wang, J.; Chen, Z.; Wang, D.; Xu, S. Risk assessment of land subsidence at Tianjin coastal area in China. *Environ. Earth Sci.* **2009**, *59*, 269–276.
2. Strozzi, T.; Wegmuller, U. Land subsidence in Mexico City mapped by ERS differential SAR interferometry. In Proceedings of the International Geoscience and Remote Sensing Symposium (IGARSS), Hamburg, Germany, 28 June–2 July 1999.
3. Holzer, T.L.; Galloway, D.L. Impacts of land subsidence caused by withdrawal of underground fluids in the United States. *Rev. Eng. Geol.* **2005**, *XVI*, 87–99.
4. Yamaguchi, R. Water level change in the deep well of the University of Tokyo. *Bull Earthq. Res. Inst.* **1969**, *47*, 1093–1111.
5. Adrian, O.G.; Rudolph, L.D.; Cherry A.J. Analysis of long-term land subsidence near Mexico City: Field investigations and predictive modelling. *Water Resour. Res.* **1999**, *35*, 3327–3341.
6. Bankher, K.A.; Al-Harthi, A.A. Earth fissuring and land subsidence in Western Saudi Arabia. *Nat. Hazards* **1999,** *20*, 21–42.
7. Gabrysch, R.K.; Neighbors R.J. Land-surface subsidence and its control in the Houston-Galveston region, TX, 1906–1995. In Proceedings of the 6th International Symposium Land Subsidence, Ravenna, Italy, 2 September 2000; pp. 81–92.
8. Abidin, H.Z.; Djaja, R.; Darmawan, D.; Hadi, S.; Akbar, A.; Rajiyowiryono, H.; Sudibyo, Y.; Meilano, I.; Kasuma, M.A.; Kahar, J.; et al. Land subsidence of Jakarta (Indonesia) and its geodetic monitoring system. *Nat. Hazards* **2001**, *23*, 365–387.
9. Teatini, P.; Ferronato, M.; Gambolati, G.; Bertoni, W.; Gonella, M. A century of land subsidence in Ravenna, Italy. *Environ. Geol.* **2005**, *47*, 831–846.
10. Bergado, D.T.; Nutalaya, P.; Balasubramaniam, A.S.; Apaipong, W.; Chang, C.C.; Khaw, L.G. Causes, effects and predictions of land subsidence in AIT campus Chao Phraya Plain, Bangkok, Thailand. *Bull Assoc. Eng. Geol.* **1987**, *25*, 57–81.
11. Phien-wej, N.; Giao, P.H.; Nutalaya, P. Land subsidence in Bangkok, Thailand. *Eng. Geol.* **2006**, *82*, 187–201.
12. Hu, J.C.; Chu, H.T.; Hou, C.S.; Lai, T.H.; Chen, R.F.; Nien, P.F. The contribution to tectonic subsidence by groundwater abstraction in the Pingtung area, southwestern Taiwan as determined by GPS measurements. *Quat. Int.* **2006**, *147*, 62–69.
13. Xu, Y.S.; Shen, S.L.; Cai, Z.Y.; Zhou, G.Y. The state of land subsidence and prediction approaches due to groundwater withdrawal in China. *Nat. Hazards* **2008**, *45*, 123–135.
14. Holzer, T.L. Ground failure induced by ground-water withdrawal from unconsolidated sediments. *Geol. Soc. Am. Rev. Eng. Geol*. **1984**, *VI*, 67–105.

15. Budhu, M.; Adiyaman, I.B. Mechanics of land subsidence due to groundwater pumping. *Int. J. Numer. Anal. Methods Geomech.* **2010**, *34*, 1459–1478.
16. Galloway, D.L.; Burbey, T.J. Review: Regional land subsidence accompanying groundwater extraction. *Hydrogeol. J*. **2011,** *19*, 1459–1486.
17. Martínez, J.P.; Cabral-Cano, E.; Wdowinski, S.; Marín, M.H.; Ortiz-Lozano, J.A.; Zermeño-de-León, M.E. Application of InSAR and gravimetry for land subsidence hazard zoning in Aguascalientes, Mexico. *Remote Sens.* **2015,** *7*, 17035–17050.
18. Pratt, W.E.; Johnson, D.W. Local subsidence of the Goose Creek oil field. *J. Geol.* **1926**, *34*, 577–590.
19. Poland, J.F.; Davis, G.H. Land subsidence due to withdrawal of fluids. *Rev. Eng. Geol.* **1969**, *2*, 187–270.
20. Bell, F.G.; Cripps, J.C.; Culshaw, M.G. A review of the engineering behavior of soils and rocks with respect to groundwater. *Geol. Soc. Eng. Geol. Spec.* **1986,** *3*, 1–23.
21. Shi, X.Q.; Xue, Y.Q.; Ye, S.J.; Wu, J.C.; Zhang, Y.; Yu, J. Characterization of land subsidence induced by groundwater withdrawals in Su-Xi-Chang area, China. *Environ. Geol.* **2007**, *52*, 27–40.
22. Inaba, Y.; Abe, I.; Iwasaki, S.; Aoki, S.; Endo, T.; Kaido, R. Review of land subsidence researches in Tokyo. In Proceedings of the Tokyo Symposium in Land Subsidence, Tokyo, Japan, September 1969, 1, pp. 87–98.
23. Perlman, H. United States Geological Survey. Land Subsidence. Available online: http://water.usgs.gov/edu/earthgwlandsubside.html （accessed on 24 February 2017）.
24. Pandey, V.P.; Shrestha, S.; Kazama, F. Groundwater in the Kathmandu Valley: Development dynamics, consequences and prospects for sustainable management. *Eur. Water* **2012,** *37*, 3–14.
25. Metcalf, Eddy. *2998-NEP: Urban Water Supply Reforms in the Kathmandu Valley;* Inc with CEMAT Consultants Ltd: Kathmandu, Nepal; 2000; Volume I–II.
26. Shrestha, S.; Semkuyu, D.J.; Pandey, V.P. Assessment of groundwater vulnerability and risk to pollution in Kathmandu Valley. *Nepal. Sci. Total Environ.* **2016**, *556*, 23–35.
27. Rana, G.; Murray, A.B.; Maharjan, D.R.; Thaku, A.K. *Kathmandu Valley Environmental Outlook*. International Centre for Integrated Mountain Development (ICIMOD): Kathmandu, Nepal, 2007.
28. Pradhanang, S.M.; Shrestha, S.D.; Steenhuis, T.S. Comphrensive review of groundwater research in the Kathmandu Valley, Nepal. In: *Kathmandu Valley Groundwater Outlook*; Shrestha, S., Pradhananga, D., Pandey, V.P., Eds.; Asian Institute of Technology (AIT): Klong Luang, Thailand; Small Earth Nepal (SEN): Kathmandu, Nepal; Center of Research for Environment Energy and Water (CREEW): Kathmandu, Nepal; International Research Center for River Basin Environment-University of Yamanashi: Kofu, Japan, 2012; 6–18.
29. Kobayashi, T.; Morishita, Y.; Yarai, H. Detailed crustal deformation and fault rupture of 2015 Gorkha earthquake, Nepal, revealed from ScanSAR-based interferograms of ALOS-2. *Earth Planets Sp.* **2015**, *67*, 201, 1–13.
30. Elliot, J.R.; Jolivet, R.; Gonzalez, P.J.; Avouc, J.P.; Hollingswort, J.; Searle, M.P.; Stevens, V.L. Himalayan megathrust geometry and relation to topography revealed by the Gorkha earthquake. *Nat. Geosci.* **2016**, *9*, 174–180.
31. Diao, F.; Walter, T.R.; Motagh, M.; Prats-Iraola, P.; Wang, R.; Samsonov, S.V. The 2015 Gorkha earthquake investigated from radar satellites: Slip and stress modeling along the MHT. *Front. Earth Sci*. **2015**, *3*, 65.
32. Lavé, J.; Yule, D.; Sapkota, S.; Basant, K.; Madden, C.; Attal, M.; Pandey, R. Evidence for a great medieval earthquake (approximate to 1100 AD) in the Central Himalayas. *Nepal. Sci.* **2005**, *307*, 1302–1305.
33. Sapkota, S.N.; Bollinger, L.; Klinger, Y.; Tapponnier, P.; Gaudemer, Y.; Tiwari, D. Primary surface ruptures of the great Himalayan earthquakes in 1934 and 1255. *Nat. Geosci.* **2013**, *6*, 71–76.
34. Avouac, J.P.; Bollinger, L.; Lave, J.; Cattin, R.; Flouzat, M. Seismic cycle in the Himalayas. *C. R. Acad. Sci. II A*. **2001,** *333*, 513–529.
35. Mugnier, J.L.; Gajurel, A.; Huyghe, P.; Jayangondaperumal, R.; Jouanne, F.; Upreti, B. Structural interpretation of the great earthquakes of the last millennium in the central Himalaya. *Earth-Sci. Rev*. **2013**, *127*, 30–47.
36. Luo, H.; Chen, T. Three Dimensional Surface Displacement Field Associated with the 25 April 2015 Gorkha , Nepal Earthquake: Solution from Integrated InSAR and GPS Measurements with an Extended SISTEM Approach. *Remote Sens.* **2016**, *8*, 599.
37. Tomás, R.; Romero, R.; Mulas, J.; Marturia, J.J.; Mallorqui, J.J.; Lopez-Sanchez, J.M.; Herrera, G.; Gutierrez, F.; Gonzalez, P. J.; Fernandez, J.; et al. Radar interferometry techniques for the study of ground subsidence phenomena: A review of practical issues through cases in Spain. *Environ. Earth Sci*. **2014**, *71*, 163–181.

38. Galloway, D.L.; Hudnut, K.W.; Ingebritsen, S.E.; Phillips, S.P.; Peltzer, G.; Rogez, F.; Rosen, P.A. Detection of aquifer system compaction and land subsidence using interferometric synthetic aperture radar, Antelope Valley, Mojave Desert, California. *Water Resour. Res.* **1998**, *34*, 2573–2585.
39. Sneed, M.; Ikeheara, M.E.; Galloway, D.L.; Amelung, F. *Detection and measurement of land subsidence using global positioning system and interferometric synthetic aperture radar, Coachella valley, California, 1996-98*. Water Resources Investigation Report 01-4193. U.S. GEOLOGICAL SURVEY: Sacramento, CA, USA.
40. Chatterjee, R.S.; Fruneau, B.; Rudant, J.P.; Roy, P.S.; Frison, P.; Lakhera, R.C.; Dadhwal, V.K.; Saha, R. Subsidence of Kolkata (Calcutta) City, India during the 1990s as observed from space by Differential Synthetic Aperture Radar Interferometry (D-InSAR) technique. *Remote Sens. Environ.* **2006**, *102*, 176–185.
41. Motagh, M.; Walter, T.R.; Sharifi, M.A.; Fielding, E.; Schenk, A.; Anderssohn, J.; Zschau, J. Land subsidence in Iran caused by widespread water reservoir overexploitation. *Geophys. Res. Lett.* **2008**, *35*, LI6403.
42. Bayuaji, L.; Josaphat, T.S.S.; Kuze, H. ALOS PALSAR D-InSAR for land subsidence mapping in Jakarta, Indonesia. *Can. J. Remote Sens.* **2010**, *36*, 1–8.
43. Bonì, R.; Herrera, G.; Meisina, C.; Notti, D.; Béjar-Pizarro, M.; Zucca, F.; González, P.J.; Palano, M.; Tomás, R.; Fernández, J.; Fernández-Merodo, J.A.; et al. Twenty-year advanced DInSAR analysis of severe land subsidence: The Alto Guadalentín Basin (Spain) case study. *Eng. Geol.* **2015**, *198*, 40–52.
44. Abidin, H.Z.; Andreas, H.; Gamal, M.; Djaja, R.; Subarya, C.; Hirose, K.; Maruyama, Y.; Murdohardono, D.; Rajiyowiryono, H. Monitoring land subsidence of Jakarta (Indonesia) using levelling, GPS survey and InSAR techniques. *Int. Assoc. Geod. Symp.* **2005**, *128*, 561–566.
45. Cascini, L.; Ferlisi, S.; Fornaro, G.; Lanari, R.; Peduto, D.; Zeni, G. Subsidence monitoring in Sarno urban area via multi-temporal DInSAR technique. *Int. J. Remote Sens.* **2006**, *27*, 1709–1716.
46. Chini, M.; Bignami, C.; Stramondo, S.; Pierdicca, N. Uplift and subsidence due to the 26 December 2004 Indonesian earthquake detected by SAR data. *Int. J. Remote Sens.* **2008**, *29*, 3891–3910.
47. Guoquinga, Y.; Jingquin, M. DInSAR technique for land subsidence monitoring. *Earth Sci. Front.* **2008**, *15*, 239–243.
48. Yan, Y.; Doin, M.P.; Lopez-Quiroz, P.; Tupin, F. Mexico City subsidence measured by InSAR time series: Joint analysis using PS and SBAS approaches. *IEEE J. Sel. Top. App. Earth Obs. Remote Sens.* **2012**, *5*, 1312–1326.
49. Amelung, F.; Galloway, D.L.; Bell, J.W.; Zebker, H.A.; Laczniak, R.J. Sensing the ups and downs of Las Vegas: InSAR reveals structural control of land subsidence and aquifer-system deformation. *Geology* **1999**, *27*, 483–486.
50. Calo, F.; Abdikan, S.; Gorum, T.; Pepe, A.; Kilic, H.; Sanli, F.B. The space-borne SBAS-DInSAR technique as a supporting tool for sustainable urban policies: The case of Istanbul Megacity, Turkey. *Remote Sens.* **2015,** *7*, 16519–16536.
51. Pandey, M.R. Ground response of Kathmandu valley on the basis of microtremors. In Proceedings of the World Conference on Earthquake Engineering, Auckland, New Zealand, 30 January–4 February 2000.
52. Piya, B.K. Generation of a Geological Database for the Liquefaction Hazard Assessment in Kathmandu Valley. Master's Thesis, International Institute for Geo-Information Science and Earth Observation, Enschede, The Netherlands, 2004.
53. Nautiyal, S.P.; Sharma, P.N. A Geological Report on the Groundwater Investigation of Kathmandu Valley. Unpublished work, 1961.
54. Moribayashi, S.; Maruo, Y. Basement topography of Kathmandu Valley, Nepal: An application of gravitational method to the survey of a tectonic basin in the Himalayas. *J. Japan Soci. Eng. Geol.* **1980**, *21*, 30–37.
55. Stocklin, J.; Bhattarai, K.D. Geology of Kathmandu Area and central Mahabharat Range, Nepal Himalaya. HMG/UNDP Mineral Exploration Project, Kathmandu. Unpublished work, 1977.
56. Kuwahara, Y.; Masudome, Y.; Paudel, M.R.; Fuji, R.; Hayashi, T.; Mampuku, M.; Sakai, H. Controlling weathering and erosion intensity on the southern slope of the central Himalaya by the Indian summer monsoon during the last glacial. *Glob. Planet. Change* **2010**, *71*, 73–84.
57. Ardiansyah. *Tutorial InSAR Menggunakan Sarscape*. Department of Geography, University of Indonesia: Indonesian. Unpublished work, 2013; p. 8.
58. Yerro, A.; Corominas, J.; Monells, D.; Mallorqui, J.J. Analysis of the evolution of ground movements in a low densely urban area by means of DInSAR technique. *Eng. Geol.* **2014**, *170*, 52–56.

59. Curlander, J.C.; McDonough, R.N. *Synthetic aperture radar: Systems and signal processing*; Wiley-Interscience: Toronto, Canada, 1991.
60. Exelis help article: Estimating the appropriate number of looks when multilooking images in SARscape. Available online: http://www.harrisgeospatial.com/Support/HelpArticles/TabId/185/ArtMID/800/ArticleID/4265/4265.aspx (accessed on 15 September 2014).
61. SAR Guidebook. Available online: www.sarmap.ch/pdf/SAR-Guidebook.pdf (accessed on 16 August 2010).
62. Goldstein, R.M.; Werner, C.L. Radar interferogram filtering for geophysical applications. *Geophys. Res. Lett.* **1998**, *25*, 4035–4038.
63. Anderssohn, J.; Wetzel, H.U.; Walter, T.R.; Motagh, M.; Djamour, Y.; Kaufmann, H. Land subsidence pattern controlled by old alpine basement faults in the Kashmar Valley, Northeast Iran: Results from InSAR and levelling. *Geophys. J. Int.* **2008**, *174*, 287–294.
64. Thrall, G.I. *Business Geography and New Real Estate Market Analysis*; Oxford University Press: Oxford, United Kingdom, 2000; p. 216.
65. Sato, H.P.; Abe, K.; Ootaki, O. GPS-measured land subsidence in Ojiya City, Niigata Prefecture, Japan. *Eng. Geol.* **2003**, *67*, 379–390.
66. Sakai, H. Stratigraphic division and sedimentary facies of the Kathmandu Basin group, Central Nepal. *J. Nepal Geol. Soc*. ***2001***, *25*, 19–32.
67. Shrestha, S.R.; Shah, S. Shallow Aquifer Mapping of Kathmandu Valley. Groundwater Resources Development Board, Babarmahal, Kathmandu. Available online: http://www.academia.edu/27155659/Shallow_Aquifer_Mapping_of_Kathmandu_Valley (accessed on 23 February 2017).
68. Pathak, D.R.; Hiratsuka, A. An investigation of nitrate and iron concentrations and their relationship in shallow groundwater systems of Kathmandu. *Desalination Water Treat.* **2010**, *19*, 1–3, 191–197.

Scientific Research Publishing

Advances in Remote Sensing, 2017, 6, 132-146
http://www.scirp.org/journal/ars
ISSN Online: 2169-2688
ISSN Print: 2169-267X

Risk Assessment of Land Subsidence in Kathmandu Valley, Nepal, Using Remote Sensing and GIS

Richa Bhattarai, Akihiko Kondoh

Graduate School of Science, Chiba University, Chiba, Japan
Email: richa_b5@hotmail.com

How to cite this paper: Bhattarai, R. and Kondoh, A. (2017) Risk Assessment of Land Subsidence in Kathmandu Valley, Nepal, Using Remote Sensing and GIS. *Advances in Remote Sensing*, **6**, 132-146.
https://doi.org/10.4236/ars.2017.62010

Received: May 7, 2017
Accepted: June 17, 2017
Published: June 20, 2017

Abstract

Land subsidence is identified as a global problem and intensive studies are being conducted worldwide to detect and monitor risk of this problem. Risk assessment of land subsidence is simply an evaluation of the probability and frequency of occurrence of land subsidence, exposure of people and property to the subsidence and consequence of that exposure. Remote sensing technology was used to extract information of land subsidence in Kathmandu Valley, Nepal. Also, Disaster Risk Index method and Analytic Hierarchy Process (AHP) along with Geographic Information System (GIS) tools were used to assess risk of land subsidence in Kathmandu Valley, Nepal. Subsidence volume for locations Central Kathmandu, Chauni, Lalitpur, Imadol, Thimi, Madhyaour Thimi, New Baneshwor, Koteshwor and Gothatar was calculated using a simple mathematical formula. The subsidence depth for these locations was found to be in a range of 1 cm to 17 cm and the maximum subsidence velocity was found to be 4.8 cm/yr. This study revealed that the location where maximum subsidence was observed (*i.e.* Central Kathmandu and Lalitpur) was found to be at high risk of experiencing land subsidence induced damage. Other location where subsidence was observed was found to be at medium risk and the rest of the Kathmandu valley was found to be at low risk with current data situation. This study can be considered as the first step towards other comprehensive study relating to land subsidence risk assessment. The outcome of this research provides a basic understanding of the current situation that can further assist in developing prevention and risk management techniques.

Keywords

Risk Assessment of Land Subsidence, Hazard, Vulnerability, Analytic Hierarchy Process, GIS

1. Introduction

1.1. Background

Land subsidence is just a geological phenomenon either triggered by natural or anthropogenic activities but when this phenomenon has the probability of resulting harmful consequences or the expected loss (of lives, property, livelihoods, economic activities or environment) then it is considered as risk [1]. Risk factors are compounded by rapid increase in urban population and economic development [2]. The physical damage caused by land subsidence can be mainly categorized into two forms: damage on artificial (manmade) infrastructures and damage on natural systems. Significant damage is seen in areas corresponding to land subsidence occurrence.

The main damage on manmade infrastructure reported worldwide is mostly related to water transport structures [3] [4]. Since land subsidence affects the elevation of the ground, and because water transportation infrastructures are very sensitive to minor gradient changes, subsidence can hugely affect such structures. Other reported problems include damage to buildings and transportation facility (*i.e.* roads, bridges, railways).

The damage to manmade infrastructures is more emphasized and noticeable unlike to the damage to natural systems, which is invisible and generally more threatening. The main reason is that artificial infrastructure damages can generally be repaired opposed to natural system damage which is generally permanent. Some of the examples of natural structure damage are permanent compaction of aquifer system, change in topography which ultimately affects the river patterns and low lying areas.

The other main factor affected by land subsidence is damage to the social environment which includes the human society and the economic development level. The physical damage caused by land subsidence will eventually affect the social environment directly or indirectly but the intensity is determined by the recoverable capability of life, property and various economic activities in the disaster affected areas. Remarkable economic losses have been caused by land subsidence throughout the world [5] [6] [7].

Kathmandu valley, the capital and the urban core of a developing country Nepal is lagging in terms of data documentation and research work regarding land subsidence and its risk assessment. The factors that make a location prone to land subsidence risk (*i.e.* geology and groundwater extraction characteristics) are in favor of the valley, yet research is not being conducted. Also, the valley is experiencing rapid increase in population and economic development in the past few decades that will ultimately contribute to increase in risk of damage induced by land subsidence if no counter measures are considered.

Therefore, it is necessary to assess land subsidence risk for decision and policy makers to prevent a huge potential disaster. Risk assessment is simply an application of a methodology for evaluating risk, where risk is defined as the probability and frequency of occurrence of a hazardous event, exposure of people and property to the hazard and consequences of that exposure [1].

Most frequently deployed approach for land subsidence risk assessment are by the means of Geographic Information System (GIS) techniques and Disaster Risk Index Method and Analytic Hierarchy Process (AHP) [1] [7] [8] [9]. GIS provides robust tools for inclusive spatial modeling and analysis. Disaster Risk Index method is an approach where the hazard, the vulnerability and the capability of disaster prevention and reduction are considered for the quantitative evaluation of a risk. AHP is a multi-criteria mathematical evaluation method used for decision making where hierarchical structures are used to quantify relative priorities for a given set of elements on a ratio scale set by the user [1].

The main objective of this study is to assess land subsidence risk in Kathmandu valley, Nepal, by using Geographic Information System (GIS) techniques, Disaster Risk Index Method and Analytic Hierarchy Process (AHP). Land subsidence map of Kathmandu valley for 2007 to 2010 was generated by applying the Differential Synthetic Aperture Radar Interferometry (D-InSAR) technique before conducting this study. Peer-reviewed paper related to this study can be found at http://www.mdpi.com/2073-445X/6/2/39.

1.2. Study Area

Kathmandu valley is the capital city of Nepal and hence has been a center of ever growing economic activities from a very long time. Kathmandu valley is an urban agglomerate with a core urban center surrounded by extended urban economic zones. The lack of decentralization of developmental activities has propagated Kathmandu valley to be one of the most desired city to live in the country consequently, increasing the internal migration rates. The population density of Kathmandu valley is 2793 people per square kilometer as per the 2011 census [10]. The increasing population and failure in implementing strict regulation has resulted in haphazard development of the valley both in terms of infrastructure and economy. The Landsat image of Kathmandu valley is shown in **Figure 1**.

2. Methodology

2.1. Data Used

Land subsidence volume and velocity obtained from D-InSAR processing (a remote sensing technique) of ALOS PALSAR data from 2007 to 2010 was used in this research. These results were obtained by the authors in a previous study considered as the first part of this study (refer http://www.mdpi.com/2073-445X/6/2/39).

Groundwater exploitation intensity data was used for hazard mapping of land subsidence and was provided by the Kathmandu Valley Water Supply Management Board (KVWSMB), Ministry of Water Supply and Sanitation, Government of Nepal.

Population density, Gross Domestic Product (GDP) and Construction Land Proportion data was used for Vulnerability mapping. Population density data was obtained from the Kathmandu Valley Development Authority (KVDA), Government of Nepal. GDP data for the study area was obtained from National Accounts Section,

Central Bureau of Statistics, Government of Nepal. Construction land proportion data was obtained from the Ministry of Land Reform and Management, Nepal.

2.2. Methodology

2.2.1. Methodology for Subsidence Volume Estimation

Through various literature review it was found that in most of the cases the shape of subsidence is very much like a cone shape. Therefore, the subsidence volume of each subsidence zone can be estimated by an assumption that the border extremities of a subsidence zone are linearly moving at a constant rate. A simple cone model designed by [11] is used to estimate the land subsidence volume (Figure 2).

Subsidence volume represented by the shaded portion in Figure 2 can be

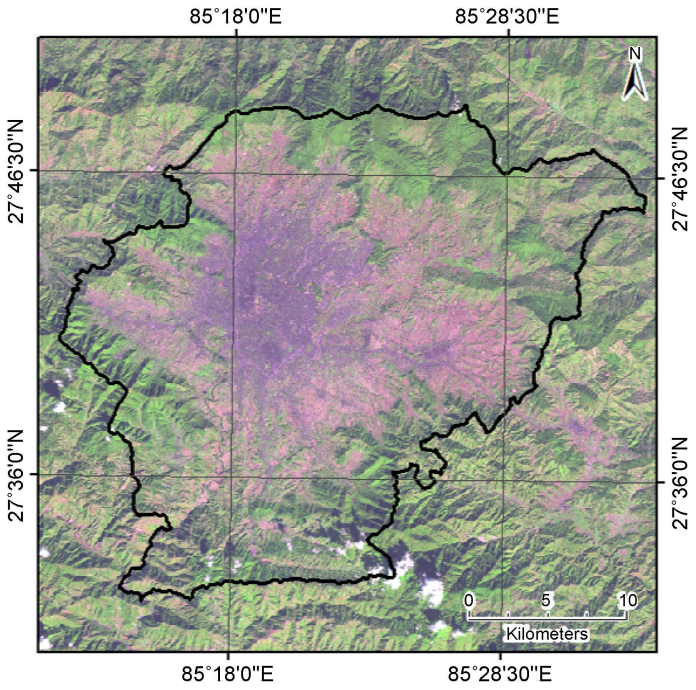

Figure 1. Landsat image of Kathmandu valley.

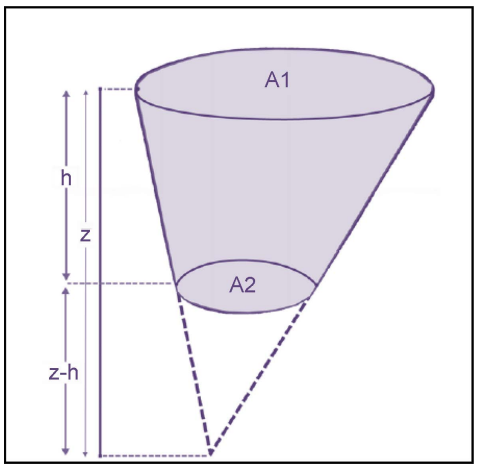

Figure 2. Cone model for volume estimation of land subsidence.

estimated by applying the formula of a volume of a cone which is shown in Equation (1) [12].

$$V = \frac{1}{3}\left[A1 + \sqrt{A1A2} + A2\right]h \quad (1)$$

where, V is the subsidence volume to be estimated, $A1$ is the upper base area, $A2$ is the lower base area and h is the height or the perpendicular distance between the surface $A1$ and $A2$. Area $A1$ and $A2$ was calculated in ArcGIS (Version 10.4.1) by converting each subsidence zone obtained by DInSAR processing into a shapefile. The subsidence depth (h) and the velocity of land subsidence was also obtained from the DInSAR processing result. The methodology for D-InSAR processing to map land subsidence in Kathmandu valley from 2007 to 2010 has been explained in detail in the first part of this study which can be found at http://www.mdpi.com/2073-445X/6/2/39.

2.2.2. Methodology for Risk Assessment

The main objective for assessing risk of land subsidence is to link the subsidence phenomenon with the damage it causes to the physical as well as social environment. The main factors that help to determine risk are hazard and vulnerability. Therefore, a hazard map and vulnerability map were generated and then combined to obtain the final risk map. The detailed methodology is explained as follows.

Disaster Risk Index Method

Risk assessment is an approach for evaluating risk, where risk is defined as the probability and frequency of occurrence of subsidence, exposure of people and property to the subsidence and consequence of that exposure [1]. The degree of risk of land subsidence significantly depends on two factors: hazard and vulnerability [7]. As per the disaster risk index method, quantitative risk can be estimated by using Equation (2) [13].

$$DR = f\left(H, V, C\right) \quad (2)$$

where, DR is the disaster risk, H is the hazard, V is the vulnerability and C is the capability of disaster prevention and reduction.

Hazard, in general can be defined as a phenomenon that has the potential to disrupt and damage people, property and their immediate environment. The hazard of land subsidence refers to the intensity and the probability that land subsidence will occur in a certain area in a certain period. As defined by the Asian Disaster Preparedness Center, Land subsidence hazard evaluation simply is the process of determining the degree of severity and the extent of the impact area. In this research, accumulative subsidence volume, land subsidence velocity and groundwater exploitation intensity was used as the indicators to evaluate hazard in the study area [14]. The former two indicators were obtained from the DInSAR processing results and the groundwater exploitation intensity data was obtained from the Kathmandu Valley Water Supply Management Board (KVWSMB), Ministry of Water Supply and Sanitation, Government of Nepal.

Vulnerability, in general can be defined as a concept that describes the factors

(including economic, social and physical) aiding to reduce the ability to cope with the potential hazards impacts. The vulnerability of land subsidence refers to the measure of susceptibility to physical harm or damage caused due to land subsidence. Vulnerability includes the ability of the human society and the economic development level of the society to cope with the disaster caused by land subsidence. Land subsidence vulnerability evaluation is the process of assessing the sensitivity of the economy, population and physical infrastructure to the land subsidence phenomenon. In this research, population density, gross domestic product (GDP) and construction land proportion data was used as the indicators to evaluate vulnerability of the study area [15]. Population density refers to the number of people per unit area and this data for the study area was obtained from the Kathmandu Valley Development Authority (KVDA), Government of Nepal. GDP is one of the primary indicators used to evaluate the economic condition of a country and this data for the study area was obtained from National Accounts Section, Central Bureau of Statistics, Government of Nepal. Construction land proportion data gives the information of the proportion of built-up space and open space. This data was obtained from the Ministry of Land Reform and Management, Nepal.

The capability of disaster prevention and reduction refers to ability of the country to prevent or reduce the effect of potential land subsidence on life, property and economy. However, the land subsidence monitoring of the study area being very poor it was assumed that the country has no ability to control land subsidence at present.

Analytic Hierarchy Process (AHP)

Analytic hierarchy process is a multi-criteria mathematical decision making process developed by Professor Thomas Saaty in (1977). This process uses hierarchical structures to derive relative priorities for criteria (indicators) employing pair wise comparisons. In this research, this process was used to give weights to the indicators identified for evaluating hazard and vulnerability in MSExcel. The basic procedure includes the following steps:

Pair-wise comparison: Pair-wise comparison matrix for hazard and vulnerability was developed separately to establish priorities among the indicators. The result of comparison is derived in terms of integer.

Normalization: The integers obtained from the above step is normalized to compute the priority vector which gives the relative weights among the indicators and ultimately helps to decide which indicator is relatively more important in determining land subsidence risk. Normalization generally means to average the values in each row to compute the corresponding weight.

Consistency Analysis: The main objective of this step is to check if the preference ratings made in the pair-wise comparison are consistent. This is measured in terms of Consistency Ratio (CR), which can be calculated using Equation (3) [16].

$$CR = \frac{CI}{RI} \tag{3}$$

where, CI is the consistency index and RI is the random inconsistency indices. RI is provided for each order of matrix by [16]. In this research, since the order of matrix was 3, the corresponding RI value 0.58 was used. The CI value can be calculated using the Equation (4).

$$CI = \frac{\lambda_{\max} - n}{n-1} \tag{4}$$

where, $\lambda_{\max}$ is the value obtained from the summation of product of each normalized weight and sum of columns of the reciprocal matrix, n is the number of indicators used. Saaty, (1980) suggests that the CR value equal to 0.1 or below shows that the comparison is consistent and hence acceptable. (For detail description of the methodology refer "The analytical hierarchy process" Saaty, 1980).

After obtaining the weights for each indicators Hazard map and Vulnerability map was generated in ArcGIS (Version 10.4.1). These two maps were then utilized to obtain the final Risk map by using Equation (2). The methodology flowchart for risk assessment is shown in **Figure 3**.

3. Result and Discussion

3.1. Volume Estimation of Land Subsidence

Figure 4 shows the interferogram image for Kathmandu valley generated by utilizing DInSAR processing to ALOS PALSAR data acquired on 2007/11/02 and 2010/02/07. The locations of subsidence are indicated by L1, L2, L3, L4, L5, L6, L7 and L8. Location L1 represents the central Kathmandu area, L2 is Chauni area, L3 is Lalitpur area, L4 is Imadol area, L5 is Thimi area, L6 is Madhyapur Thimi, L7 is New Baneshwor and Koteshwor area and L8 is Gothatar area. The details of this result have been described in "Detection of Land Subsidence in Kathmandu Valley, Nepal, using DInSAR Technique (Bhattarai *et al.*, 2017)" (refer http://www.mdpi.com/2073-445X/6/2/39) considered as the first part of this study.

The subsidence volume for each location was estimated using Equation (1). The subsidence volume estimation for each location is shown in **Table 1**. These values were further used for hazard mapping of land subsidence in this research.

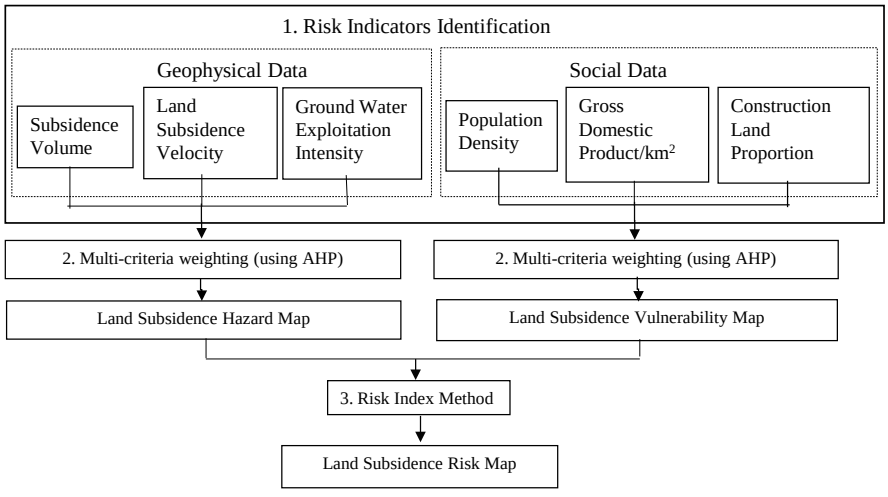

Figure 3. Methodology flowchart for risk assessment.

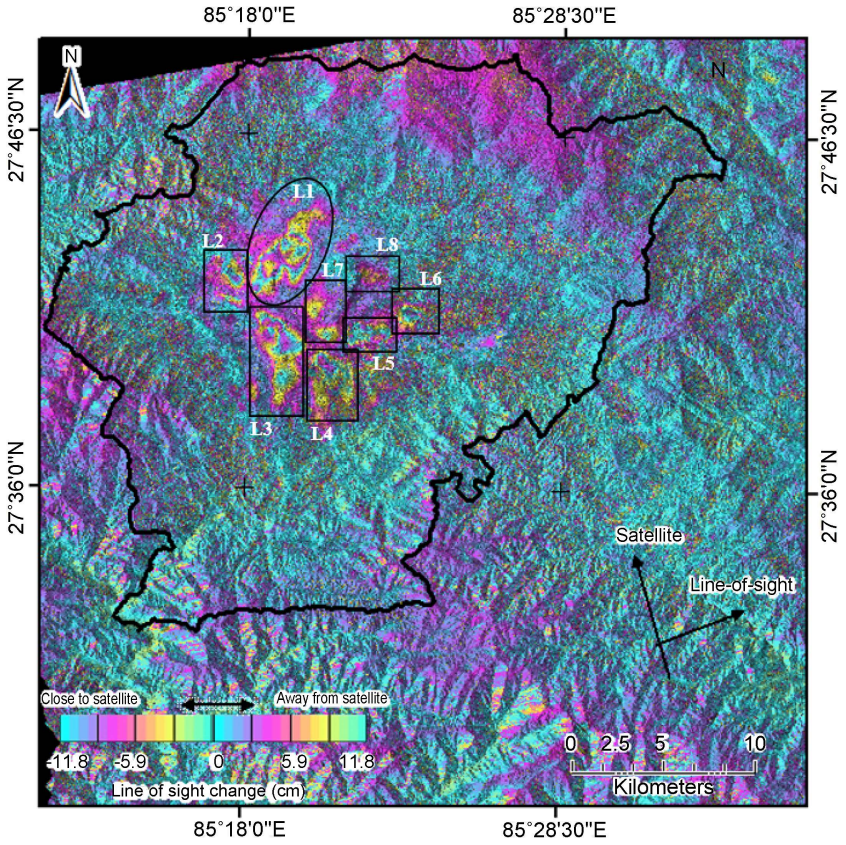

Figure 4. Differential interferogram for Kathmandu valley from 2007/11/02 to 2010/02/07 showing the subsidence locations L1 - L8.

Table 1. Volume estimation of land subsidence locations.

Location	Area 1 (m^2)	Area 2 (m^2)	Height (m)	Volume (m^3)
Cone 1	124,000	41,000	0.04	3151
Cone 2	162,000	44,000	0.04	3872
Upper part	5,179,000	3,800,00	0.12	278,474
Location L1			Total	**285,498**
Location L2	1,369,000	12,000	0.11	55,336
Location L3	4,290,000	900,000	0.11	262,348
Location L4	3,696,000	399,000	0.11	194,677
Location L5	536,000	424,000	0.11	52,680
Location L6	1,092,000	194,000	0.11	64,030
Cone 1	1,079,000	211,000	0.05	29,452
Cone 2	784,000	52,000	0.05	17,299
Location L7			Total	**46,751**
Location L8	1,000,000	1,000,000	0.02	20,000

3.2. Risk Assessment of Land Subsidence

An indicator framework based on the Disaster Risk Index method was prepared with two significant factors for risk assessment along with three indicators for each factor. The indicators were weighted by its significance to govern land sub-

sidence risk using the AHP multi-criteria decision making process. The values of each indicator were classified into three classes Low, Medium and High where low indicates the lowest hazard/vulnerability level and high indicates the highest hazard/vulnerability level. Table 2 shows the weighted values and grade and values for the respective indicators.

3.2.1. Land Subsidence Hazard Evaluation

Kathmandu valley was divided into three zones corresponding to the major cities Kathmandu, Bhaktapur and Lalitpur along with the subsidence locations obtained from previous processing for hazard evaluation. The data values of indicator for each zone and location is shown in Table 3. The volume and maximum subsidence velocity for the three zones were considered to be nil as no subsidence was detected in these areas.

Table 2. Weighted values and grade and values for indicators of land subsidence risk assessment.

Index			Grade and value		
			Low	Medium	High
Factor	Indicator	Weighted value	[1]	[2]	[3]
Hazard	Accumulated Subsidence volume (mm)	0.63	0 - 10000	10000 - 100000	>100000
	Subsidence velocity (mm/yr.)	0.26	0 - 30	30 - 50	>50
	Groundwater exploitation intensity (10^4 m^3/yr.)	0.11	0-8	8-16	>16
Vulnerability	Population density (person/km^2)	0.67	0 - 1000	1000 - 10000	>10000
	GDP per km^2 (10^4 $)	0.24	0 - 99	100 - 499	>500
	Construction land proportion (%)	0.09	0 - 49	50 - 79	>80

Table 3. Data values of indicators used for land subsidence hazard evaluation of Kathmandu valley.

Location	Volume (m^3)	Maximum subsidence velocity (mm/yr.)	Average Discharge (10^4 m^3/yr.)
Location L1	285,498	48	32
Location L2	55,336	26	4
Location L3	262,348	33	3
Location L4	194,677	30	2
Location L5	52,680	35	4
Location L6	64,030	29	1
Location L7	46,751	18	3
Location L8	20,000	11	2
Kathmandu zone	-	-	4
Lalitpur zone	-	-	4
Bhaktapur zone	-	-	3

The land subsidence hazard map of Kathmandu valley is shown in Figure 5. Land subsidence in Kathmandu valley mainly situates in low hazard area (indicated by yellow colour in Figure 5). High hazard areas can be seen scattered in the subsidence locations L1, L3 and L4 (indicated by red colour in Figure 5) whereas medium hazard areas can be seen scattered in the subsidence locations L2, L5, L6, L7 and L8 (indicated by green colour in Figure 5).

This indicates that there is a high probability that land subsidence occurrence is bound to intensify in locations L1, L3 and L4 considering there is no reduction in the average groundwater discharge.

3.2.2. Land Subsidence Vulnerability Evaluation

In the same manner to hazard evaluation, Kathmandu valley was also divided into three zones corresponding to the major cities Kathmandu, Bhaktapur and Lalitpur along with the subsidence locations obtained from previous processing. The data values of indicator for each zone and location is shown in Table 4. The individual subsidence locations were categorized into their respective municipality since it is difficult to acquire social and economic data (*i.e.* population density and GDP) for such small zones.

The land subsidence vulnerability map for Kathmandu valley is shown in Figure 6. The evaluation results show that subsidence location L1, L2, L3 L7 and L8 (indicated by red colour in Figure 6) are highly vulnerable areas. These locations are situated in the main urban core of the Kathmandu valley where the population density is the highest and the economy is the most developed. Kathmandu zone, Lalitpur zone and subsidence locations L4, L5 and L6 are found to be in medium vulnerable zone (indicated by green colour in Figure 6). Lowest

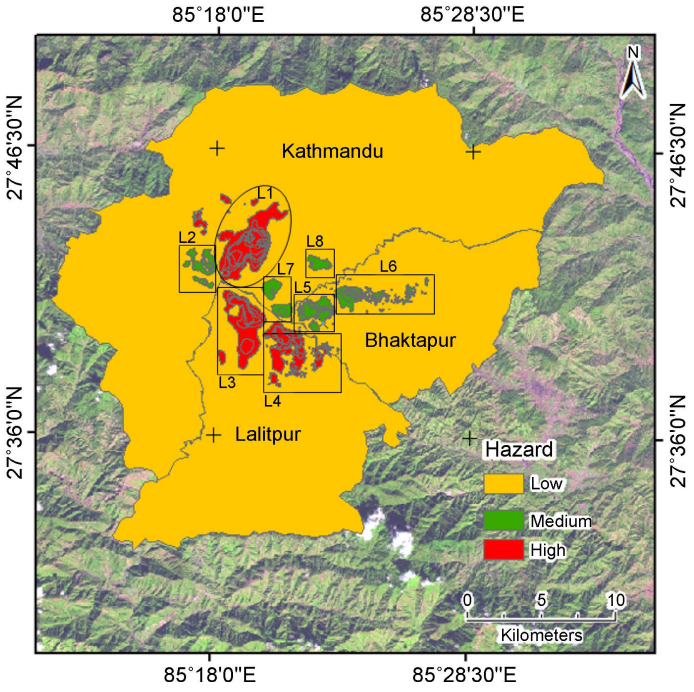

Figure 5. Land subsidence hazard map of Kathmandu valley generated through GIS processing.

Table 4. Data values of indicators used for land subsidence vulnerability evaluation of Kathmandu valley.

Location	Municipality	Population density	GDP ($)	Construction land Proportion (%)
Location L1	Kathmandu	19,726	749,582	80
Location L2	Kathmandu	19,726	749,582	95
Location L3	Lalitpur	14,574	1,014,539	80
Location L4	Lalitpur District	3241	4,562,750	30
Location L5	MadhyapurThimi	7717	1,916,042	60
Location L6	MadhyapurThimi	7717	1,916,042	20
Location L7	Kathmandu	19,726	749,582	70
Location L8	Kathmandu	19,726	749,582	50
Kathmandu zone		2382	6	60
Lalitpur zone		1197	12	40
Bhaktapur zone		680	22	30

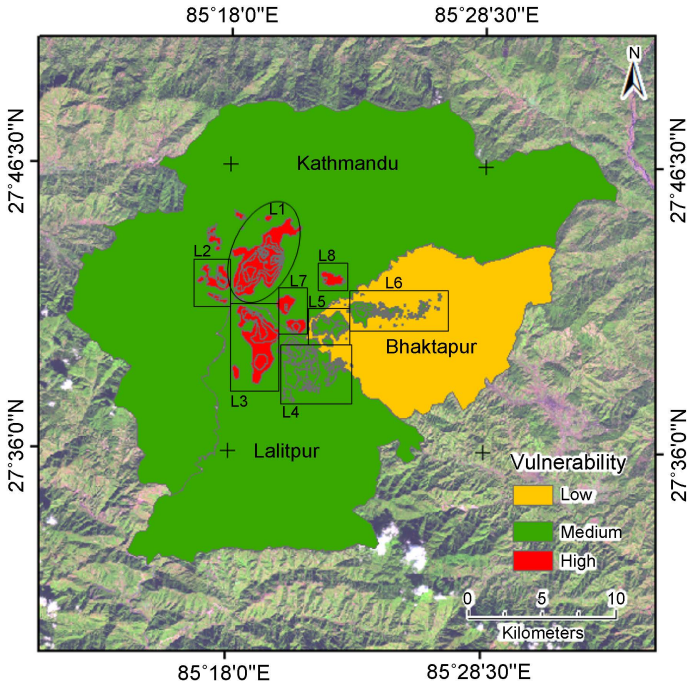

Figure 6. Land subsidence vulnerability map of Kathmandu valley generated through GIS processing.

vulnerability is seen in Bhaktapur zone as the population density and economic activity is lowest in this area. The result indicates that Location L1, L2, L3 L7 and L8 are most sensitive to damage caused by land subsidence.

3.2.3. Land Subsidence Risk Assessment

Land subsidence risk map of Kathmandu valley was generated based on the hazard and vulnerability evaluation in ArcGIS (Version 10.4.1) using Equation (2) (**Figure 7**). The areas where land subsidence was detected through DInSAR processing were found to be in high (Location L1 and L3; indicated by red colour in

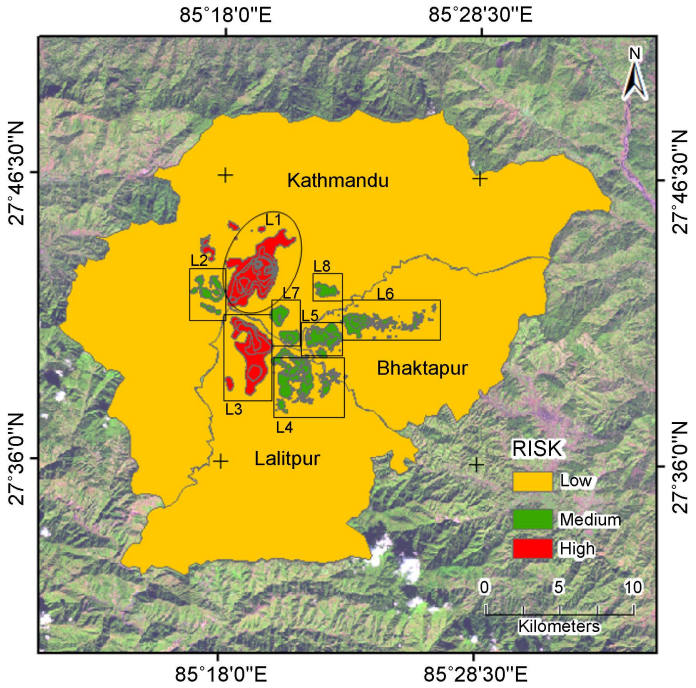

Figure 7. Land subsidence risk map of Kathmandu valley generated through GIS processing.

Figure 7) and medium (Location L2, L4, L5, L6, L7 and L8; indicated by green colour in Figure 7) risk areas. However, rest of the Kathmandu valley was found to be at low risk of land subsidence (indicated by yellow colour in Figure 7).

Shrestha, *et al.*, (2017) [17] also predicted that Kathmandu valley is at low risk through a model-based estimation of land subsidence. Even though the prediction has not been validated, it resembles the result of this study.

Due to lack of proper scientific data and research, evidence of damage caused by land subsidence has not been reported in Kathmandu valley till date. Case studies from around the world can be referred to utilize the knowledge and experience in planning and policy making to reduce if not prevent the disastrous effect of land subsidence. The location of Kathmandu valley has a very close resemblance with the location of Mexico City where land subsidence has been documented very well. Hence, case study of land subsidence in Mexico City is discussed here.

Mexico City is the capital city of Mexico located in the valley of Mexico Basin. It is surrounded by volcanic chain and mountains with elevations reaching up to 5000 m [18]. Like the origin of Kathmandu Valley, Mexico City emerged where there was once Lake Texcoco, therefore the geology consists of highly saturated clay [19]. The geology is classified into three zones namely Foothill zone, Transition zone and Lake zone. The Foothill zone comprises heterogeneous volcanic deposits and lava. The Transition zone mainly comprises of sand and gravel alluvial deposits along with volcanic materials. The lake zone comprises of highly compressible lacustrine clays [20].

The city has been suffering from groundwater extraction related subsidence

since decades [21]. The city has been reported with subsidence reaching up to 38 cm/yr. [20]. The main cause has been identified to be the drying and compaction of soft clay layers which has less permeable capacity and is mainly triggered by excessive groundwater exploitation from the aquifers [22].

The main problems reported relating to land subsidence in Mexico City are

- Decrease in runoff and wastewater drainage ability, that ultimately results in flooding during rainy season [19].
- Disruption to the water transportation structures (*i.e.* pipelines, canals) resulting in interference with water supply [20].
- Damage to the stability of manmade infrastructure (Buildings, transportation facilities like highways, roads and bridges) due to changes in surface gradients [20].

Since, there is a close resemblance in Kathmandu Valley and Mexico City, it can be expected that these problems may be encountered in Kathmandu Valley in near future if current situations prevail. The high-risk areas indicated by red color in **Figure 7**, Central Kathmandu and Lalitpur which are the main urban core of the valley has the highest probability to suffer from such damages. Other locations that are at medium risk to such damages are Chauni, Imadol, Thimi, Madhyapur Thimi, New Baneshwor and Koteshwor and Gothatar. Since, these damages are not limited to a point location, the periphery areas are also bound to suffer.

4. Conclusion

Land subsidence risk assessment based on current data revealed that the identified subsidence areas are at high and medium risk of suffering from subsidence induced damages like decrease in runoff and wastewater drainage ability, disruption to water transportation structures and damage artificial infrastructure stability whereas the rest of the Kathmandu valley is at low risk under the circumstance that similar conditions prevail. The outcomes of this research even though it is not directly validated can be used as a base for further detailed study. The results could also serve beneficial for developing disaster prevention policies. In addition, a more comprehensive risk assessment of land subsidence can be done by considering other indicators like the geological characteristics and land use type of the location. This would give a more detailed outlook on factors that can be controlled to reduce if not prevent a huge disaster. Also, in this study, it was assumed that the study area had no capacity for disaster prevention and reduction for risk assessment. However, different case scenarios like with government action to reduce groundwater exploitation and with government action to reduce or prevent construction land proportion can be employed to judge the situation in a different perspective.

Acknowledgements

The authors would like to thank Kathmandu Valley Water Supply Management Board (KVWSMB), Ministry of Water Supply and Sanitation, Kathmandu Val-

ley Development Authority (KVDA) and National Accounts Section, Central Bureau of Statistics, Government of Nepal for providing necessary data to conduct this study. The authors would also like to express a hearty gratitude to Mr. Suyesh Bhattarai for his help in obtaining the required data.

References

[1] Hu, B., Wang, J., Chen, Z., Wang, D. and Xu, S. (2009) Risk Assessment of Land Subsidence at Tianjin Coastal Area in China. *Environmental Earth Sciences*, **59**, 269-276. https://doi.org/10.1007/s12665-009-0024-6

[2] Wang, J., Gao, W., Xu, S., Yu, L. (2012) Evaluation of the Combined Risk of Sea Level Rise, Land Subsidence and Storm Surges on the Coastal Areas of Shanghai, China. *Climatic Change*, **115**, 537-558. https://doi.org/10.1007/s10584-012-0468-7

[3] Sato, H.P., Abe, K. and Ootaki, O. (2003) GPS-Measured Land Subsidence in Ojiya City, Niigata Prefecture, Japan. *Engineering Geology*, **67**, 379-390.

[4] Faunt, C.C., Sneed, M., Traum, J. and Brandth, J.T. (2015) Water Availability and Land Subsidence in Central Valley, California, USA. *Hydrogeology Journal,* **24**, 675-684. https://doi.org/10.1007/s10040-015-1339-x

[5] Zhang, W.R., Duan, Z.L., Zeng, Z.Q. and Shi, H.P. (2003) Evaluation on Economic Losses Resulted from Land Subsidence in Shanghai: 1921-2000. *Journal of Tongji University*, **31**, 743-748.

[6] Holzer, T.L. and Galloway, D.L. (2005) Impacts of Land Subsidence Caused by Withdrawal of Underground Fluids in the United States. *Reviews in Engineering Geology*, **XVI**, 87-99. https://doi.org/10.1130/2005.4016(08)

[7] Liu, J., Wang, H. and Yan, X. (2015) Risk Evaluation of Land Subsidence and Its Application to Metro Safety Operation in Shanghai. *The Proceedings of the International Association of Hydrological Sciences*, **372**, 543-553. https://doi.org/10.5194/piahs-372-543-2015

[8] Westen, C.J., Alkema, D., Damen, M.C.J., Kerle, N. and Kingma, N.C. (2011) Multi-Hazard Risk Assessment. Distance Education Course Guide Book, United Nations University – ITC School on Disaster Geo-Information Management (UNU-ITC DGIM).

[9] Zhu, L., Chen, Y., Gong, H.L., Liu, C. and Wang, R. (2013) Spatial Risk Assessment on Land Subsidence in Beijing, China. 20*th International Congress on Modelling and Simulation,* Adelaide, 1-6 December 2013.

[10] CBS (2012) National Population and Housing Census. National Report. Central Bureau of Statistics, Kathmandu.

[11] Bayuaji, L., Josaphat, T.S.S. and Kuze, H. (2010) ALOS PALSAR D-Insar for Land Subsidence Mapping in Jakarta, Indonesia. *Canadian Journal of Remote Sensing*, **36**, 1-8. https://doi.org/10.5589/m10-023

[12] Gibilisco, S. (2006) Technical Math Demystified. McGraw-Hill, New York, 191-196.

[13] Lirer, L. and Vitelli, L. (1998) Volcanic Risk Assessment and Mapping in the Vesuvian Area Using GIS. *Natural Hazards*, **17**, 1-15. https://doi.org/10.1023/A:1007977110144

[14] Wang, G.L. (2006) Preliminary Studies on Dangerous Grading Standard of Land Subsidence. *Shanghai Geology*, **4**, 39-43.

[15] Zhou, C.H., Wan, Q. and Huang, S.F. (2000) A GIS-Based Approach to Flood Risk Zonation. *Acta Oceanologica Sinica*, **55**, 15-24.

[16] Saaty, T.L. (1980) The Analytic Hierarchy Process. McGraw-Hill, New York.

[17] Shrestha, P.K., Shakya, N.M., Pandey, V.P., Birkinshaw, S.J. and Shrestha, S. (2017) Model-Based Estimation of Land Subsidence in Kathmandu Valley, Nepal. Geomatics, Natural Hazards and Risk. https://doi.org/10.1080/19475705.2017.1289985

[18] National Research Council Staff (1995) Mexico City's Water Supply: Improving the Outlook for Sustainability. National Academies Press, Washington DC.

[19] Maricela, Y. and Pierre, M. (2002) Air Pollution in Mexico City. Project Study Paper, University of Salzburg, Austria. http://biophysics.sbg.ac.at/mexico/air.htm

[20] Yan, Y., Doin, M.-P., Lopez-Quiroz, P. and Tupin, F. (2012) Mexico City Subsidence Measured by Insar Time Series: Joint Analysis Using PS and SBAS Approaches. *IEEE Journal of Selected Topics in Applied Earth Observations and Remote Sensing*, **5**, 1312-1326. https://doi.org/10.1109/JSTARS.2012.2191146

[21] Cabral-Cano, E., Solano-Rojas, D., HernÃ¡ndez-Espriu, J., Cigna, F., Wdowinski, S., Osmanoglu, B., Falorni, G., Bohane, A. and Colombo, D. (2012) Subsidence Induced Faulting Hazard Risk Maps in Mexico City and Morelia, Central Mexico. NASA Astrophysics Data System (ADS).

[22] Lapez-Quiroz, P., Doin, M., Carreon-Freyre, D. and Cerca, M. (2012) Analysis of Nonlinear and Subsidence in Mexico City Lacustrine Plain. NASA Astrophysics Data System (ADS).